2019

Adsorption Induced Solid Phase Transition of MIL-53(Al)

Rushik G. Bandodkar

ADSORPTION INDUCED SOLID PHASE TRANSITION OF MIL-53(Al)

RUSHIK G. BANDODKAR

Bachelor of Engineer in Chemical Engineering

Mumbai University

June 2015

Submitted in partial fulfillment of requirements for the degree

MASTER OF SCIENCE in Chemical Engineering

at the

CLEVELAND STATE UNIVERSITY

August 2019

We hereby approve this thesis

For

RUSHIK G. BANDODKAR

Candidate for the Master of Science in Chemical Engineering degree

For the Department of

Chemical and Biomedical Engineering at the Washkewicz College of Engineering

And

CLEVELAND STATE UNIVERSITY'S

College of Graduate Studies by

_____

Thesis Chairperson, Dr. Orhan Talu

Department of Chemical & Biomedical Engineering

_____

Thesis Committee Member, Dr. Geyou Ao

Department of Chemical & Biomedical Engineering

_____

Thesis Committee Member, Dr. Christopher Wirth

Department of Chemical & Biomedical Engineering

Date of Defense: July 17, 2019

ACKNOWLEDGEMENT

First and foremost, I would like to offer my sincerest gratitude to Dr. Orhan Talu for his guidance, support and patience throughout my time learning under him. It has been a pleasure to work under him and his insight into adsorption has been invaluable. Without him I would not have learned nearly as much as I did throughout the process of writing this thesis.

I am very thankful to Dr Sasidhar Gumma for his support during the period of my studies under him and for giving me the opportunity to be a part of his research group. I would like to thank Dr Ao and Dr Wirth for their willingness to serve as members of my Thesis Committee and also for their input and critique of my work. They provided beneficial inputs to the final draft of my thesis.

Additionally, I wish to thank Dustin Bowden for his help with experimental setup of Rubotherm process and countless synthesis batches. He was extremely helpful in providing the necessary improvements to the apparatus in order to allow me to conduct the experiments as I wished to perform.

Finally, my sincere gratitude goes to god for giving me this opportunity to pursue Master's degree at Cleveland State University. I am also very thankful to my parents for their selfless sacrifices which allowed me to accomplish my dream of studying in the United States.

ADSORPTION INDUCED SOLID PHASE TRANSITION OF MIL-53(Al)

RUSHIK BANDODKAR

ABSTRACT

Metal organic frameworks (MOFs) are nano-porous solids with potential applications in a wide range of fields including gas separation and catalysis. A number of metal organic frameworks show structural transformation and exceptional flexibility on changing the temperature, pressure and adsorption of certain guest molecules. On the contrary, most of the porous solids like zeolites and activated carbon used in applications are rigid. The structural flexibility makes MOF materials very interesting to study and show promise in applications such as sensors, actuators, membrane separation and adsorptive separation.

In this study, we examine the chemical potential difference ($\Delta\mu$) of MIL-53 (Al), a MOF which exhibits a "breathing" phenomena by transitioning between its narrow pore (np) and large pore (lp) conformation. It is important to measure $\Delta\mu$ between the two phases of the solid to be able to predict and/or model gas adsorption. Single component adsorption equilibria of carbon dioxide (CO_2), methane (CH_4), nitrogen (N_2) and oxygen (O_2) were measured over a pressure range of 0-20 bar at 273K, 293K and 306K, using a magnetic suspension microbalance. The adsorption measurements show that experimental sample of MIL-53(Al) behaves differently in case of CO_2 when compared with other gases. The data obtained is used to investigate these differences in the adsorption characteristics of narrow pore and large pore phases. A modified form of Langmuir model is fitted to the experimental data and corresponding chemical potential differences between the two pore conformations is determined. The effect of temperature dependency is also investigated.

TABLE OF CONTENTS

Page

LIST OF TABLES

Table Page

LIST OF FIGURES

Figure Page

NOMENCLATURE

b = Henry's law constant

b_1 = Henry's law constant for lp phase

b_2 = Henry's law constant for np phase

E = Activation energy

ε = Volumetric strain

F = Helmholtz free energy

F_{host} = Helmholtz free energy of solid adsorbent

$F_{host}^{(i)}$ = Helmholtz free energy of solid phases

ΔF_{host} = Helmholtz free energy difference between the solid phases

G = Gibbs free energy

ΔG = Free energy Change

ΔH_0 = Difference in enthalpy of adsorption

ΔH = Change in Enthalpy

K = Bulk modulus

k = Rate constant

K_0 = Adsorption entropy change

K_a = Rate constant for adsorption

K_d = Rate constant for desorption

m = Mean of normal distribution

N_i = Number of moles of species i

N_{max} = Saturation capacity of adsorbent

N_{1max} = Maximum saturation capacity of lp the phase

N_{2max} = Maximum saturation capacity of np the phase

N = Number of moles of gas adsorbed by the adsorbent

ΔN_i = Difference in the amount of species (i) adsorbed between two phases

P^0 = Partial pressure

P_s = Solvation or disjoining pressure

p_{ext} = External pressure

P_{trans} = Transition pressure

q = Amount of gas in adsorbed phase

R = Ideal Gas Constant

s = Standard deviation

ΔS = Change in Entropy

T = Temperature

μ_i = Chemical Potential of adsorbent species i

$\Delta\mu$ = Difference in chemical potential of adsorbed species

V = Volume of gas adsorbed

V_c = Unit cell capacity

ΔV_c = Variation of cell volume

ΔV_{host} = Difference in volume of two host phases

V_p^1 = Pore volume of starting phase

V_p^2 = Pore volume of second phase

ψ = Grand Potential of adsorbed phase

ψ_{lp} = Grand potential of lp phase

ψ_{np} = Grand potential of np phase

φ = Degree of transition

σ_s = Adsorption induced stress

σ_o = Pre-stress

σ^* = Critical stress

σ^*_{lp} = Critical stress associated with lp to np transition

σ^*_{np} = Critical stress associated with np to lp transition

Ω_{os} = Osmotic potential

θ = Fractional coverage

CHAPTER I

INTRODUCTION

1.1 Adsorption

Adsorption is defined as a process in which a fluid, when exposed to a solid substance, tends to form a bond with the particles of the solid[1]. The bonds are formed as a result of the attraction of fluid molecules to the surface of a solid based on its size or molecular interactions with the solid. Due to adsorption, there is an increase in the density of the fluid or enrichment of the material of the gas near the solid interface[2]. In usual terminology, gas molecules that are adsorbed onto the surface of a solid are called as the adsorbate molecules while, the solid surface which adsorbs the gas is referred to as the adsorbent. Adsorbed molecules have at the most two degrees of translational freedom on the surface since they lose the rotational freedom compared to gas phase molecules [3]. This makes adsorption an exothermic process.

Based on the interaction between gas molecules and solid surface, adsorption is classified into two categories: physical adsorption also referred to as 'Physisorption' and chemical adsorption which is also referred to as 'Chemisorption'. Physisorption results from the attachment of adsorbate molecules to the adsorbent surface due to weak

Van der Waals forces and hence is an easily reversible process. It is nonspecific in nature and is significant only at relatively low temperatures. It has a low heat of adsorption comparable to the latent heat of evaporation. Almost all the industrial adsorptive separation processes are based on physisorption since it is a reversible phenomenon which makes it possible to regenerate the adsorbent. Heat of adsorption of physisorption is typically in the range of 10 KJ/mol to 40 KJ/mol[3].

Chemisorption on the other hand, involves the formation of chemical bonds between adsorbate molecule and surface of adsorbent by transferring or sharing electrons. Hence, it is an irreversible phenomenon at constant temperature. This type of adsorption is highly specific and can be carried out over a wide range of temperature. It has a high heat of adsorption in the range of 80 to 400 KJ/mol [3] comparable to chemical bond energies.

If single gas is being adsorbed, it is called pure component adsorption while, if the gas involved in adsorption is a mixture, it is called multi-component adsorption. In the latter case, the success of adsorption depends on the composition of the mixture and the interaction of the adsorbate molecules of interest with the solid surface. The adsorbents have selectivity of species and preferentially adsorb some species over others. Almost all of the industrial processes involve separation. It is therefore important to know the behavior of adsorbate-adsorbent system under consideration before designing any adsorption process[4].

Departure of the sorbate-adsorbent system from equilibrium[4] is the main driving force for all separation processes involving adsorption. Equilibrium data is therefore vital which is typically represented in the form of an isotherm i.e. change in the amount of gas adsorbed at a constant temperature. Just like any other data, chemical engineers are interested in predicting or at least correlating the equilibrium data. But, in order to

make such predictions or develop correlations, it is important to measure the actual data. Although most of the industrial separation processes involve mixtures, pure component isotherm data helps understand the interactions between individual molecules and adsorbent.

1.2 Adsorbent

Most of the industrially significant adsorbents are microporous in nature. They have a high surface area or micro pore volume which is required for adsorption. Activated carbon, activated alumina, silica gel, zeolites are some of the widely used solids in the industry. Silica gel, activated carbon and activated alumina are examples of traditional amorphous microporous adsorbents whereas aluminosilicates (zeolites) and recently developed metal-organic frameworks (MOFs) are adsorbents which have a crystalline structure. Zeolites are fundamentally different from others; they do not have a pore size distribution since crystal structure defines the micropore size. Amorphous adsorbents contain a wide pore size distribution which is controlled by the manufacturing process [3]. Generally, adsorbents have similar properties which can be explored for applications. Silica gel, activated alumina, zeolite and metal-organic frameworks are hydrophilic because their surface is polar. They have a higher affinity for polar molecules such as water. Activated carbon surface mainly made of graphene sheets is non-polar and as a result has no specific affinity for polar molecules. It adsorbs large quantities of non-polar hydrocarbons.

The choice of an adsorbent depends on adequate adsorptive capacity. This requirement limits the selection to microporous adsorbents which could be used for practical separation processes. Porosity is one of the important properties which governs the capacity of the material. Usually, higher the porosity, higher is the surface area and pore volume of a material. Based on this property, adsorbent materials are

categorized into three groups: microporous adsorbents (< 2nm), mesoporous adsorbents (2-50nm) and macroporous adsorbents (> 50nm) [3]. It is important to optimize the pore size of an adsorbent to maximize its potential.

(As a point of reference, kinetic diameter of methane at room temperature is only 3.6 Å or 0.36nm)

1.3 Metal Organic Frameworks

Metal-organic frameworks (MOFs) represent a rapidly expanding class of nanoporous adsorbent materials that display an extremely wide range of crystal structure and host-guest properties due to the tunable porosity allowed by coordination chemistry and the versatility enabled by functionalization of organic linkers[5]. It is anticipated that MOFs may have a major impact in many areas of science and technology[6]. MOFs are made up of metal ions interconnected by organic linkers like carboxylates, tetrazolates, sulfonates etc. Compared to other classes of microporous materials (*e.g.*, zeolites, activated carbon, and silica gels) currently used in processes such as gas storage, catalysis and sensing, adsorptive gas separation, MOFs show a great potential due to the wide possibilities of pre- or post- synthetic functionalization of these linkers. Moreover, many of these materials exhibit an exceptionally flexible porous framework and stimulus-responsive behavior by undergoing structural transformations as a result of changes in temperature, pressure, and adsorption of guest molecules [5]. In some cases, variations in structure are progressive i.e. swelling upon exposure to water and various alcohols while, in other materials, the structural response is displayed by an abrupt transition between two distinct crystal structures of the framework [5,7].

1.4 Flexible Framework/MIL-53(Al)

1.4.1. MIL-53. MIL-53 belongs to the group of metal terephthalate MOF first synthesized by Ferey. The crystal structure is shown in Figures 1.1 and 1.2. The framework structure is formed from the chains of $MO_4(OH)_2$ octahedra [M= Al for MIL-53(Al)], held together by the dicarboxylate groups of the terephthalate linkers. The chemical formula of MIL-53 is $M(OH)(O_2C–C_6H_4–CO_2)$. The hydroxyl groups are located at the metal-oxygen-metal links within the structure. This results in a different adsorption mechanism compared to other members of MIL family [8]. It has a three-dimensional microporous framework with one-dimensional diamond shaped channels with a free internal diameter of about 0.85nm (Figure 1.1)[9]. The corner sharing hydroxyl groups present in the framework are accountable for a high degree of flexibility upon hydration/dehydration [9, 10, 11]. There is a strong interaction between the adsorbed water molecules and the hydroxyl groups present in the framework because of hydrogen bonding, coupled with the flexibility of relatively deformable hinge like units of the structure which pull the oppositely positioned metal octahedra towards each other thereby reducing the pore size [referred to as the narrow pore (np)]. The pores open up on removal of the water molecules [referred to as the large pore (lp)]. This structural flexibility is referred to as the "breathing" phenomena which has attracted a lot of attention. The cell volume decreases by approximately 35% during its transformation from the lp domain to the np domain[12]. A similar behavior is observed during CO_2 adsorption.

In the aluminum form of MIL-53, the crystal framework consists of corner sharing octahedral chains of hydroxyaluminate $[AlO_4(OH)_2]$ which are linked together by 1,4-benzenedicarboxilate (BDC) organic ligand[12]. MIL-53(Al) is sometimes also referred to as aluminum terephthalate because of the presence of terephthalate group in

its framework structure. The structural transition described above can also be achieved by applying mechanical pressure, or by sole effect of temperature on empty sample [13]. At room temperature, and in the absence of a guest molecule, the lp phase is the most stable form [13]. A considerable amount of research work has been published on this material because of its fascinating breathing behavior and good stability[14]. Figure 1.2 shows crystal projection of MIL-53(Al) on the two pore phases.

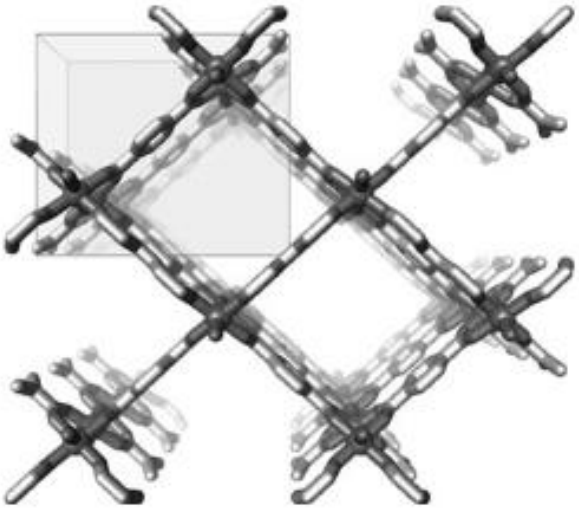

Figure 1.1 Structure of MIL-53. The box represents one unit cell [9]

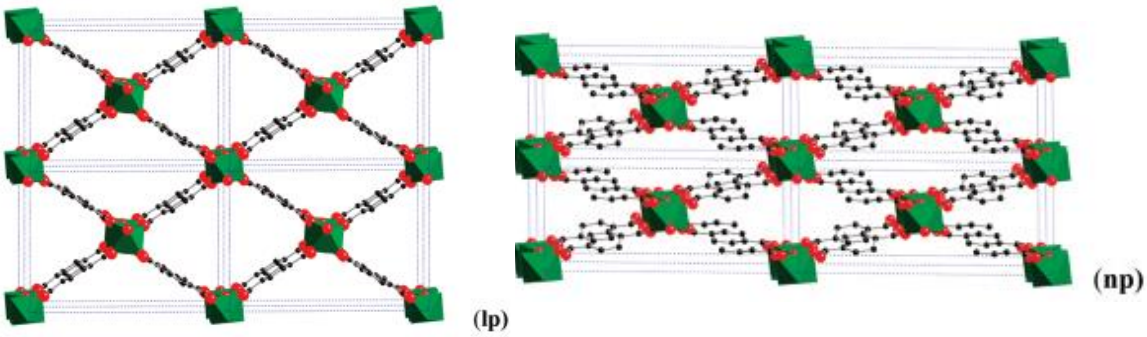

Figure 1.2 Representation of the metastable lp and np structures of MIL-53(Al) material, as a 2 x 2 x 2 supercell viewed along the axis of the unidimensional channel [13].

1.5 Research Objective

In this work we present a consistent method to quantify chemical potential difference $\Delta\mu$ between the two pore conformations of MIL-53(Al) as a function of temperature and adsorbed species.

The purposes are:

1. Collect adsorption equilibrium data for np and lp forms of MIL-53(Al) for methane, oxygen, nitrogen and carbon dioxide at three temperatures.
2. Show that $\Delta\mu_s$ is independent of the adsorbing compound and solely a property of MIL-53(Al).
3. Show that the transition is an activated process depending on the exponential of absolute temperature.
4. Investigate the double transition caused by CO_2 adsorption commonly referred to “breathing”

CHAPTER II

THEORY

2.1 Adsorption Fundamentals

Molecular interactions resulting from attraction between adsorbate and adsorbent molecules, are a combination of van der Waals forces (dispersion-repulsion) and electrostatic interactions which include polarization, dipole (permanent and induced), and quadrupole interactions[3]. Uneven charge distribution in the electron cloud results in permanent dipole in polar molecules. Polarity can also be induced in non-polar molecules if they are close enough to a polar molecule on a polar surface. Non-polar molecules do not have a permanent dipole when their charge is averaged over time. However, they have a dipole at any instantaneous moment which has the potential of inducing a dipole on another molecule. This results in London Dispersion forces. Molecules experience repulsive forces when they are too close to each other and their electron clouds start overlapping. Adsorption occurs when the repulsive forces and attractive forces are at equilibrium. Figure 2.1 depicts the relationship between potential energy (sum of all the interactions between an adsorbate molecule and the molecules in the lattice of the adsorbent)[15] and distance of sorbate molecules from the surface of the adsorbent.

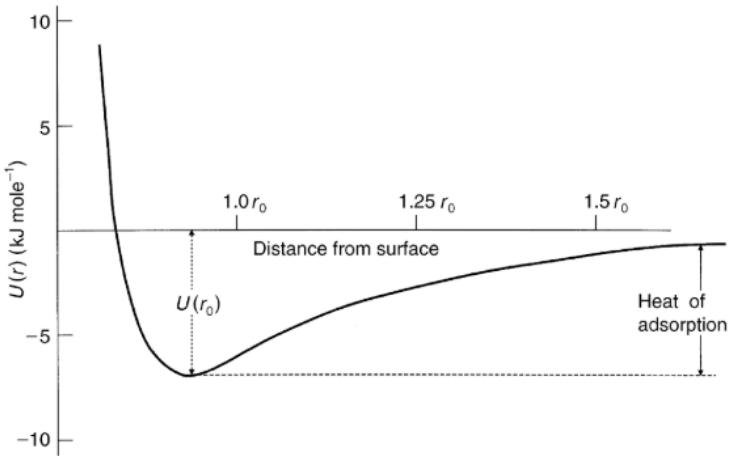

Figure 2.1 Potential energy diagram for adsorption [16,15]

The depth of the potential well, $U(r_0)$, relates to the strength of attractive forces between adsorbate and adsorbent surface. The larger the potential energy difference, the higher the sorbate molecules would be attracted to the surface. For a given adsorbate-adsorbent system, $U(r_0)$ also equates closely with the measured heat of adsorption [15]. The heat of adsorption provides a direct measure of the strength of attraction between sorbate and surface[3].

2.2 Adsorption Thermodynamics

Adsorbed molecules have at the most two degrees of translational freedom on the surface; surface restricts the molecules to move along the surface of the adsorbent. Also, the rotational freedom of the adsorbed species is always less than that of the gas phase molecules. This results in a decrease in the entropy i.e. negative entropy ($\Delta S = S_{ads} - S_{gas}$ where S_{ads} and S_{gas} are entropies of adsorbed phase and bulk gas phase). For significant adsorption to occur, the free energy change on adsorption (ΔG) reduces as well. Thus, from the thermodynamic equation 2.2.1, ΔH (change in enthalpy) must also decrease, which causes a release in heat making adsorption an exothermic process.

$$\Delta G = \Delta H - T\Delta \qquad 2.2.1$$

Isotherms are a way of representing primary equilibrium data as amount adsorbed versus pressure at constant temperature. For pure component adsorption, these are the primary properties of concern. Five classes of adsorption isotherms have been observed as illustrated in the Figure 2.2[17]:

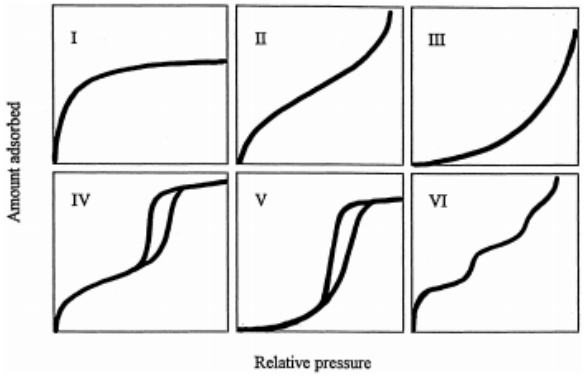

Figure 2.2 The IUPAC classification of Adsorption Isotherm for Gas-Solid Equilibria[17]

Microporous adsorbents in which the pore size is not very much greater than the molecular diameter of the sorbate, are normally of type I[3]. The adsorbents which exhibit this type of isotherm have a definite saturation limit that corresponds to complete filling of the micropores. Types II and III describe adsorption on macroporous adsorbents which have a wide range of pore size with strong and weak adsorbate-adorbent interaction respectively[17,3]. Types IV and V represent mono and multi layer adsorption either on the plane surface or the walls of a pore whose diameter is much larger compared to the diameter of the sorbate. While, type VI illustrates that isotherm can have multiple steps [17].

2.3 Reference States

An adsorbed phase only exists at the interface between a solid phase and a fluid phase.Therefore, any thermodynamic property (amount adsorbed, enthalpy, entropy, etc.) of an adsorbed phase is measured as its value for the two-phase system relative to a value in some reference state [18]. There is no apparent “correct” reference state. If a

thermodynamic reference state is defined completely, its choice is somewhat arbitrary. However, it is usually dictated by the specific application. There are three common reference states viz. *absolute*, *excess* and *net* adsorption. [**Note:** All measurements in this thesis are based on *net* adsorption reference state for which volume of the gas in bulk phase is simply the volume of the container i.e. volume is constant[18].]

2.4 Gibbs Dividing Surface

Adsorption results in changes in the density profile of a gas near the surface of a solid. Generally, the density increases near the surface because of the potential field imposed by the solid. This perturbation in adsorbate density results in three regions from left to right as shown in Figure 2.3

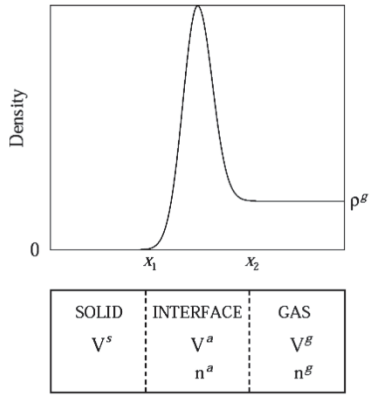

Figure 2.3 Illustration of density profiles [19]

(1) zero density in the solid region

(2) Substantially higher density in interfacial region as a result of potential field of the solid

(3) Decay in density to the bulk gas density far away from the surface

However, the interfacial limits (X_1 and X_2) are ill-defined. The location of X_1 will depend on the size of the gas molecule i.e. the type of gas adsorbed whereas, the location of X_2 will depend on thermodynamic properties such as temperature T and pressure P.

In order to overcome this ambiguity, Gibbs proposed partitioning the ill-defined interfacial region with changing properties into two separate phases with uniform properties [18]. Thus, the Gibbs dividing surface separates the fluid phase (where gas density is ρ_g) from the impenetrable solid phase (where gas density is zero) (see Figure 2.4 below). As a result, the ill-defined upper-limit (X_2) extends to infinity i.e. becomes independent of the thermodynamic properties. The location of lower-limit (X_1) depends on where the Gibbs dividing surface is placed. The placement of the low limit actually defines the reference state for adsorption thermodynamics. The Gibbs approach is purely mathematical and applicable regardless of where the dividing surface is placed as long as it is not a function of thermodynamic properties such as T and P [18].

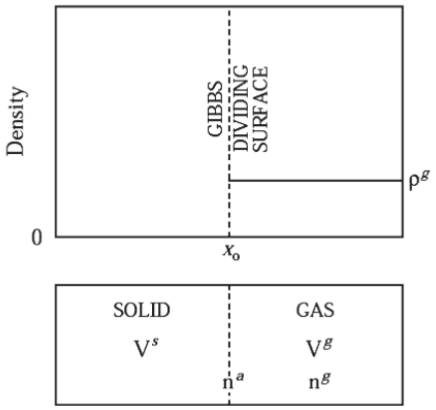

Figure 2.4 Gibbs dividing surface near a flat surface [19]

The Gibbs definition described above applies to a 2D surface phase which uses surface area as the necessary extensive property to complete the thermodynamic definition (since adsorption is a surface phenomenon). Since most industrially relevant adsorbents require a high surface area-to-volume ratio, they are typically nanoporous or microporous in nature. As the radius of curvature for such solids is of the order of a few angstroms, surface area loses its physical importance because it cannot be defined or measures. Hence, the adsorbent mass is used as the extensive property.

2.5 Grand Potential

Grand potential is the free energy change associated with isothermal immersion of fresh adsorbent in a bulk fluid. The absolute value of grand potential is the minimum amount of isothermal work needed to regenerate the adsorbent[20]. It plays a vital role in adsorption thermodynamics. Mathematically, grand potential is defined as

$$\psi = F - \sum N_i \mu_i = - P^0 V \quad [20] \qquad 2.5.1$$

In the above equation, F is the Helmholtz free energy of the empty solid, μ_i is the chemical potential of the adsorbent species i and N_i is the number of moles of species i adsorbed. Temperature, volume and chemical potential are the independent variables of grand potential[20].

In case of pure component adsorption, grand potential is obtained from an isothermal integration as shown in equation 2.5.2

$$\psi = -RT \int_0^{P^0} \frac{N}{P^0} dP^0 \quad [20] \qquad 2.5.2$$

The integral term in the equation represents spreading pressure which is used to characterize the adsorbed phase and correlates to the decrease in the surface tension of adsorbent as a result of adsorption. Grand potential (ψ) is expressed as J Kg^- of solid adsorbent[20].

2.6 Equilibrium Models

The ability to be able to model equilibrium data correctly is crucial not only for MOF's, but for other application also. An accurately developed model not only helps us understand how adsorption occurs, but also saves us time and tedious process of collecting data. There are several models for single component adsorption. Some of the models used in this study are discussed in this section starting with the most basic. All the text in this section is drawn from D.M. Ruthven's "Principles of Adsorption & Adsorption Processes".

2.6.1 Henry's Law. Equilibrium relationship between an adsorbent and adsorbate for a uniform surface and at low concentration resembles a linear function. This linear relation is called the Henry's law shown in the equation below:

$$N = bP^0 \qquad 2.6.1.1$$

Where N is the amount of gas in the adsorbed phase, b is the Henry's law constant (adsorption equilibrium constant) and P^0 is the partial pressure of adsorbate in the gas phase. Temperature dependency of the Henry constant obeying the vant Hoff equation is represented below:

$$b = K_0 \, e^{-\Delta H/RT} \qquad 2.6.1.2$$

Where ΔH represents difference in enthalpy (i.e. isosteric heat of adsorption), R is the ideal gas constant, K_0 is related to the adsorption entropy change, and T is the temperature. The equation relates the change in constant b to the change in temperature T. A plot of ln b versus 1/T is usually linear with a wide temperature range. Since Henry's law has no saturation capacity, adsorption increases with pressure and reaches infinity. This cannot occur in microporous adsorbents as they have a finite pore volume. Never the less, Henry's law forms the basis for other isotherm models explained later. Thermodynamics requires that as the density approaches zero at low pressures, adsorbed amount must be linearly dependent hence, all adsorption systems thermodynamically approach Henry's law.

2.6.2 The Langmuir Isotherm. It is the simplest and most commonly used theoretical model for monolayer adsorption on microporous solids which includes saturation capacity with finite number of sites. The Langmuir model was originally developed to represent chemisorption on a set of distinct localized adsorption sites. But the equation is also obeyed by a number of systems at a relatively low coverage. A dynamic equilibrium is assumed between the adsorbed phase and the vapor phase while

formulating the isotherm. The rate at which adsorbate gas molecules strike the surface of the adsorbent is proportional to the product of partial pressure P^0 of the gas and the fraction (1- θ) of sample remaining uncovered i.e. available adsorption site [15]. Also, the model assumes that the rate of desorption is directly proportional to the fractional surface coverage θ. The Langmuir model reduces to Henry's Law at low concentrations, which is a requirement for thermodynamic consistency in any physical adsorption system [16].

Basic assumptions in the model are stated as [3]:

a) Molecules are adsorbed at a fixed number of well-defined localized sites.
b) Each site can hold one adsorbate molecule.
c) All sites are energetically equivalent.
d) There is no interaction between molecules adsorbed on neighboring sites.

Langmuir contended that rates of adsorption and desorption are equal at equilibrium. The rate equation for a single adsorbate molecule is represented below:

$$K_a P^0 (1- \theta) = K_d \theta \qquad 2.6.2.1$$

Where, K_a and K_d are the rate constants for adsorption and desorption.

$\theta = N/N_{max}$ is the fractional coverage, N_{max} is the saturation capacity of the adsorbent, N is the actual amount adsorbed. Since K_a and K_d cannot be determined experimentally, they are combined. This leads to a typical representation of the Langmuir isotherm as shown in equation 2.6.2.2:

$$\frac{\theta}{(1-\theta)} = \frac{K_a}{K_d} P^0 = b P^0 \qquad 2.6.2.2$$

Where $b = K_a/K_d$ is the adsorption equilibrium constant also referred to as the Henry's law constant.

$$\theta = \frac{N}{N_{max}} = \frac{bP^0}{(1+bP^0)} \qquad 2.6.2.3$$

Equation 2.6.2.3 correctly expresses the asymptotic behavior for monolayer adsorption as the sites fill up. At low adsorbate concentration, the equation simplifies to Henry's law as stated before. The variables N_{max} and b in the above equation are referred to as the Langmuir model parameters/fits.

2.6.3 Dual Site Langmuir Model. This model is developed by assuming that adsorption on each phase of the solid i.e. MIL-53(Al) follows Langmuir model[12].

Langmuir Model for lp phase:

$$\frac{N}{N_{1max}} = \frac{b_1 P^0}{1+ b_1 P^0} \qquad 2.6.3.1$$

In the above equation, N_{1max} and b_1 represent the maximum saturation capacity and the adsorption equilibrium constant of lp phase respectively.

Langmuir Model for np phase:

$$\frac{N}{N_{2max}} = \frac{b_2 P^0}{1+ b_2 P^0} \qquad 2.6.3.2$$

In the equation, N_{2max} and b_2 represent the maximum saturation capacity and the adsorption equilibrium constant of np phase.

The history of the solid and affinity parameter for the adsorbate affects the amount of gas adsorbed (discussed in sections 3.3 and 3.5). Hence, the total amount adsorbed (loading) is the sum of the number of moles of gas adsorbed in both the phases. Equation 2.6.3.3 below represents the dual site Langmuir model which also forms the basis for the model used in this thesis. A weighting fraction [or pore opening parameter (φ)] is introduced to the model to represent fraction of np and lp phases of MIL-53(Al).

$$N = \left(\frac{N_1 b_1 P^0}{1+ b_1 P^0}\right)(\varphi) + \left(\frac{N_2 b_2 P^0}{1+ b_2 P^0}\right)(1 - \varphi) \qquad 2.6.3.3$$

2.7 Proposed Model

In this work, the pure component adsorption isotherms of N_2, O_2, CH_4 and CO_2 are modelled using the modified dual site Langmuir model proposed by Mishra et al. (2014)[12]. According to this model, the pore opening parameter (φ) is a function of pressure (P^0) at a given temperature. The model equations are described as follows:

Langmuir equations for each phase:

$$N_{lp} = \left(\frac{N_{1max}\, b_1 P^0}{1+ b_1 P^0}\right) \quad 2.7.1$$

$$N_{np} = \left(\frac{N_{2max}\, b_2 P^0}{1+ b_2 P^0}\right) \quad 2.7.2$$

Grand Potential for each phase:

$$\frac{\psi}{RT} = \int_0^{P^0} \left(\frac{N}{P^0}\right) dp \quad 2.7.3$$

$$\frac{\psi_{lp}}{RT} = N_{1max} \ln(1 + b_1 P^0) \quad 2.7.4$$

$$\frac{\psi_{np}}{RT} = N_{2max} \ln(1 + b_2 P^0) \quad 2.7.5$$

Difference in grand potential between the phases:

$$\delta = \frac{\psi_{lp}}{RT} - \frac{\psi_{np}}{RT} \quad 2.7.6$$

Overall total amount adsorbed:

$$N = \left(\frac{N_1 b_1 P^0}{1+ b_1 P^0}\right)(\varphi) + \left(\frac{N_2 b_2 P^0}{1+ b_2 P^0}\right)(1 - \varphi) \quad 2.7.7$$

Fraction of sample that will be in the lp phase at P^0:

$$\varphi = \text{Norm.Dist}\ (P^0, m, s) \quad 2.7.8$$

In the above equations, N is the total amount adsorbed, N_{1max}, N_{2max} are the saturation capacities and b_1, b_2 are the affinity parameters of the large pore and narrow pore phases, φ is the parameter accountable for degree of transition (pore opening), m is the mean of the normal distribution which represents the critical pressure (P_c) and s is the standard deviation of the normal distribution.

2.8 Arrhenius Equation

Temperature plays a major role in influencing equilibrium during an adsorption process. In order to analyze the effect of temperature dependency of crystal phase transition, a logarithmic form of the Arrhenius equation represented by equation 2.8.2 was used.

$$k = Ae^{-E/RT}\ ^{21} \qquad 2.8.1$$

Equation 3.8.1 is the well-known Arrhenius equation where k is the ration of forward and backward rate constants, A is the pre-exponential factor, R is the universal gas constant, T is the temperature and E is the activation energy.

$$\ln k = \ln A - \frac{E}{R}\left(\frac{1}{T}\right) \qquad 2.8.2$$

The above equation has the form of a straight line i.e. $y = mx + c$ where x represents T^{-1}. A plot of ln k versus T^{-1} (also known as Arrhenius plot) gives a straight line whose slope and intercept are used to determine E and A. In this work, ln k is replaced by $\ln(\delta)_{Pc}$ and a similar Arrhenius plot is obtained (detailed discussion in chapter V). The slope of a line is equal to $(-U/R)$ where U represents the internal energy with unit of energy/solid mass. This ratio is also equivalent to the change in Helmholtz energy (ΔF). At constant temperature and volume (i.e. net adsorption), F and chemical potential (μ) are the same.

CHAPTER III

LITERATURE REVIEW

3.1 Crystal Structure

Loiseau et al., in 2004[10], characterized the crystal structure of MIL-53(Al). According to them, the crystals have three forms i.e. MIL-53(Al)*as* (after synthesis), MIL-53(Al)*ht* (calcined) and MIL-53(Al)*lt* (at room temperature) with same topology as shown in Figure 3.1. The framework is made up of infinite trans chains of corner-sharing $AlO_4(OH)_2$ (via OH group) octahedra interconnected by BDC ligands as shown in Figure 3.2. Hydroxide anions are formed on two oxygen atoms of BDC, which are required to maintain the electroneutrality balance of the structure. These two carboxylate anions of BDC are then connected to two distinct adjacent aluminum cations of the corner sharing $AlO_4(OH)_2$ octahedra. The interatomic distances for Al-O in an octahedra are typically in the range of 1.82 -2.00 Å. For C-C, C-O and C = C of the BDC ligand, the distances range from 1.43-1.51Å, 1.39-1.23Å and 1.35-1.46Å respectively. Depending on the nature of the inserted molecules, 1D channels with different pore sizes are generated as a result of these connection modes throughout the framework. It is also responsible for the large breathing effect.

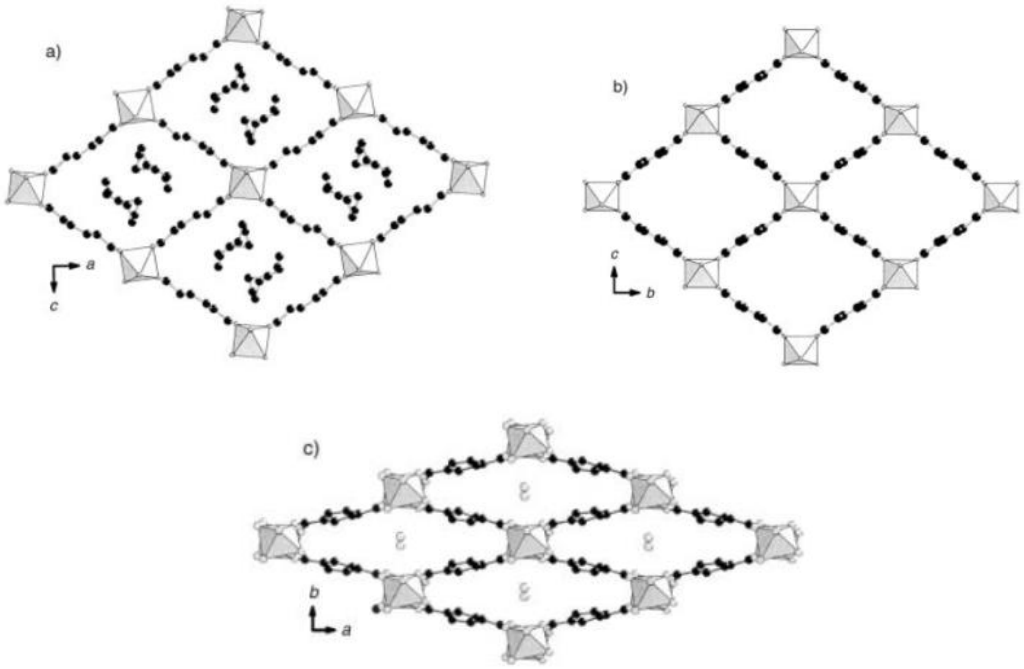

Figure 3.1 Views of the 3D structure of MIL-53(Al) showing the channel system: a) $Al(OH)[O_2C\text{-}C\text{-}C_6H_4\text{-}CO_2H]_{0.70}$ or MIL-53(Al)*as*, in which the channels are occupied by free disordered 1,4-benzenedicarboxylic acid molecules; b) calcined form, MIL-53(Al)*ht* or $Al(OH)[O_2C\text{-}C\text{-}C_6H_4\text{-}CO_2]$ with empty channels; c) room temperature form, MIL-53(Al)*lt* or $Al(OH)[O_2C\text{-}C\text{-}C_6H_4\text{-}CO_2]$. H_2O in which a water molecule is located at the center of the channel. Gray octahedra: $AlO_4(OH)_2$; black circles: carbon; gray circles: oxygen [10].

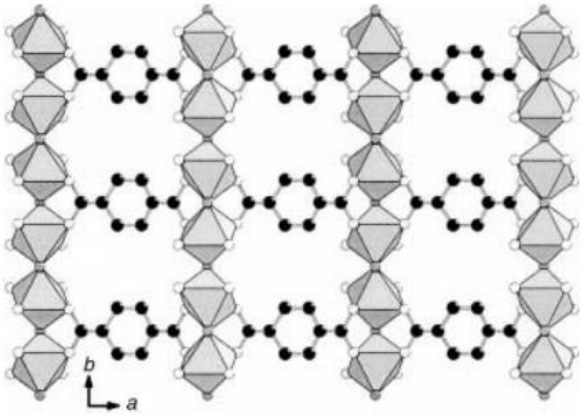

Figure 3.2 View of the infinite chains of corner-sharing octahedral AlO4(OH)2 units connected through the 1,4-benzenedicarboxylate ligands; gray circles indicate the hydroxyl groups bridging the aluminum atoms [10].

In MIL-53(Al)*as* form, the pores are filled with BDC ligand molecules in their protonated form with pore dimensions of 7.3 x 7.7$Å^2$. In order to unblock the channels, synthesized sample is calcined overnight at about 548-553K which yields a high temperature form of MIL-53(Al)ht with pore dimensions of 8.5 x 8.5$Å^2$. On adsorption of one H_2O molecule per aluminum at room temperature, it forms a pair of hydrogen bonds between the hydrophilic part i.e. quadrupole of aromatic ring and water although the walls of the channel are hydrophobic in nature. This significantly changes the pore dimensions to 2.6 x 13.6$Å^2$ as shown in Figure 3.1c.

3.2 Structural Transformation in MIL-53(Al)

A more complicated system evolves when CO_2 is involved. Mishra et al. in 2013, described the structural transition caused by CO_2. The process involves activating the sample by subjecting it to high temperature of 493K. This yields a lp structure (shown in Figure 3.3). The pore conformation is retained even after the sample is cooled to experimental/room temperature (293 K). On exposing the activated sample to CO_2 at low pressure of about 1 bar, it undergoes a transition from lp to np phase. The sample remains in np pore conformation up to 4.5 bar. The framework then goes through a second transition as it slowly starts opening i.e. transitioning from np back to lp phase between 4.5 – 10 bar CO_2 pressure range. At high pressure (10 bar and beyond), the sample is completely in lp conformation. As depicted in Figure 3.3, the structure undergoes a reverse transformation on complete CO_2 desorption at room temperature or any other experimental temperature. However, the sample stays in lp conformation for other desorbing gas.

In order to tune the sample back to large pore conformation after desorbing other gases, they suggested two ways: (a) by activating (heating) the sample again after

completely desorbing from high pressure or (b) by first adsorbing and then desorbing the sample with CO_2 at sub atmospheric pressures as shown in Figure 3.3.

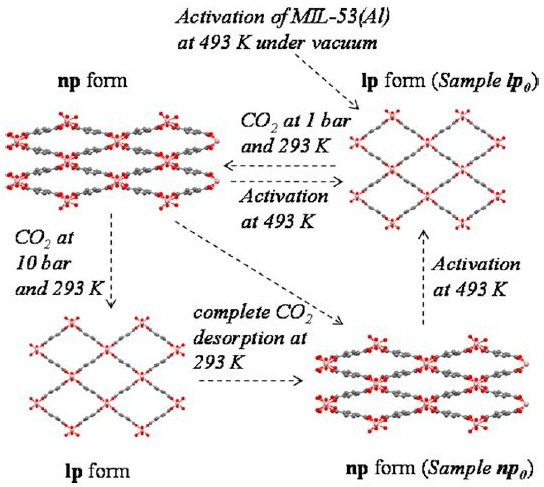

Figure 3.3 Structural transformation in MIL-53(Al) [14]

3.3 Effect of History

In 2013, Mishra et al. also reported a procedure which demonstrated that the adsorption capacity of MIL-53(Al) is dependent on the history of the material. The group measured CO_2 adsorption isotherm at 293k on activated sample in lp phase [denoted as lp_0 in Figures 3.4 (a, b)]. The sample underwent a similar structural transition as explained in the previous section which is exhibited by the isotherm.

However, a hysteresis was seen in sub-atmospheric pressure region which attributes to difference in structure during adsorption and desorption.

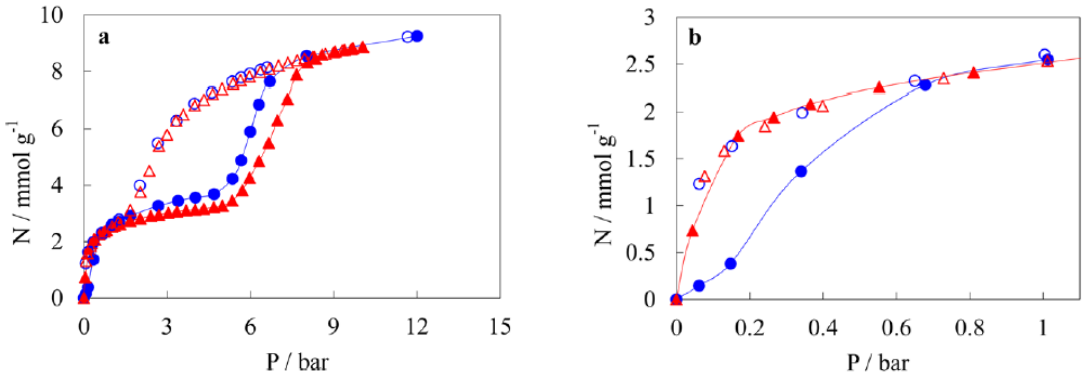

Figure 3.4 (a) CO_2 isotherm at 293K on different structures of MIL-53(Al). (b) Enlarged portion of the isotherms in the low-pressure region. Blue filled circles represents adsorption on sample lp_o; blue open circle represents desorption on sample lp_o; red filled triangle represents adsorption on sample np_o; red open triangle represents desorption on sample np_o [14].

On adsorbing CO_2 again on the sample which was now in the np phase (represented by np_0), the isotherm was different compared to isotherm measured when sample was in lp_0 phase. One can notice from the figure that the uptake capacity on sample np_0 was higher than on sample lp_0 and matched with desorption branch on lp_0. This increase in the CO_2 loading capacity on sample np_0 was a result of large Henry constant of np phase. Since the sample np_0 was already in the narrow pore domain, lp to np transition was absent and the hysteresis below 1 bar disappeared. Beyond this pressure, Other characteristics of the adsorption isotherm were like isotherm on sample lp_0, the only difference being in the adsorption capacity.

3.4 Breathing Behavior in MOFs

Bourrelly et al in 2005[22] studied the adsorption of CO_2 and CH_4 at 304K on MIL-53 (M = Cr, Al) and its isostructural Vanadium^{4+} analogue, MIL-47 using direct calorimetric measurements which give useful information about the energetic nature of adsorbents which could be used to characterize adsorption sites. The chemical formula of the metal-benzenedicarboxylate MIL-53 is $M(OH)(O_2C\text{-}C_6H_4\text{-}CO_2)$ where M denotes the trivalent chromium14 or aluminum15. The corner-sharing μ_2-OH groups of

MIL- 53 are replaced by μ_2-oxo groups in MIL-47 to give a chemical formula of $V^{IV}O(O_2C\text{-}C_6H_4\text{-}CO_2)$. The striking feature of the adsorption isotherms obtained with both MIL-53 samples for CO_2 was the presence of step at around 6 bar. However, the step was absent for CH_4 isotherms on both MIL-53 (Cr and Al) as shown in Figure 3.5. The significant step was attributed to the role of permanent dipole moment (- 1.4 x 10^{-35} C.m) of CO_2 in the adsorption process.

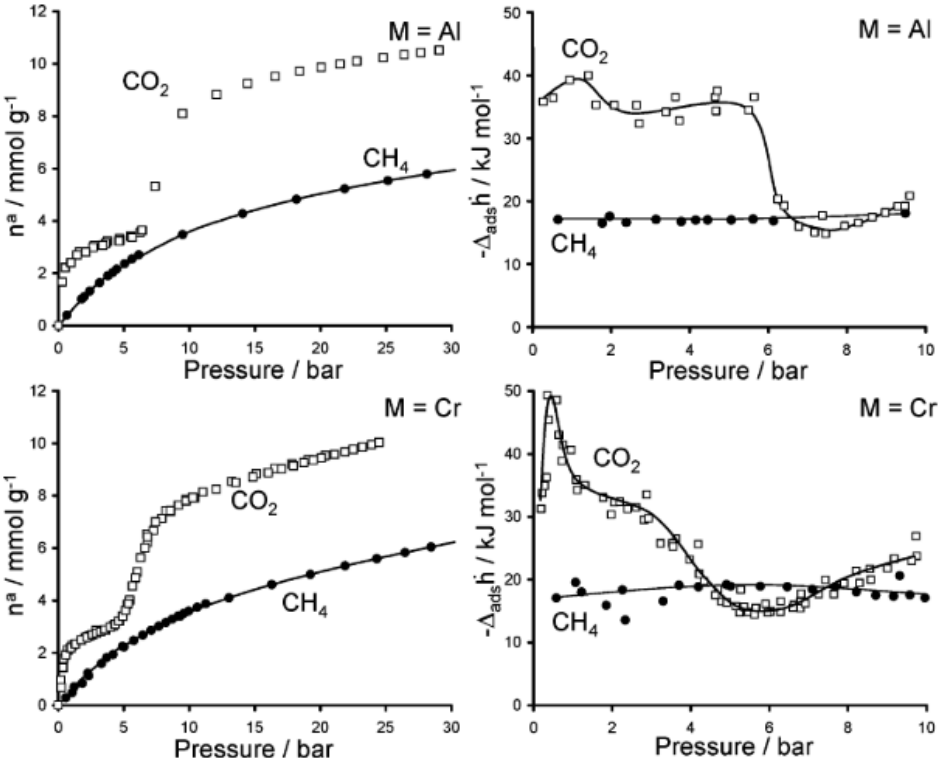

Figure 3.5 Isotherms (left) and differential enthalpies (right) at 304K for the adsorption of CH_4 and CO_2 MIL-53(Al) (top) and MIL-53(Cr) (bottom) [22].

In order to understand the reasons behind this unusual breathing behavior, isotherms and corresponding pseudo differential enthalpies for both the gases were compared. The adsorption enthalpies for CH_4 were found to be relatively constant at about 17 kJmol^{-} for both the samples throughout the pressure range. However, in case of CO_2 on MIL-53(Al), it is around 35 kJmol^{-}during pore filling (around 6 bar) followed by a sharp decline. The curve showed a distinct peak during initial adsorption

before a region at 32 kJmol⁻ in case of chromium containing sample followed by a similar decline. It was hypothesized that the CO_2 probe molecules interacted with specific adsorption sites (i.e. metallic centers) before completely filling up the pores. Also, the initial shrinkage in pore volume on gas adsorption upon activating the sample was assumed to be a consequence of the interaction between the probe molecule and the OH group of the framework.

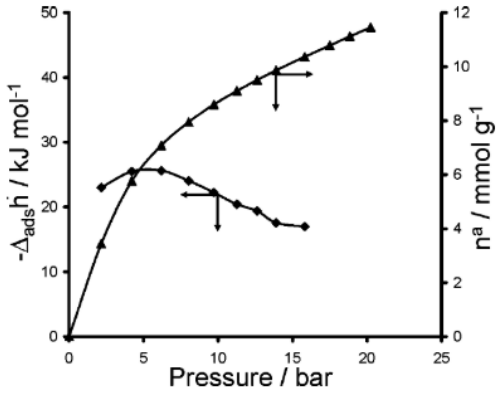

Figure 3.6 Isotherm (triangle) and differential enthalpies of CO_2 adsorption (square) at 304 K on MIL-47 (V) [22].

In order to verify the hypothesis, the CO_2 isotherm were obtained on MIL-47(V). As shown in Figure 3.6, a distinct step was absent. This result confirmed that the distinct step observed during CO_2 adsorption on MIL-53 was due to the presence of interaction between the probe molecule and OH group.

3.5 Parameters Affecting Adsorption

Rallapalli et al. in 2010[23], studied adsorption of various industrially important gases like CO_2, CH_4, CO, N_2, O_2 and Ar on MIL-53(Al) at 288K and 304K upto 1 bar. The authors calculated Henry's constant, heat of adsorption in the low-pressure region and adsorption selectivity's based on the adsorption isotherms (see Table 1 below). The absolute adsorption capacity followed an order of $CO_2 > CH_4 > CO > N_2 > Ar > O_2$. The difference in adsorption behavior and adsorption capacity of CO_2 compared to

other gases as shown in Figure 3.7 was explained based on the molecular size and quadrupole moment of the adsorbate described by Bourrelly et al., 2005. Although, probe molecules of CO, N_2 and O_2 possess significant quadrupole moment, their adsorption capacities were found to be less compared to CH_4 with high polarizability. Adsorption capacity of Ar was less than methane inspite both being spherical molecules because, polarizability of Ar is much lower than CH_4.

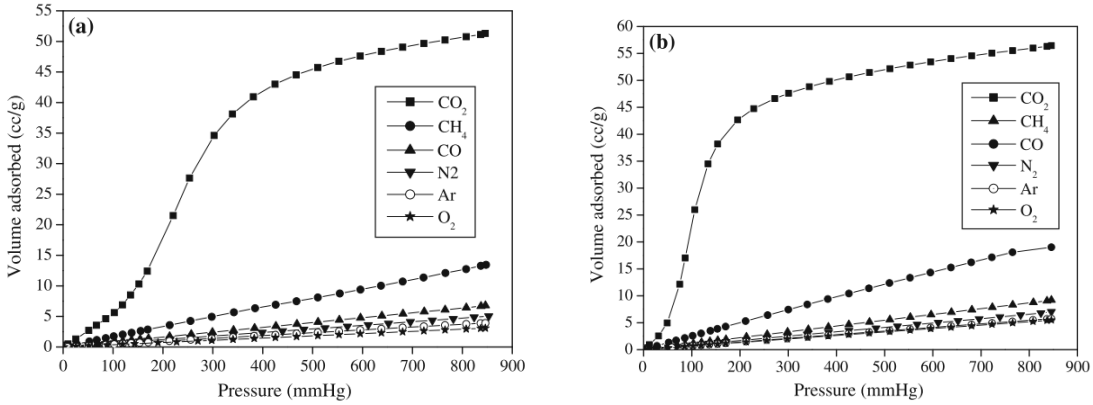

Figure 3.7 Adsorption isotherms of CO_2, CH_4, CO, N_2, Ar and O_2 on MIL-53(Al) (a) at 303 K up to 860 mmHg and (b) at 288 K up to 860 mmHg [23]

Table 1 Adsorption capacity, quadrupole moment, polarizability, henry constant and heat of adsorption of the adsorbate gases on MIL-53(Al)[23].

Adsorbate gas	Volume adsorbed (cc/g)		Quadrupole moment ($\times 10^{40}$ cm^2)	Polarizability ($\times 10^{-25}$ cm^3)	Henry's constant (cm^3/g mmHg) $\times 10^{-2}$	Heat of adsorption in Henry's region (kJ/mol)
	288 K	303 K				
CO_2	56.5	51.3	−13.71	29.1	4.0	26.4
CH_4	19.9	13.5	0.00	25.9	1.77	18.3
CO	9.2	6.8	−6.92	19.5	0.79	16.4
N_2	7.1	5.1	−4.91	17.4	0.63	15.9
Ar	5.8	3.9	0.00	16.4	0.46	15.1
O_2	5.5	3.1	−1.33	15.8	0.45	14.5

The polarizability followed an order of CO_2>CH_4>CO>N_2>Ar>O_2 (see Table 1). Though there is a significant difference in the quadrupole moments of N_2, O_2 and Ar, their polarizabilities are almost similar. As a result, the uptake capacity of these gases on MIL-53(Al) is the same. Thus, the isotherms shown in the above figures follow the order of polarizability rather than their quadrupole moment.

The Henry's law constants (b) were calculated using a Virial isotherm method provided by Himeno et al. 2006 and Peter et al. 2005. Henry's constant helps to determine interaction between sorbate molecule and adsorbent surface at infinite dilution. Since the adsorbate-adsorbent molecules are dispersive in nature, the extend of adsorption depend on these interactions. In other words, higher value of b for an adsorption process, indicates a steep isotherm. The isotherms follow a similar trend in the figures above.

3.6 Modeling Flexible Framework behavior

3.6.1 Stress Model. In 2010, Neimark et al.[5] proposed a stress model to describe the structural transformation exhibited by MIL-53(Al) because of adsorption induced stress (σ_s). The adsorption stress (σ_s) is evaluated by taking a derivative of the thermodynamic grand potential ψ of the adsorbed phase per unit cell with respect to the unit cell volume V_c at constant temperature T and adsorbate chemical potential μ.

$$\sigma_s\,(V_c) = -\left(\frac{\partial \psi}{\partial V_c}\right)_{\mu,\,T} \qquad 3.6.1.1$$

The model states that the magnitude of frameworks elastic deformation in terms of volumetric strain ε ($\varepsilon = \Delta V_c / V_c$, where ΔV_c is the variation of the cell volume) is determined by solvation or disjoining pressure P_s assuming linear Hooke law with an effective framework bulk modulus K. Solvation pressure (P_s) is defined as the difference between adsorption stress, σ_s, and the external pressure.

$$P_s = \sigma_s - p_{ext} = K\varepsilon + \sigma_o \qquad 3.6.1.2$$

σ_o is the pre-stress in the reference state at which the cell volume V_c is defined.

The model hypothesizes that the structural transition occurs when the solvation pressure approaches a certain critical stress σ^* which the framework cannot resist. The critical stress associated with lp to np transition (σ^*_{lp}) should be negative because the framework undergoes a contraction, while the critical stress associated with np to lp

transition (σ^*_{np}) should be positive as a result of framework expansion. Another important aspect of this model is that critical stress depends on crystal size. Later this fact is used to postulate a normal distribution of crystal sizes around a mean which in turn relates to a distributed transition pressure. The model was tested with low temperature xenon adsorption which shows a similar breathing behavior to CO_2 in Figure 3.8 below.

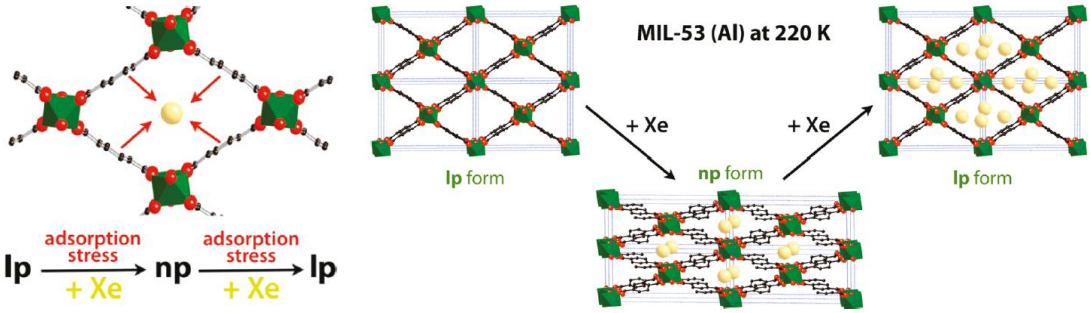

Figure 3.8. Schematic representation of the breathing phenomenon of MIL-53 (Al), exhibiting two successive structural transitions upon adsorption of some gases (here, Xe at 220 K). The two possible states of bistable MIL-53 (Al) are called np (narrow pore) and lp (large pore).[5]

In this study, Langmuir equations were used in the further development of the stress model. The adsorption stress was calculated directly by invoking the general integral relationship between the grand thermodynamic potential and the adsorption isotherm.

$$\psi(P^0) = -RT\int_0^{P^0} N(P^0)d(\ln P^0) = -RTN_{max}\ln(1 + bP^0/N_{max}) \qquad 3.6.1.3$$

In the above equation, N_{max} is the unit cell capacity and b is the Henry constant. From equations 3.6.1.1 and 3.6.1.3, adsorption stress as a function of vapor pressure was expresses as shown in the following equation:

$$\sigma_s(P^0) = RT\left\{\frac{dN_{max}}{dV_c}\left[\ln(1 + bP^0/N_{max}) - \left(\frac{bP^0/N_{max}}{1+ bP^0/N_{max}}\right)\right] + \frac{db}{dV_c}\left(\frac{P^0}{1+bP^0/N_{max}}\right)\right\} \qquad 3.6.1.4$$

The quantity dN_{max}/dV_c is positive while db/dV_c is negative in the above equation. This gives rise to a nonmonotonic variation in the adsorption stress and solvation pressure.

3.6.2 Osmotic Ensemble. Coudert et al. in 2008[26] proposed a model based on osmotic ensemble to rationalize the thermodynamics of adsorption in flexible frameworks when guest-induced structural transitions of the host are involved. The osmotic ensemble is an extension of the grand canonical ensemble that accounts for the presence of a flexible host material with variable unit cell volume. The group proposed an expression for the osmotic potential represented by equation 3.6.2.1:

$$\Omega_{os}(T, P^0) = F_{host}(T) + P^0V - \int_0^{P^0} N\,(T, P^0)\,\frac{RT}{P^0}\,dP^0 \qquad 3.6.2.1$$

The equation can be used to evaluate the potential of the host phases (np and lp in case of MIL-53(Al)). The three key parameters involved in the expression are: the free energy (Helmholtz energy) of the solid (F_{host}), the amount of gas adsorbed (N) as a function of temperature (T) and pressure (P^0) and the molar volume of pure fluid expressed as the ratio of the product of gas constant (R) and temperature (T) over pressure (P^0). The comparison of Ω_{os} for each host phase allows to determine relative stability of the phases, the number of structural transitions that will occur and the pressure at which they occur for a given crystal size.

Among the parameters involved, the prediction of the relative free energies of the solid phases $\left(F_{host}^{(i)}\right)$ is very difficult to evaluate experimentally and by simulation methods compared to other two parameters. But the difference in two forms of the solid can be determined from absolute properties. For that reason, the group proposed a method to determine the relative free energy of solid phases $\left(F_{host}^{(i)}\right)$ from readily available experimental quantities like the phase transition pressure and the amount of

fluid adsorbed. The method involved analysis of the experimental adsorption isotherms for each phase and the transition pressure to determine Helmholtz free energy difference between the host structures. According to this method, the osmotic potentials (Ω_{os}) of both the phases must be equal at transition pressure which can be determined from experimental adsorption and desorption isotherms. However, when Neimark's stress model is combined with osmotic ensemble results, the transition pressure is unique for a fixed crystal size. Also, the authors proposed to obtain the rigid-host isotherms for each phase: these phases correspond to each of the solid phases assuming no transition over the entire pressure range (see Figure 3.9). In order to solve this problem, they proposed fitting the distinct parts of a stepped isotherm to obtain full rigid host isotherms needed for each phase.

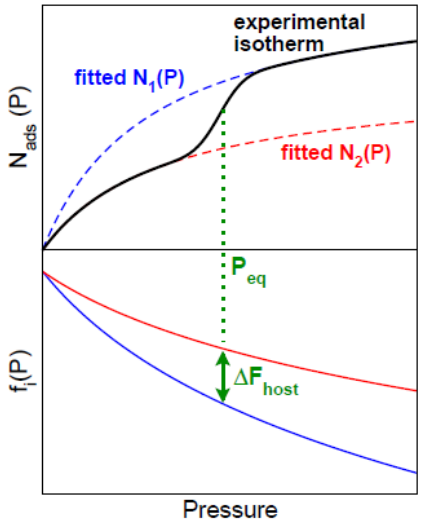

Figure 3.9. Schematic representation of the determination of free energy difference ΔF_{host} from an experimental adsorption isotherm (upper panel) by calculation of $f_i(P)$, the pressure-dependent part of the thermodynamic potential of the osmotic ensemble (lower panel)[26].

This gives a way to calculate the free energy difference between the host phases using the following equation:

$$\Delta F_{host} = RT \sum \int_0^{P_{trans}} \frac{\Delta N_i(T,P^0)}{P^0} dP^0 - P_{trans}\, \Delta V_{host}\ ^{26} \quad 3.6.2.2$$

ΔF_{host} is the free energy difference between the host phases, ΔV_{host} is the difference in volume of two host phases (i.e. np and lp phase), P_{trans} is the pressure at which transition occurs, ΔN_i is the difference in the amount of species (i) adsorbed between two phases and R, T represent temperature and ideal gas constant respectively. The group also identified three distinct cases for framework with two metastable phases (lp and np):

Case 1: If the pore volume of the second phase (V_p^2)is greater than the starting phase (V_p^1), then irrespective of the values of b_1, b_2, only one transition will occur. Starting phase will be favored at low pressure and as pressure is increased, second phase with large accessible pore volume will be more favorable resulting in a transition.

Case 2: If $V_p^1 > V_p^2$ and $b_1 > b_2$: No transition will occur because all the factors favor starting phase. This is because the empty structure has low free energy, high affinity and high pore volume.

Case 3: If $V_p^1 > V_p^2$ and $b_2 > b_1$: Two different behaviors are observed. At low pressure, starting phase is favored. At high pressure, it is also favored because it has high pore volume. However, in between, there might exist a regime where second phase is thermodynamically favored because of higher affinity. This results in two successive structural transitions (as seen in case of CO_2).

CHAPTER IV

MATERIALS AND METHODS

The adsorption characteristics of narrow pore and large pore conformations of MIL-53(Al) were studied by measuring pure component adsorption isotherms of N_2, O_2, CH_4 and CO_2. These isotherms were measured gravimetrically. The sample used in this thesis was synthesized using hydrothermal method. It was characterized using thermogravimetric analysis (TGA) and Brunauer−Emmett−Teller (BET) surface area analysis.

4.1 Synthesis

The MIL-53(Al) sample used in this study was synthesized using a hydrothermal process suggested by Loiseau et al. in 2004. Materials used for synthesis were aluminum nitrate nonahydrate ($Al(NO_3)_3.9H_2O$), 1-4 benzene dicarboxylic acid (BDC), dimethylformamide (DMF) and deionized water. Aluminum nitrate, BDC and deionized water were used in a molar ratio of 1:0.5:80 and mixed together. The mixture was then transferred to a batch reactor with a removable Teflon® liner. Once sealed, the reactor was then placed in a pre-heated oven at 493K for approximately 72–75 hours. At the end of heating, the batch remained in the oven until it cooled to room temperature.

The resulting product was then centrifuged in DMF. It was mixed with excess amount of DMF in a 2-liter conical flask. The setup was then placed in a large beaker containing steel balls which acted as a heat bath. To ensure uniform heat distribution, a magnetic stirrer was introduced in the mixture and the entire assembly was placed on a heating plate. The batch was heated at 423K overnight in a furnace head to remove unreacted BDC. It was then cooled and washed three times with 300ml of methanol each time to replace DMF in the pores and calcined at 453K overnight in an oven. The batch produced about 11g of MIL-53(Al) sample.

4.2 Characterization

MIL-53 sample was characterized using TGA and BET analysis.

4.2.1 Thermogravimetric Analysis (TGA). The TGA analysis of MIL-53(Al) was done in a Mettler TOLEDO (model no. TGA/SDTA 851e) thermogravimetric analyzer. The temperature was ramped up from 298K to 853K at the rate of 5 K min^{-1} under a nitrogen atmosphere. The result is shown in the figure below:

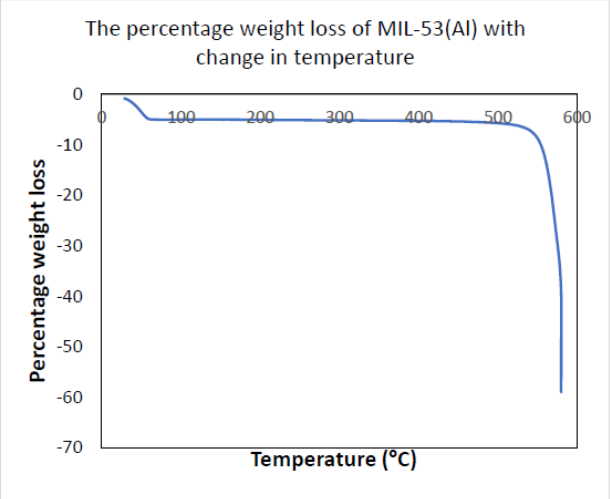

Figure 4.1 Thermal stability of MIL-53(Al) [27]

The initial weight loss at low temperature was a result of loss of water molecules from the pores. The solid maintains its weight up to about 540°C (813K) as depicted in the figure. The drastic weight loss beyond this temperature was attributed to the

collapse of BDC linker which is holding the structure together. This result shows that MIL-53(Al) has a high thermal resistance.

4.2.2 BET Surface Area Analysis. A micrometric ASAP 2010 was used for surface area analysis by carrying out a nitrogen physisorption at 77K. The sample was degassed at 493K for about 4 hours prior to nitrogen physisiorption. Brunauer−Emmett−Teller (BET) model and a relative pressure (P/P0) range of 0.03 – 0.3 was used for calculating the surface area. A pre-determined relative pressure of 0.98 was used for calculating the pore volume. The BET surface area and pore volume were estimated to be 1284 m^2/g and 0.64 cm^3/g respectively, which are in agreement with the previously reported values[27].

4.3 Isotherm Measurements

The Rubotherm magnetic suspension balance was used to collect isotherm data of different gases. Data is collected during the process by a computer data acquisition system and is displayed systematically on the computer screen.

4.3.1 Rubotherm System Schematics. Schematic is shown in Figure 4.2. The entire system is divided into three sections. First is the feed section along with bypass (also called as manifold) where gases of interests are fed into the system. The gas lines have needle valves (NV1-NV3) attached to limit the flowrate of gas going into the system. The type of gas feed into the system is controlled by the switch valves V1, V2 and V3 are at the gas inlet to choose between gases. Gases used in this study are nitrogen (Grade 5.0, >99.999%), carbon dioxide (Grade 4.4, >99.99%), helium (Grade 4.7,>99.997%), Oxygen and Methane (Grade 4.0), which are all stored in compressed gas cylinders. Next is the adsorption section comprising of the balance containing known amount of sample enclosed in an adsorption chamber. This section can be isolated from the system using valves V5 and V7 which act as the inlet and the outlet

to the adsorption chamber as shown in the figure. Finally, the exit section which lies below the chamber made up of vent and vacuum lines. Bypass along with valve V6 links all the sections together. All the gas can be forced through the balance (whenever needed) only if the bypass is closed. It is closed during activation and equilibrium steps. During other steps however, bypass provides the way to flow gases through the system when the balance is isolated. A large tank is attached to the system to prevent from over pressurizing the experimental setup because of its small volume since it is made up of stainless-steel pipes of 1/4th inch diameter.

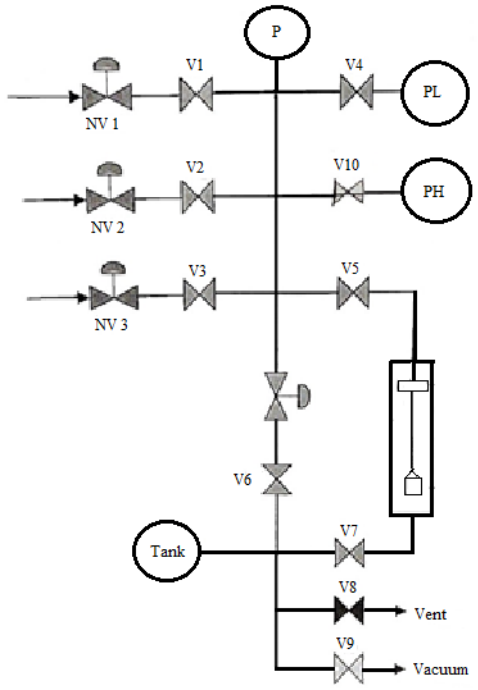

Figure 4.2 Schematic of experimental setup.

Valve V1 is always connected to the Helium gas cylinder while valves V2 and V3 can be attached to other gas cylinders interchangeably. Gas flow to the low pressure and high-pressure transducers is controlled by valves V4 and V10 respectively. Bypass is connected to the manifold via valve V6 and the flow is controlled by a needle valve.

Valves V5 and V7 control the inlet and outlet of adsorption section. A vacuum pump is connected at the bottom of the manifold to allow for vacuum pressure in the

system during degassing. It is connected to a switch valve (V9) which can take it offline from the system. A vent line controlled by valve V8 is provided to vent out high pressure from the system until the pressure is close to atmospheric pressure before turning on the vacuum pump. This is done to protect the pump.

Figure 4.3 shows a schematic diagram of the balance (Following detailed description is taken from Weireld et.al 1999 study of "Automated determination of high-temperature and high-pressure gas adsorption isotherms using a magnetic suspension balance"). The crucible (C) containing the adsorbent sample is suspended from a permanent magnet (PM) by a coupling system (CS). The whole system is in an adsorption chamber (AC) kept at the experimental conditions (temperature, pressure, adsorbate). The permanent magnet is kept in a suspension state with an external electromagnet (EM) which hangs from the hook of an analytical balance (AB). The balance and the electromagnet are completely disconnected from the adsorption chamber. The balance and the upper part of the electromagnet are at ambient conditions. The lower part of the electromagnet, although it is not in the adsorption chamber, is at the experiment temperature. The force change due to mass uptake during the adsorption process is transmitted from the adsorption chamber to the analytical balance due to the magnetic suspension (coupling of the permanent magnet and electromagnet). The position of the permanent magnet is kept constant by a regulation system including the sensor core (SCR), the sensor coil (SCL) which detects the position of the permanent magnet and the PID controller which regulates the position of the magnet by changing the current input to the electromagnet. The force transmitted to the analytical balance by the permanent magnet is equal to the force exerted on the permanent magnet since, its position is constant. This force is a result of weight change. Figure 4.4 represents the pictorial representation of the Rubotherm balance.

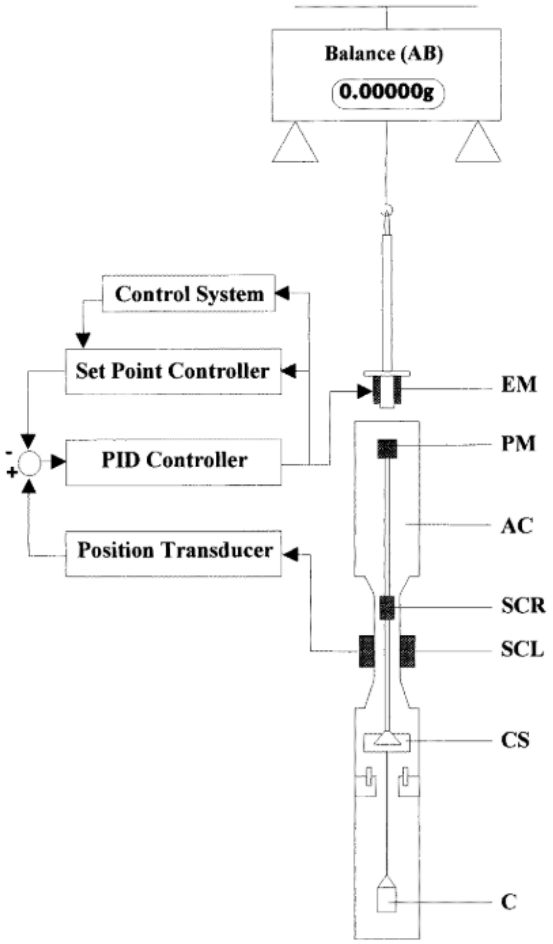

Figure 4.3 The magnetic suspension balance: AB, analytical balance; AC, adsorption chamber; C, crucible; CS, coupling system; EM, electromagnet; PM, permanent magnet; SCL, sensor coil; SCR, sensor core. [28]

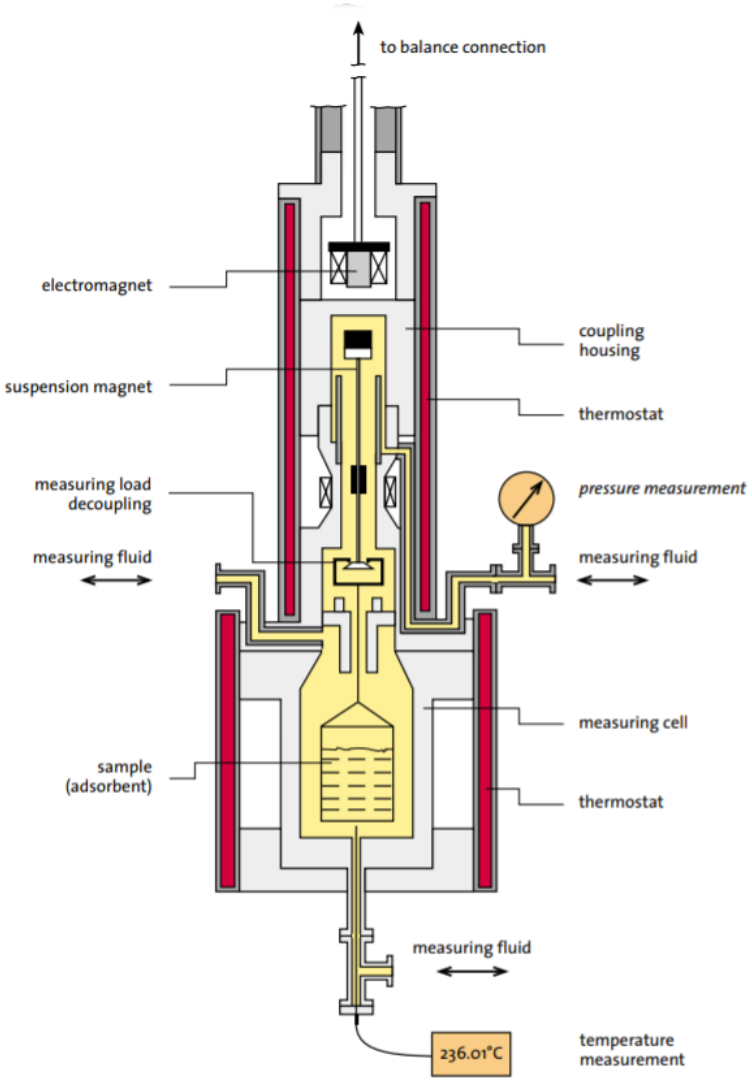

Figure 4.4 The Rubotherm Magnetic Suspension Balance [29].

4.3.1.1. The magnetic coupling system. The magnetic suspension balance offers the possibility of lifting the suspension magnet in a controlled way to three measuring positions viz zero point (ZP), measuring point 1 (MP 1) and measuring point 2 (MP2) as shown in Figure 4.5.

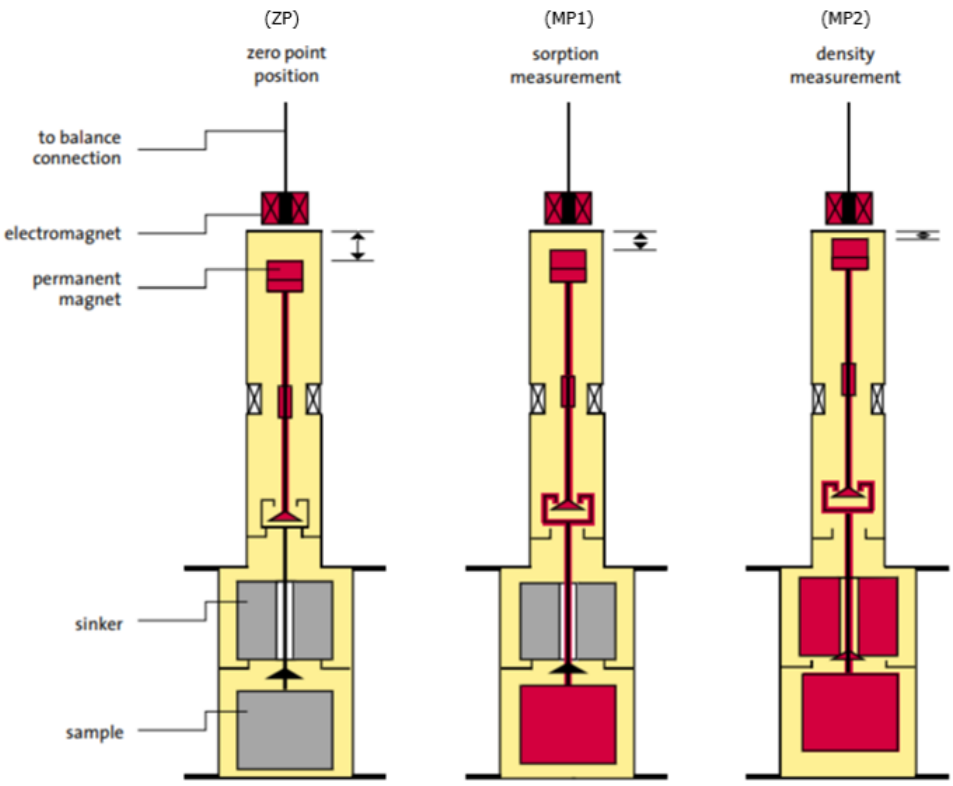

Figure 4.5 Three measuring positions [29].

While in first position i.e. ZP, the permanent magnet is freely suspended and only its weight is transmitted to the analytical balance. During this step, both the sample and sinker (made of titanium with a known mass of 19.5963 gm and volume of 17.0551 cm^3 used for buoyancy correction measurements) are decoupled from the permanent magnet. This position allows calibration and taring of the balance even during an experimental run. In second position i.e. MP1, only the sample is lifted by the permanent magnet which allows measuring its weight under experimental conditions. Finally, in the MP2 position, both the sinker and sample are lifted and weighed together. The buoyancy correction measurements obtained from sinker allows for the measurements of gas density under experimental conditions. These corrections are vital for adsorption calculations at high pressure where equations of state are not reliable.

4.3.2 Rubotherm Instrumentation, Process Control, and Data Collection

There are two types of valves used in the system, needle valve and pneumatic valve. The needle valves are used to manually limit the flow of gas into the system in order to prevent large pressure waves. The pneumatic valves can be switched on/off by solenoid coils which are controlled either manually or by a computer program. The computer provides automated control of the pneumatic valves through a programmed repeated sequence of events in which the valves open and close at different pressures to create a process. It is located on a controller switch board that contains fourteen manual switches that put the valves in manual, computer, or off mode. The mode is determined by the position of switch on the controller switch board. The up position represents control to the controller, the middle position switches the valves off while, the down position puts them into manual control.

Four pressure transducers are used in the system for accuracy reasons. Three of which are placed on the inlet manifold as shown in Figure 4.2. The first is an MKS transducer represented by PL which is a 1000 torr gauge isolated by valve V4 at higher pressures. It is used to measure sub atmospheric pressures. Next is a Sensotec transducer (model GM) represented as PH. It is a 100 psia gauge isolated by valve V10. Finally, the Omega transducer represented as P. This is a 500 psia gauge not controlled by any valve. In addition, a Themovac TM23 pressure guage (not shown in the figure) connected to the vacuum manifold is also used to check vacuum level.

Temperature during the process is measured using three thermocouples. One of which is on the outside to measure ambient temperature. A digital Omega temperature controller is used to read this temperature. Other two thermocouples are inside the adsorption chamber and they measure temperatures of the sample and the chamber. Omega DP20 digital temperature controller reads temperature inside the chamber

while, the sample temperature is displayed on a Rubotherm JUMO IMAGO 500 temperature controller (not shown in the schematic). The temperature controller (JUMO IMAGO 500) is a ramp soak single output Solid State Relay (SSR) control action controller, with dual alarms manufactured by Omega Engineering Inc. It is used for a controlled rate heating during activation process[30]. High temperature activation process is controlled by Rubotherm temperature controller while, the experimental temperature is controlled by an external jacket around the crucible. For the program to proceed to the next data point, the sample and jacket temperatures should be within 2°C. A high precision (up to five decimal points) Rubotherm weighing balance is used to measure the change in weight (in grams) of the sample during the experiment. Since the data collected is used to plot an isotherm, a Fisher Scientific Isotemp Refrigerated Circulator (Model 9500) water bath was used to maintain the temperature at desired experimental temperature.

Data collection from the pressure transducers, thermocouples and the weighing balance is done with a National Instruments SCXI-1000 data acquisition system. Lab Windows software is then used to display the data on a computer. The collected data is stored as a log file which is then analyzed using MS-Excel.

4.4 Experimental Procedure

The experimental procedure is divided into two parts. The first part included preliminary experiments to check for leaks in the system, calibration of the instrumentation, measurement of volume of the bucket with the sample and activation of the sample used. The later part is the measurement of actual isotherm data.

4.4.1 Preliminary Experiments. It was necessary to determine if the system had any leaks that would affect the experiment. The basic method used was to fill the system with Helium at a high pressure (50 – 60 psia) and observe the reading on the

transducers over a period. The pressure drop was found to be negligible over experimentally relevant time i.e. several hours.

All the instruments on the system were calibrated and zeroed before carrying out any experiments. The pressure gauges used were zeroed with the help of a vacuum pump and an external McLeod gauge. Temperature controllers were calibrated using a water bath and standard mercury thermometers.

Weights of the crucible, glass wool, glass fiber sheet and wire mesh (chrome Al) were measured using high precision Mettler Toledo (Model number MS 204S) weighing scale. During the later stages of experiments, crucible, glass wool and wire mesh were replaced by wire mesh bucket and glass fiber sheet. Next, the volume of empty crucible along with wool and wire mesh was determined by N_2 expansion in the first stage and later the volume of empty mesh bucket and glass fiber was determined using the same method. The sample is not present in the system at this step to measure buoyancy volume of balance parts.

The final preliminary test conducted was the activation of two different aliquots of same synthesis batch of 1.574 g and 1.474 g of MIL-53(Al) sample used in the first and later stages of experiments. It is done by heating the sample between 503-523K for at least three to four hours. The temperature is ramped up slowly in order to prevent the sample from experiencing a thermal shock. A continuous flow of Helium at the rate of 50-100 cc/min is maintained to ensure a uniform heat distribution throughout the sample. Throughout the activation process, the adsorption chamber is wrapped up in a glass wool cloth to prevent heat loss to the surrounding. At the end of four hours of heating, the chamber is unwrapped and allowed to cool to room temperature before turning on the water bath to set it to experimental temperature. The entire activation process takes about 7-8 hours. At the end of this process, helium expansion

measurements were conducted to measure the volume of filled crucible and mesh bucket with the sample (see Figures 4.6(a, b)). The slope on these figures gives the volume of the crucible and bucket with sample while, the intercept represents total weight under vacuum.

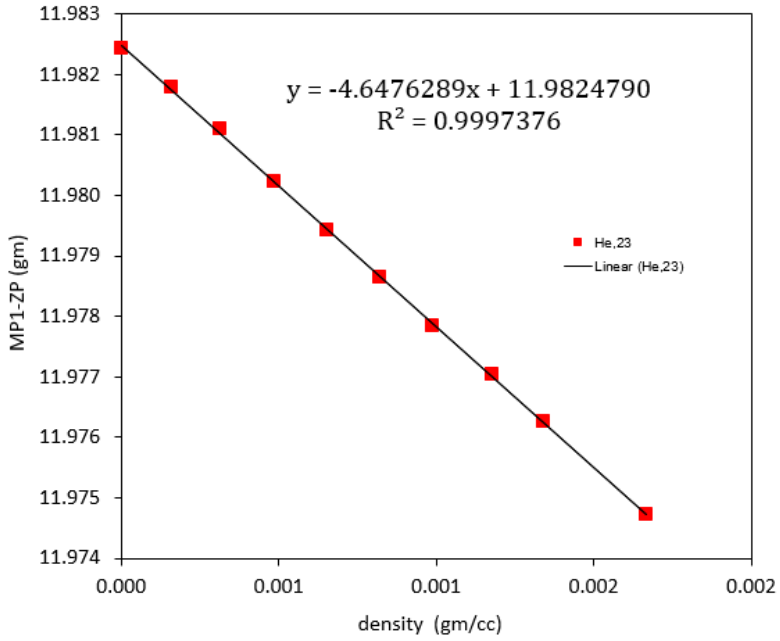

Figure 4.6.a Helium Expansion measurement for sample weighing 1.574 g.

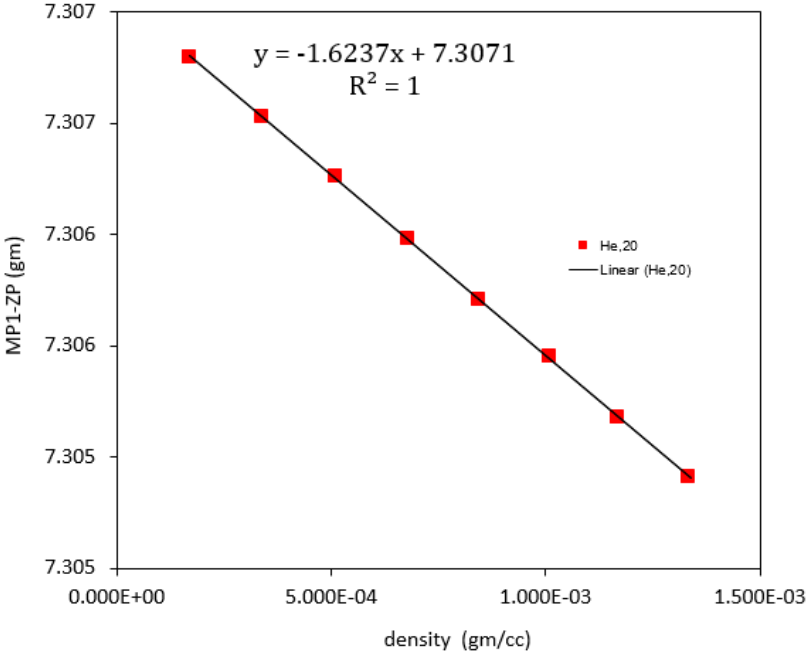

Figure 4.6.b Helium Expansion measurement for sample weighing 1.474 g.

4.4.2 Pure Component Isotherm Measurement. A certain protocol is followed while operating the Rubotherm since it is an automated system. Before logging into Lab Windows/CVI software, an "Instruction file" indicating total number of steps along with marcos modules is prepared. As the name suggests, it provides instructions to the software to perform automated experimental measurements. It is a text file which is prepared using notepad text editor. A macro is a way of performing repeated task automatically on a regular basis. It is a set of commands and actions which takes in "Input" i.e. the control values that must be set (manually or read from an instruction file). Control values involved are P-target, section in the system to be filled with gas of interest, experimental temperature, the gas of interest and equilibration time. A step is a combination of macro along with its control parameters separated by a delimiter comma ",". Macros used throughout the experiments are listed below[30]:

- Idle State- This macro brings the system to an idle state also known as stand-by position.
- Empty_Manifold- Isolates the balance by closing valves V5 and V7 before vacuuming down the rest of the system. The high-pressure transducer (500 psia) monitors the pressure change. This macro is called during the FILL macro if the pressure of the gas in the system is above the target pressure
- Empty_Balance- vacuums down the manifold and the balance section to a specified rate of pressure change. This macro is usually run before starting a new run. The system is set to an idle state after the execution of this macro
- FILL- This macro is used to fill the system with a gas of interest to a specified target pressure by user or by instruction file. Appropriate valves are opened as per section type and gas type. There are three sections first, inlet manifold which includes inlet part up to bypass valve, second section is the inlet manifold and

tank and finally inlet manifold plus balance. Empty_manifold macro is called if the pressure inside the system is greater than P-target before filling the system to target pressure. After the execution of this macro, the balance or the manifold is filled to the target pressure as specified by the user and the system is set to idle condition

- Equilibration- Equilibrate macro is used to obtain isotherm data as per the user specified conditions. This macro determines when equilibrium is attained within the system. It has three options to choose an equilibrium condition viz time equilibrium where system waits for a specified time before taking data, mass equilibrium where the system checks for change in rate of mass over a specified time before proceeding to the next data point and finally pressure equilibrium where system checks for rate of pressure change over a specified time.

Time and temperature are used as constraints to estimate equilibrium in this thesis i.e. the program will not proceed to measure the next data point until the experimental temperature is maintained within the adsorption chamber for a stated time. This sequence is repeated till the end of the experiment. In this study, the isotherms were measured in the pressure range of 0 – 290 psi.

As mentioned earlier, activation process always results in a large pore conformation on the sample. In order to change the pore conformation to narrow pore, sample is charged with CO_2 to a pressure of 60 psi and equilibrated for about 100 minutes. It is then desorbed under vacuum without applying heat until the sample stops degassing. The process described above is used to measure isotherms on both pore phases.

CHAPTER V

RESULTS AND DISCUSSION

5.1 Isotherms

The figures in this chapter show isotherm phase diagrams. All data are shown as points in the figures. The modified Dual Site Langmuir model results are shown as curves. All data is also tabulated in Appendix A.

5.1.1 N_2 Adsorption Equilibria and Data Analysis. Figure 5.1 show adsorption isotherms for N_2 on np and lp phase of MIL-53(Al) at three experimental temperatures. As reported in literature, the isotherm shows some interesting features. In case of adsorption at 279K and at pressure below 3 bar, the uptake capacity of N_2 in np phase is negligible. However, at 293K and 306K, isotherms show some adsorption. This low uptake is because the np form of sample excludes N_2 molecules with a larger kinetic diameter and low adsorption energies [14]. Beyond 5 bars, the isotherm shows a gradual step change and an increase in the adsorption capacity which can be readily attributed to np - lp transition. After a certain pressure (beyond 8 bars) the transition is complete, and the adsorption branch coincides with that on the lp structure. On desorption, hysteresis is observed in all isotherm. Only one transition is observed (i.e. np to lp) on the adsorption branch when starting with np phase. This observation is in agreement with Coudert et al., 2008 who suggested if the starting volume of the pore is

smaller than the final pore volume, only one transition will occur irrespective of the affinities.

In subsequent adsorption on lp form, the sample does not exhibit any structural transition as reported in literature. It stays in large pore phase throughout the pressure range (0 – 30 bar) and does not exhibit any hysteresis on desorption. The uptake capacity increases monotonically with increase in pressure. This is because, the empty large pores have a lower free energy and are thermodynamically more stable at low and high pressures, they have a higher adsorption capacity and higher pore volume [26]. The adsorption behavior of the sample aligns with the distinct cases discussed in section 3.6.2 for framework with two metastable phases.

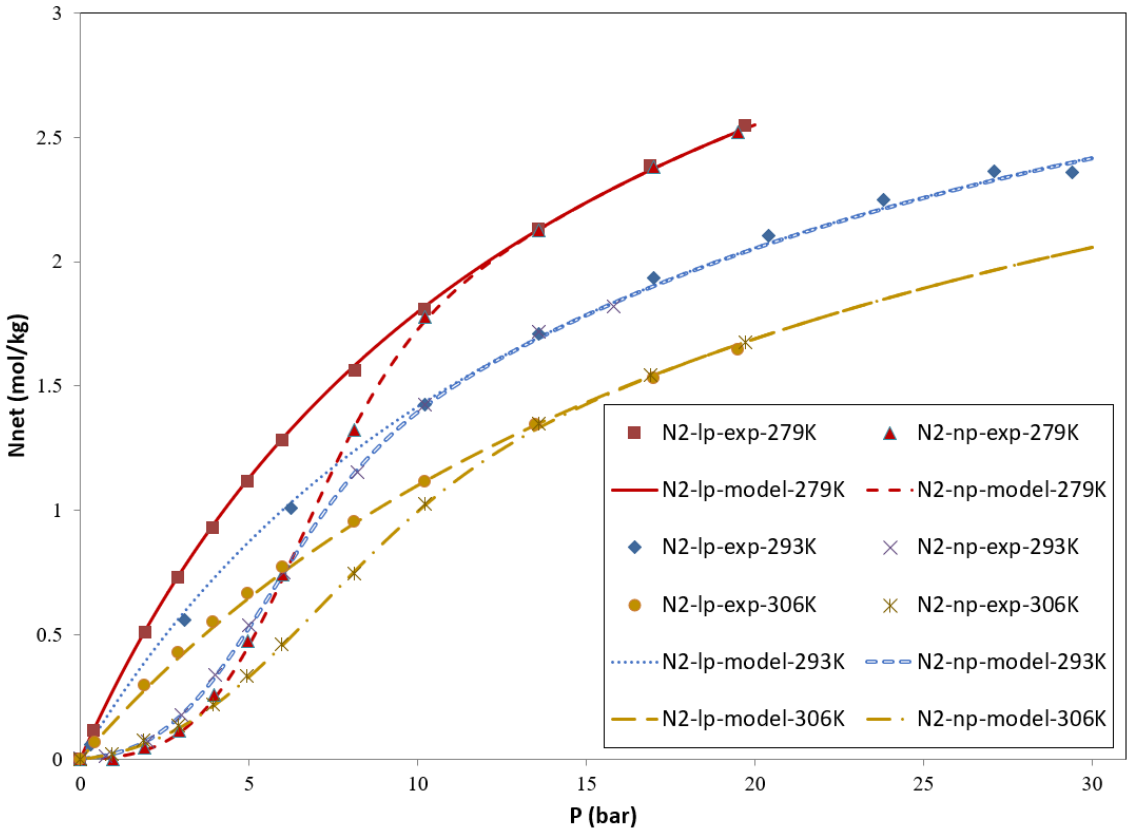

Figure 5.1 Nitrogen pure component adsorption equilibria on np and lp phase of MIL-53(Al) at three experimental temperatures along with model fits.

5.1.2 O_2 Adsorption Equilibria and Data Analysis. Figure 5.2 reported here show adsorption equilibrium isotherms for pure O_2 gas at three experimental temperatures on both np and lp phases. The plot shows similar characteristics like nitrogen, only difference being the amount of oxygen adsorbed is higher. The difference is attributed to molecular size i.e. O_2 is slightly smaller than N_2. It is interesting to note however that, in case of both the gases, transition from np to lp is complete when loading is between 1.0 – 2.0 mol kg^{-} as shown in Figure 5.3 comparing the two gases at 293K. A similar trend is observed for other two temperatures also.

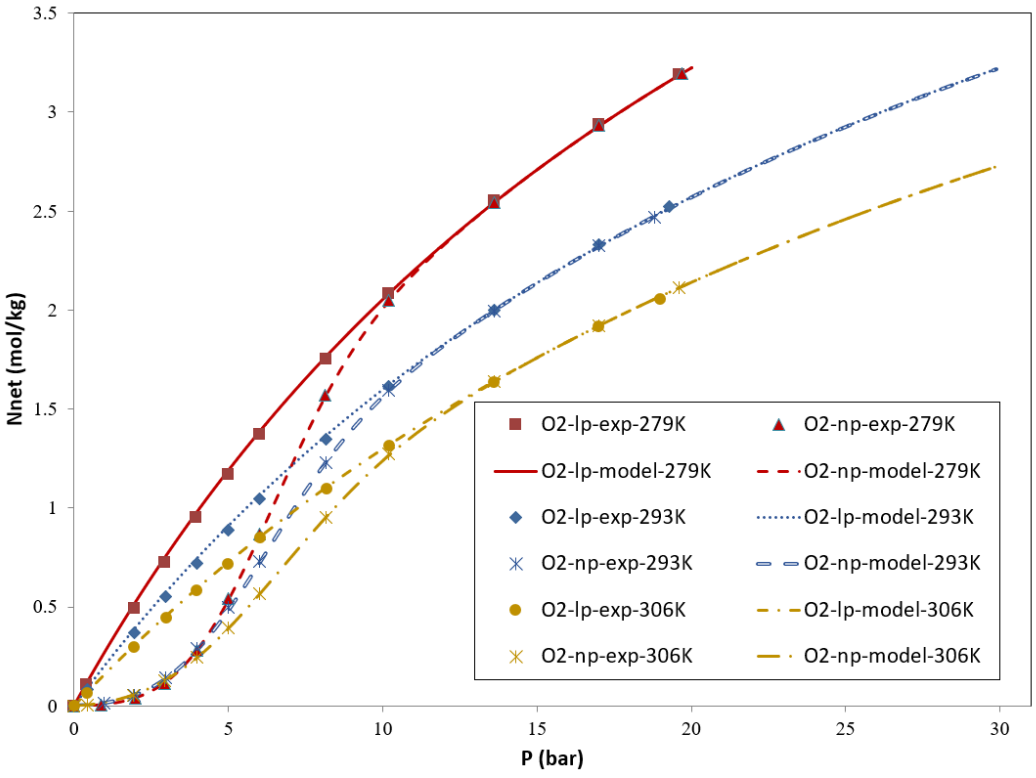

Figure 5.2 Oxygen pure component adsorption equilibria on np and lp phase of MIL-53(Al) at three experimental temperatures along with model fits.

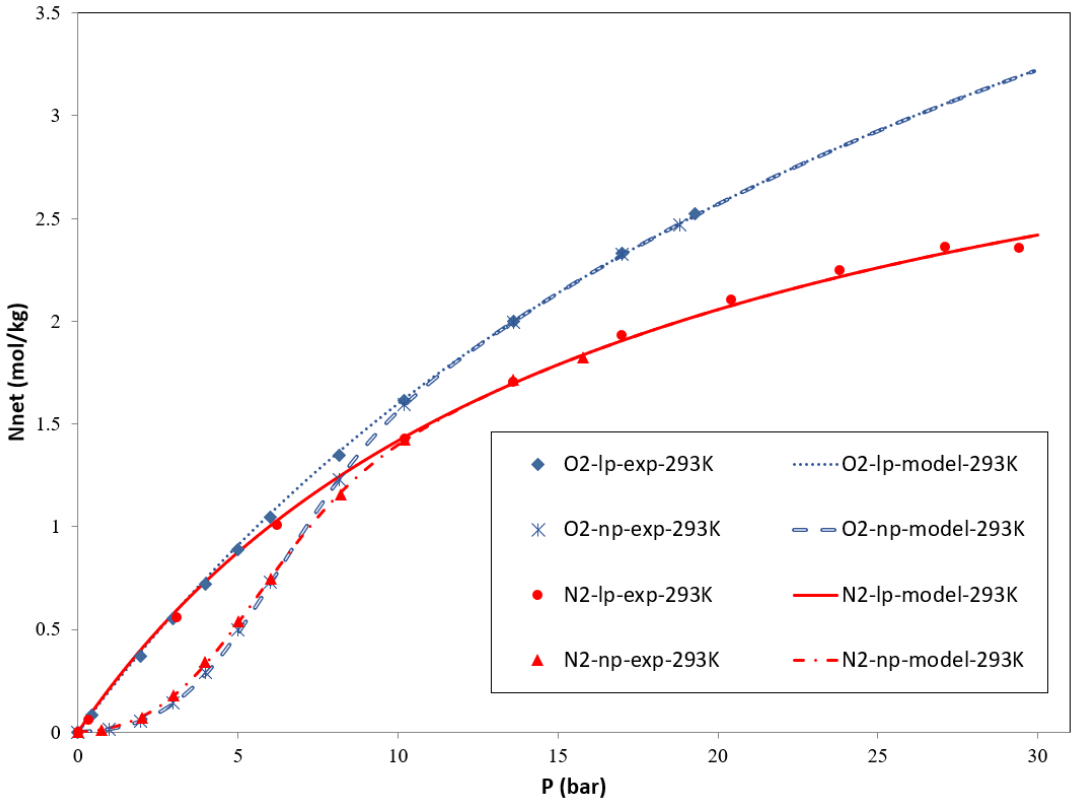

Figure 5.3 Comparison between amount of Nitrogen and Oxygen adsorbed on np and lp phase of MIL-53(Al).

5.1.3 CH_4 Adsorption Equilibria and Data Analysis. Figures 5.4 (a, b, c) show adsorption equilibrium isotherms for pure CH_4 gas at experimental temperatures of 273K, 293K and 306K on both np and lp phases. As can be seen, unlike in the case of nitrogen and oxygen, where isotherms on lp and np phases overlap at higher pressures for all the temperatures, this characteristic is not observed for methane at temperatures of 273K and 293K. There is a significant difference in the amount of gas adsorbed between the two phases. To the best of our knowledge, this behavior has never been reported in the literature. We speculate that the sample never attained equilibrium when the experiments were performed and that the critical pressure was not reached for np phase at 273K and 293K resulting in a huge difference in the amount of gas adsorbed. While at a higher temperature of 306K probably due to faster kinetics, equilibrium is attained and isotherm characteristics exhibited are similar to that of

nitrogen and oxygen. The solid undergoes transition at a pressure of about 2.5 bar with CH_4 as compared to about 12 bar in case of nitrogen and oxygen (see Figure 5.5). A noticeable feature however is a significantly higher amount of methane gas adsorbed as compared to other two gases. This difference in behavior is attributed to a larger kinetic diameter of methane (Table 2)[31] which induces a stress on the pore walls causing the sample to undergo transition in order to fit the large molecules at a low pressure. The sample is in large pore form for majority of the pressure range which leads to a higher uptake of methane. The results reported in this thesis are in good agreement with Mishra et al., 2013 "Effect of Adsorbent History on Adsorption Characteristics of MIL- 53(Al) Metal Organic Framework" and Rallapalli et al., 2011 "Sorption studies of CO_2, CH_4, N_2, CO, O_2 and Ar on nanoporous. aluminum terephthalate [MIL-53(Al)]" who suggested that the range of pressure at which the transformation occurs is related to the adsorption affinity of gases on the sample and the adsorption capacities depend on their polarizabilities respectively.

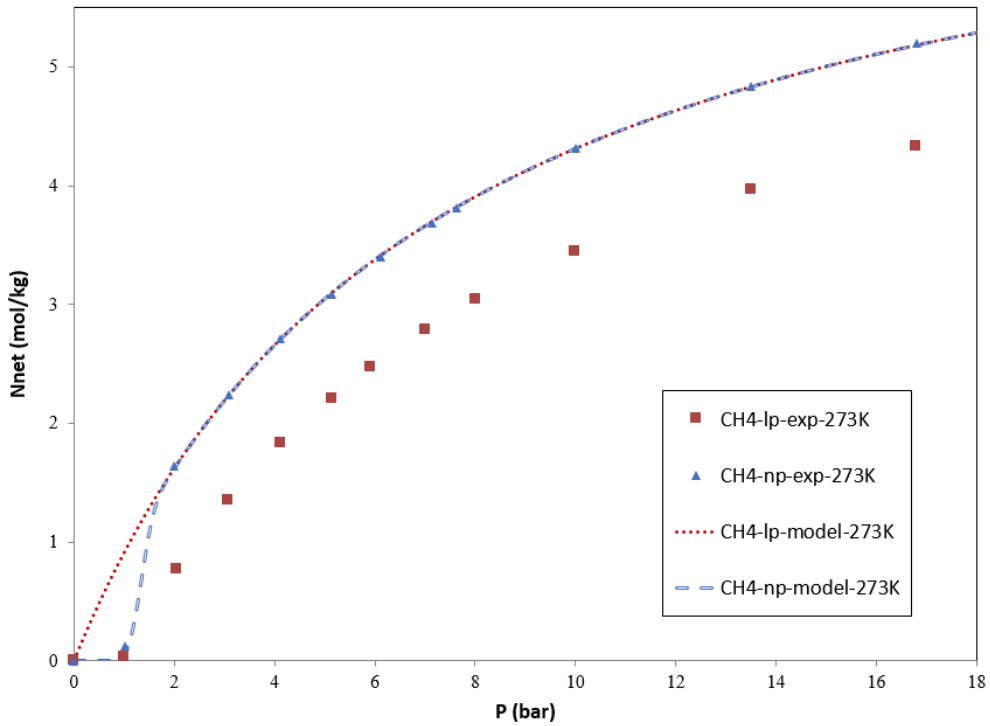

Figure 5.4 (a) Methane pure component adsorption equilibria on np and lp phases of MIL-53(Al) at 273K.

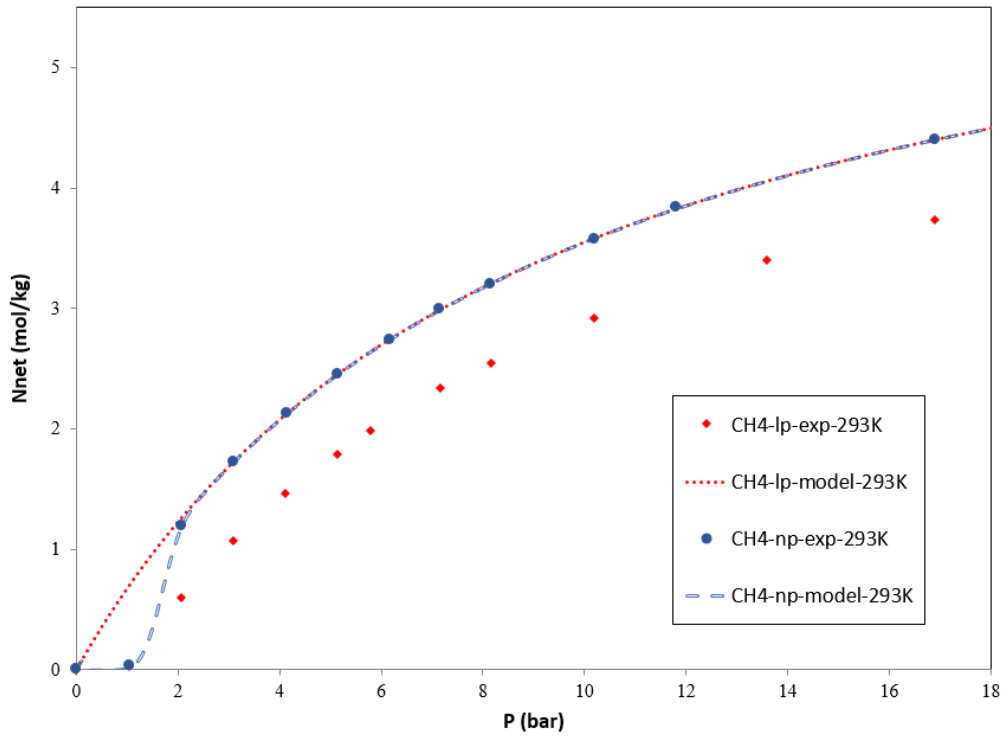

Figure 5.4 (b) Methane pure component adsorption equilibria on np and lp phases of MIL-53(Al) at 293K.

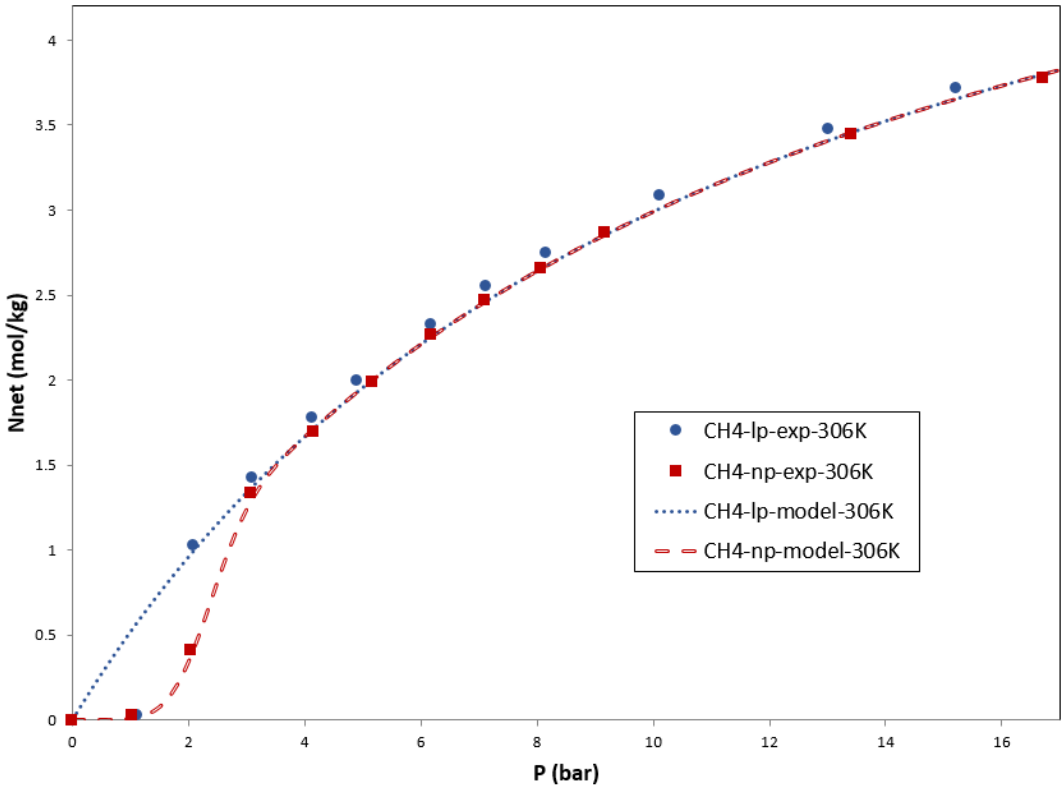

Figure 5.4 (c) Methane pure component adsorption equilibria on np and lp phase of MIL-53(Al) at 306K.

Table 2. Kinetic Diameter (Å) of Gases[31].

Molecule	Kinetic Diameter (Å)
CH_4	3.80
N_2	3.64
O_2	3.46
CO_2	3.30

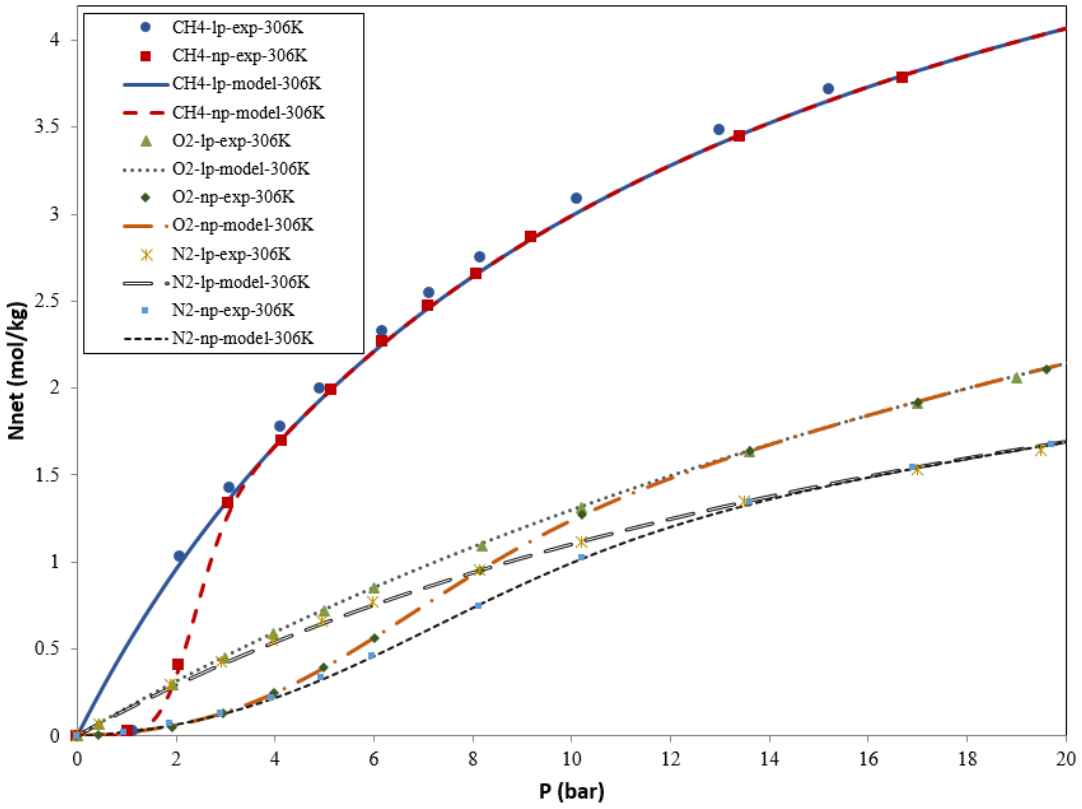

Figure 5.5 Isotherms for N_2, O_2 and CH_4 at 306K on np and lp phases of MIL-53(Al)

5.1.4 CO_2 Adsorption Equilibria and Data Analysis. Compared to other gases in this study, CO_2 shows a different behavior since it is small with a kinetic diameter of 3.3Å[31] and has a high quadrupole moment. The pure component adsorption isotherms for CO_2 on narrow pore of MIL-53(Al) are shown in the Figure 5.6 below.

The sample is predominantly in np phase between 0 – 4.5 bar for isotherms measured at 273K and 293K respectively, while at 306K, the sample stays in np phase until a pressure of 6 bar. For a pressure range during which the sample stays in np, the CO_2 uptake capacity increases steadily from 2.2 – 4 mol/kg. At pressure greater than 4 bar (for 273K and 293K) and 6 bar (for 306K) respectively, a step is evident in the isotherm which represents pore opening i.e. np to lp transition. This results in a significant increase in the uptake capacity to approximately 10 mol/kg. [**Note**- In case of adsorption isotherm measured at 306K, the lp phase data point (represented by *) was fitted by back calculating using the Langmuir parameters for 273K and 293K. This was done because the data point was outside the pressure range used for measuring the experimental data at 306K.]

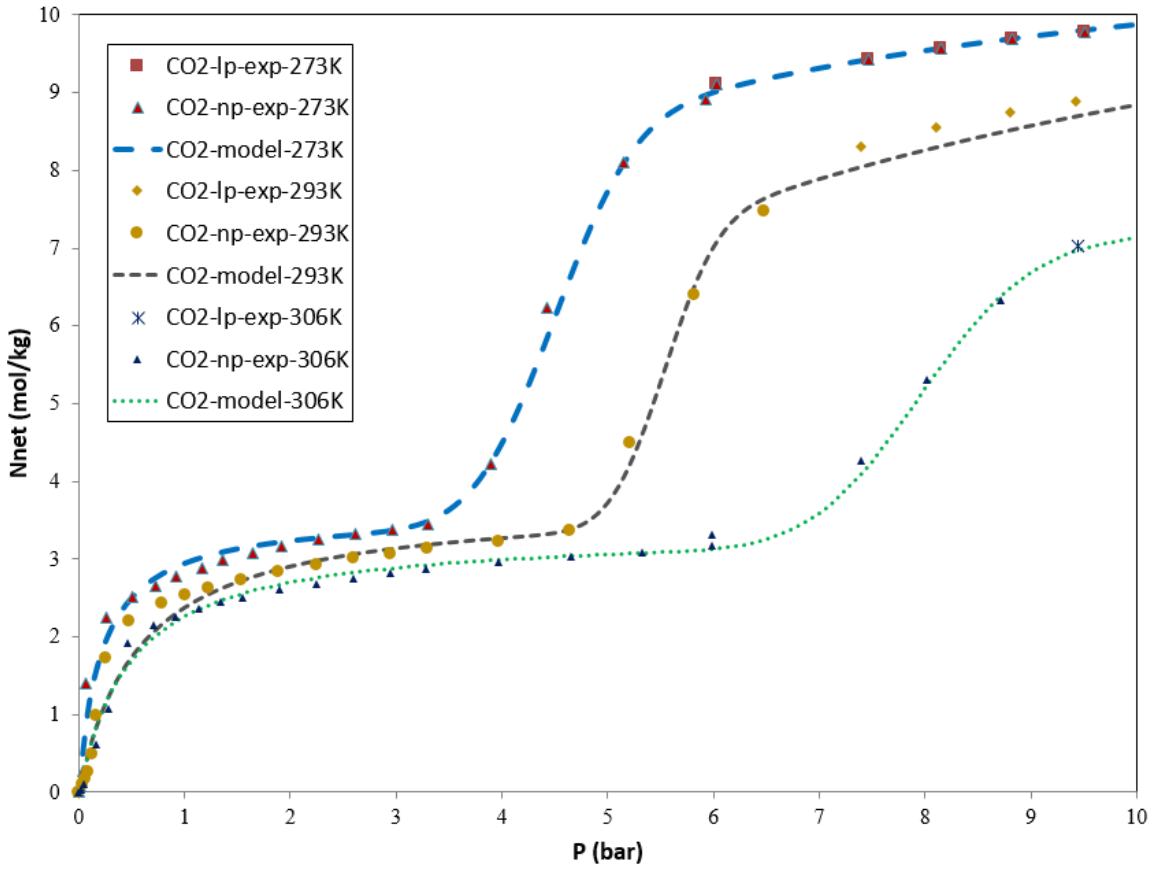

Figure 5.6 Carbon dioxide pure component adsorption equilibria on both phases of MIL-53(Al) at three experimental temperatures along with model fits.

As one can notice, the isotherms show distinct characteristics compared to N_2, O_2 and CH_4. The main reason being the amount of gas adsorbed in the low-pressure region (np phase) is significantly higher in case of CO_2. This occurs because of a significantly higher affinity of the sample for CO_2 (detailed explanation in section 5.4). As a result, the pores of the solid are already filled with gas while it undergoes the np to lp transition.

The step change corresponding to np – lp transition in present study occurs at different pressure on increasing the temperature i.e. at 4 bar for 273K, 4.5 bar for 293K and 6 bar for 306K respectively. This indicates that structural transition is a function of absolute temperature and the pressure range at which it occurs increases with temperature. In addition, the characteristic adsorption behavior of CO_2 exhibited in the figures above is in good agreement with the predictions made by Coudert et. al in 2008 in their study of "Thermodynamics of Guest-Induced Structural Transition in Hybrid Organic – Inorganic Frameworks".

5.2 Literature Comparison

The following sections compare data collected in this work to data reported in literature wherever available. As will be seen the data is in good agreement with similar published in literature noting the differences in temperature and considering completely different samples and techniques are utilized in two different laboratories to measure these complicated phase behaviors.

5.2.1 N_2 at 293K. Figure 5.7 shows a comparison between experimental data and literature as reported by Kara,2018[27] on narrow pore form of MIL-53(Al). In both the isotherms, the distinct "S-shape" of the isotherm synonymous with type IV is clear on both isotherms. The solid undergoes a complete transition from np to lp phase beyond a pressure of about 8 bar. The spread of transition (i.e. standard deviation of

underlying normal distribution) depends on particle size, and two different samples were used in these experiments. The amount of N_2 gas adsorbed in the low-pressure region is significantly higher in this study, where as it is marginally lower when compared with the literature values as we move along the high-pressure range. The isotherm however, follows a similar trend and matches with that reported in literature.

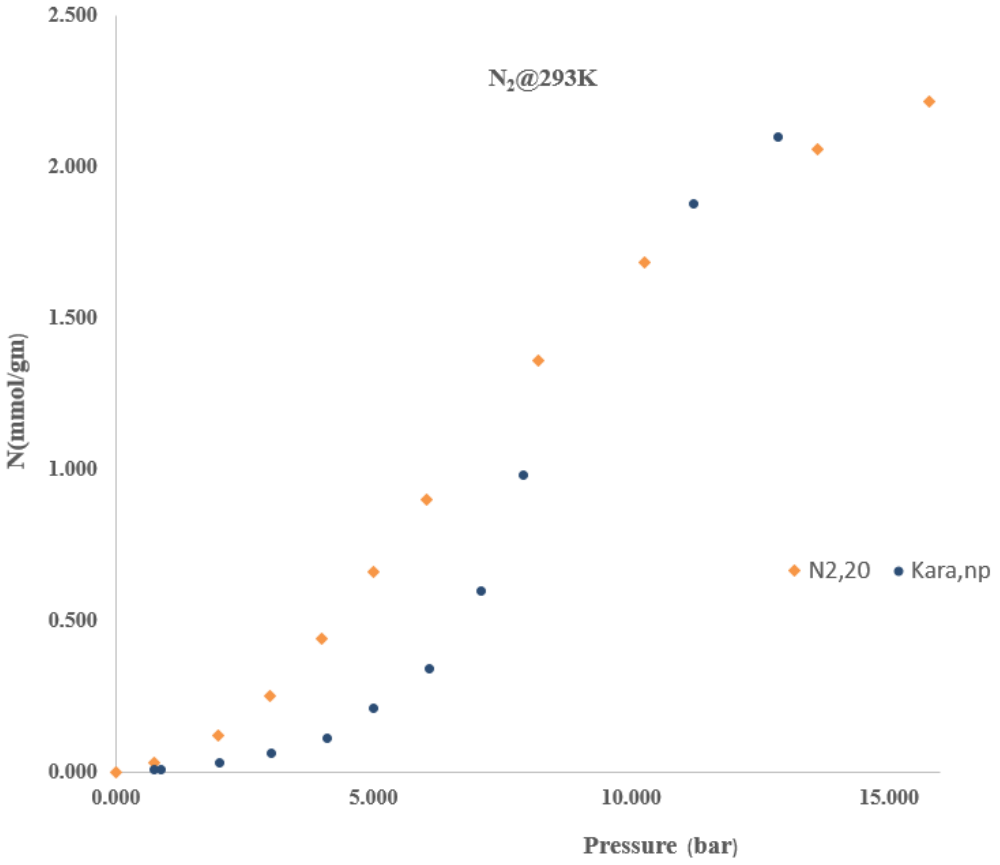

Figure 5.7 Comparison of the experimental data with literature values for N_2 at 293K on np form of MIL-53(Al).

Figure 5.8 below shows a comparison between experimental and literature data reported by Gumma et.al, 2014[12] and Kara, 2018[27] on large pore form of MIL-53(Al) at 293K. The uptake capacity of the experimental isotherm is lower at higher pressures when compared with the reported values but, the isotherm exhibits a similar trend and matches well with literature.

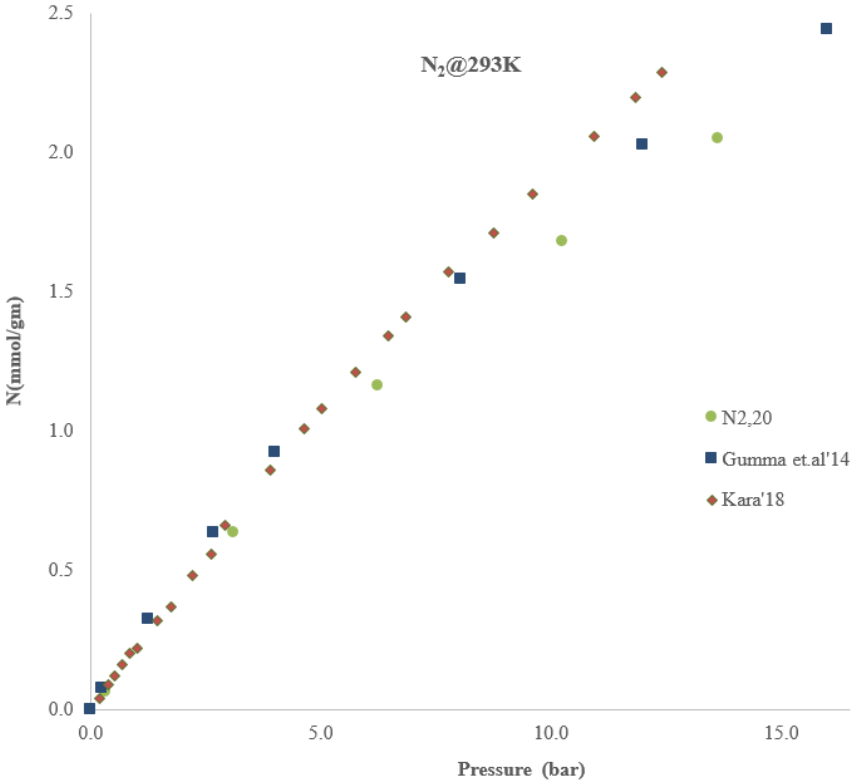

Figure 5.8 Comparison of the experimental data with literature values for N_2 at 293K on lp form of MIL-53(Al).

5.2.2 O_2 at 293K. Figure 5.9 shows the comparison between experimental data and literature values for oxygen on narrow pore and large pore forms of MIL-53(Al) at 293K. As exhibited in the figure, the experimental data fits very well with Gumma et.al, 2013[14]. In case of isotherms measured on the np phase, both undergo a complete transition from np to lp phase beyond a pressure of about 6 bar with an identical uptake capacity of gas at that pressure. As we move towards high pressure range, the np phase and lp phase isotherms align almost perfectly with each other for both sets of data with identical uptake of oxygen gas.

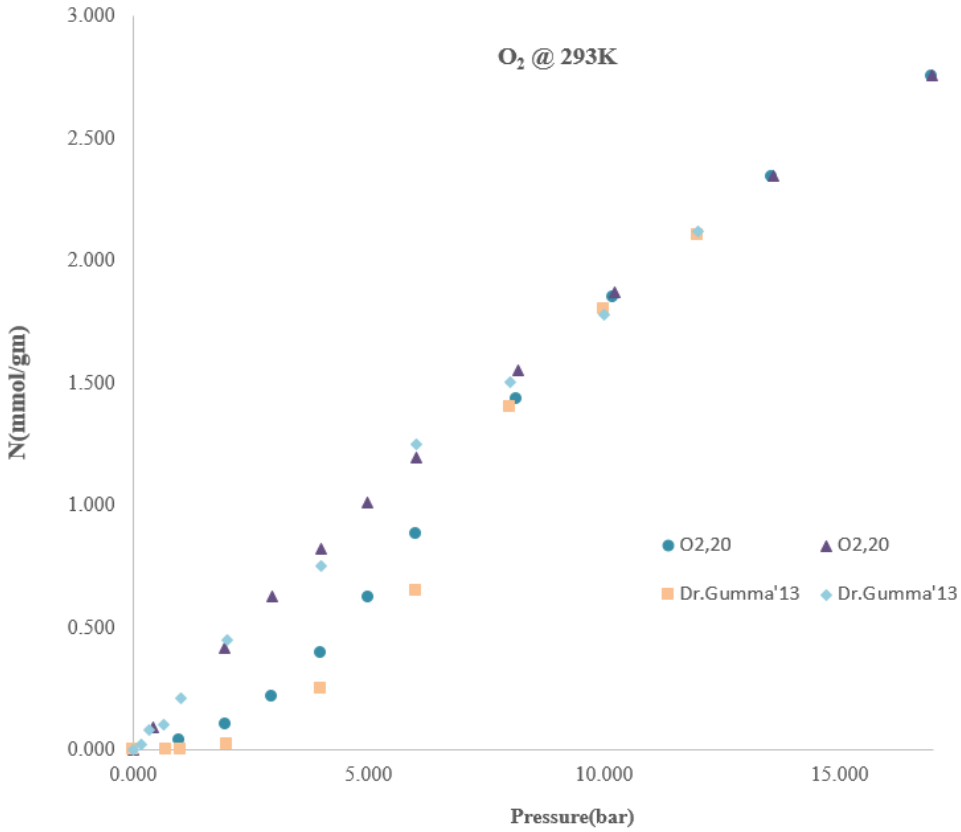

Figure 5.9 Comparison of the experimental data with literature values for O_2 at 293K on np and lp forms of MIL-53(Al).

5.2.3 CH_4 at 293K. Figure 5.10 shows the comparison between experimental and literature data for methane reported in "Adsorption and Separation of Carbon Dioxide Using MIL-53(Al) Metal-Organic Framework" by Gumma et.al, 2014 on large pore form of MIL-53(Al) at 293K. Both sets of data were measured gravimetrically using the automated Rubotherm Magnetic Suspension balance. The uptake capacity of solid [MIL-53(Al)] in this work is lower. The primary reason for this could be the difference in length of time allowed for equilibration. However, the isotherm exhibits a similar trend and is in good agreement with the published data.

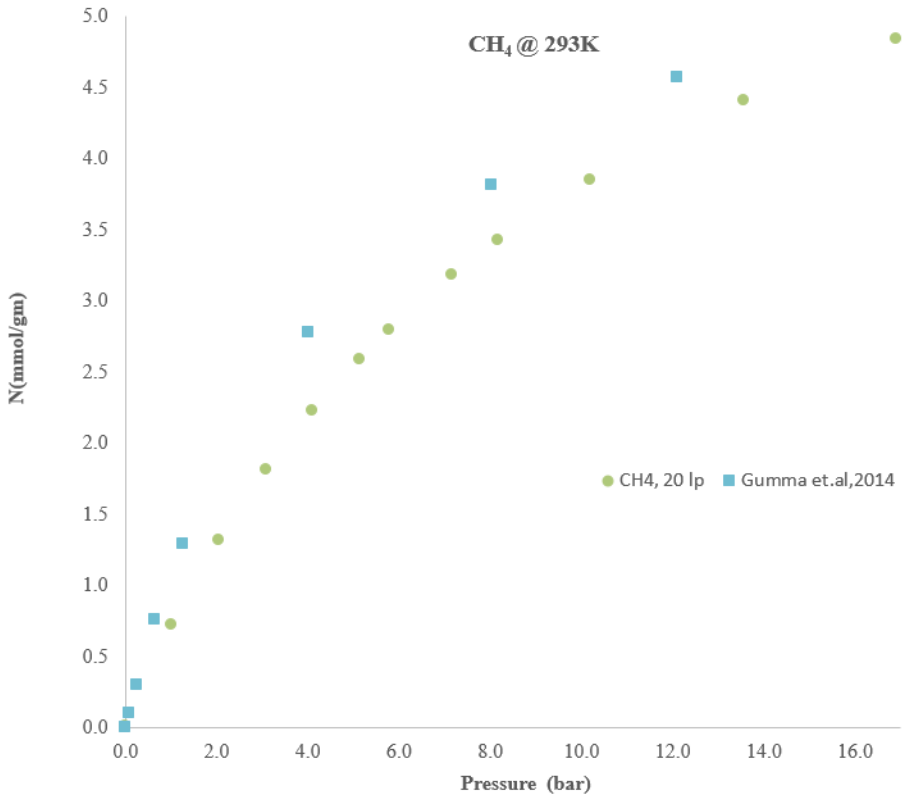

Figure 5.10 Comparison of the experimental data with literature values for CH_4 at 293K on lp forms of MIL-53(Al).

5.2.4 CO_2 at 293K. Figure 5.11shows a comparison between experimental and literature data for CO_2 reported by Gumma et.al, 2014[12] and Kara, 2018[27]. The critical pressure at which the solid undergoes transition i.e. 4.5 bar and the pressure range (i.e. $5 - 7$ bar) during which the transformation from np to lp phase is complete matches very well with the reported data. The gas uptake capacity is also identical for the entire pressure range. Thus, the isotherm at 293K is in good agreement with literature. In case of data reported by Boutin et al, 2010[13], the uptake capacities are different. The temperatures are different which may account part of the difference. Another reason may be solid impurities in one sample, the shape of curves match remarkably well. The critical pressure is about 5 bar and the transition pressure range is between 4-7 bar.

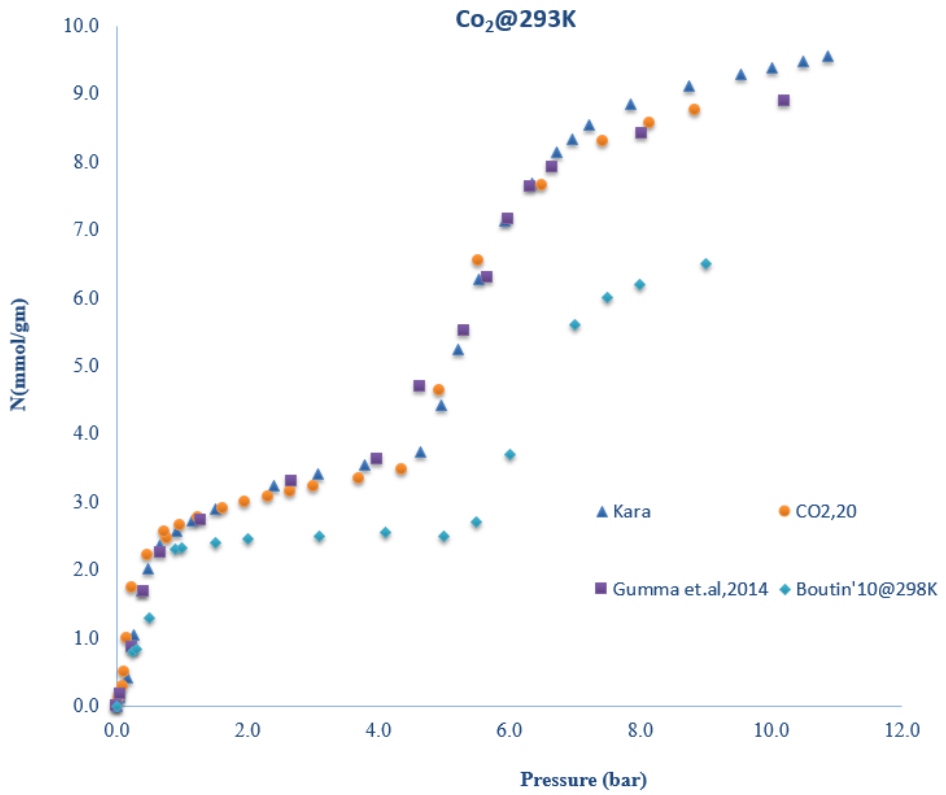

Figure 5.11 Comparison of the experimental data with literature values for CO_2 at 293K on np form of MIL-53(Al).

5.2.5 CO_2 at 304K. Figure 5.12 shows a comparison between experimental and literature data for CO_2 reported by Boutin et al[13]. The critical pressure in this case is between 6-6.5 bar followed by a pressure transition region between 7-9.5 bar. The uptake capacity reported in this work however is higher than the literature value despite both data sets being collected gravimetrically. The main reason for difference in the uptake capacity could be the time length allowed for equilibration. Measurement of the entire data set reported in literature was completed between 4-6 hours whereas, our experimental data is measured overnight. None the less, experimental isotherm is in good agreement with that reported in literature as shown in the figure below.

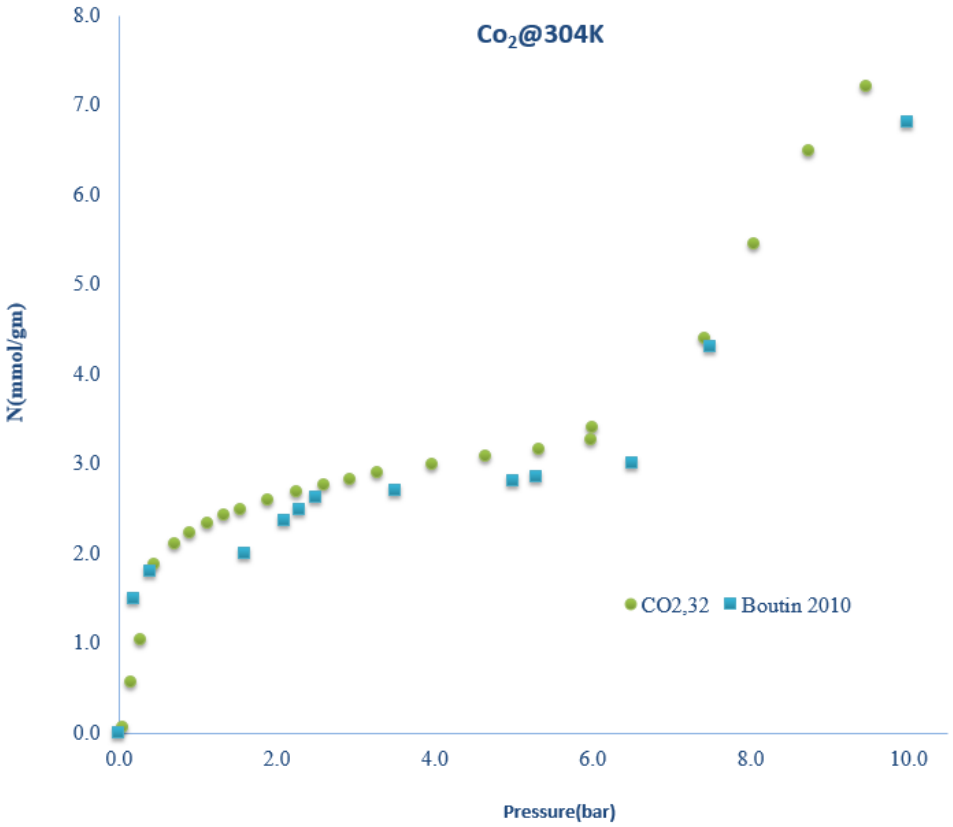

Figure 5.12 Comparison of the experimental data with literature values for CO_2 at 304K on np form of MIL-53(Al).

5.3 Model Parameters

Utilizing the convenience of having a mathematical model, several underlying phenomena can be examined. Following discussion analyzes physical parameters of the model.

The pure component adsorption isotherms for all the gases studied in this thesis were modelled with the revised dual site Langmuir model as discussed in chapter 3 section 3.7.4. The two sets of model parameters were obtained from experimental data in the low-pressure region for np phase and in high pressure region for lp phase with the help of linear regression (Table 3). While performing regression analysis, adsorption of N_2, O_2 and CH_4 in np phase was set equal to zero as evident in the table. The standard deviation (s) and mean (m) of normal distribution for transition pressure

were obtained by a trial and error method until the model branches fit the experimental data.

The parameters obtained from the regression domain provide a good fit of the experimental data as shown graphically in Figures 5.1to 5.6. The experimental data points align with the model branches on fitting the model parameters but, deviates in the low-pressure region also known as the Henry's law region. This can be seen particularly in figure 5.6 for CO_2 at 32°C. Henry's region is very important in adsorption as it denotes the affinity between a solid and the gas of interest.

Table 3. Model Parameters for Adsorption Isotherms.

Coefficient	Adsorbent			
	CO_2	N_2	O_2	CH_4
T = 279 K				
N_{1max} (mol/Kg)	11.494	4.593	8.210	8.039
N_{2max} (mol/Kg)	3.589	0.000	0.000	N/A
b_1 (1/bar)	0.611	0.064	0.033	0.074
b_2 (1/bar)	4.560	0.000	0.000	N/A
s	0.600	2.450	2.250	N/A
m	4.450	5.500	5.250	N/A
T = 293 K				
N_{1max} (mol/Kg)	9.737	4.039	7.519	7.800
N_{2max} (mol/Kg)	3.530	0.000	0.000	N/A
b_1 (1/bar)	0.760	0.052	0.027	0.058
b_2 (1/bar)	2.590	0.000	0.000	N/A
s	0.500	2.450	2.500	N/A
m	5.400	4.150	4.700	N/A
T = 306 K				
N_{1max} (mol/Kg)	8.660	3.346	6.431	6.333
N_{2max} (mol/Kg)	3.351	0.000	0.000	N/A
b_1 (1/bar)	0.472	0.050	0.025	0.094
b_2 (1/bar)	2.070	0.000	0.000	N/A
s	0.800	3.950	3.150	N/A
m	7.900	5.000	4.750	N/A

5.4 Langmuir Parameters

A plot of pressure (P) vs ratio of pressure (P) and amount of gas adsorbed (N) i.e. (P/N) is used to obtain the Langmuir parameters viz. saturation capacity (N_{max}) and (b) which is also known as the affinity parameter related to Henry's constant. N_{max} represents the maximum amount of gas that can be adsorbed by the solid phases (i.e. np or lp) of an adsorbent. Henry's constant represents the affinity of the adsorbent for the gas of interest. The plot is typically straight whose slope and intercept are calculated using a simple linear regression. Inverse of slope is equivalent to the saturation capacity (N_{max}) while the ratio of slope over intercept gives the Henry's constant (b). The parameters obtained are then used to fit the model to the experimental data.

In case of nitrogen, oxygen and methane, since the amount adsorbed in the np phase is negligible it is not possible to compute the Langmuir parameters and hence they are assumed to be zero. For carbon dioxide, parameters for both the np and lp phases are calculated. All the parameters are reported in Table 3 above where N_{1max}, b_1, N_{2max}, and b_2 are Langmuir parameters for lp and np phases respectively. The plots to determine Langmuir parameters for all the gases used in this work can be found in **Appendix B**.

5.4.1 Temperature Dependency of Langmuir Parameters.

The temperature dependency of Henry's constant is plotted for all three experimental temperatures in Figure 5.13 below which follows the vant Hoff's equation (see section 3.6.1). The equation relates the change in constant b to the change in temperature T. A plot of ln b vs $T^{-1}$is essentially found to be linear over a wide temperature range with the slope equal to the ratio of change in isosteric heat of adsorption (ΔH) at zero loading and gas constant (R) $[-\Delta H/R]$. The isosteric heat determines the strength of interaction between adsorbent and gas molecules. It is also a function of surface coverage and

temperature[33]. As can be seen, in case of nitrogen and oxygen, the slopes are fairly close to each other which implies that ΔH values are also similar for both the gases. The ΔH value for CO_2 in lp phase is substantially lower than the np phase as is expected since the molecular interactions would be higher in a tighter fitting pore environment.

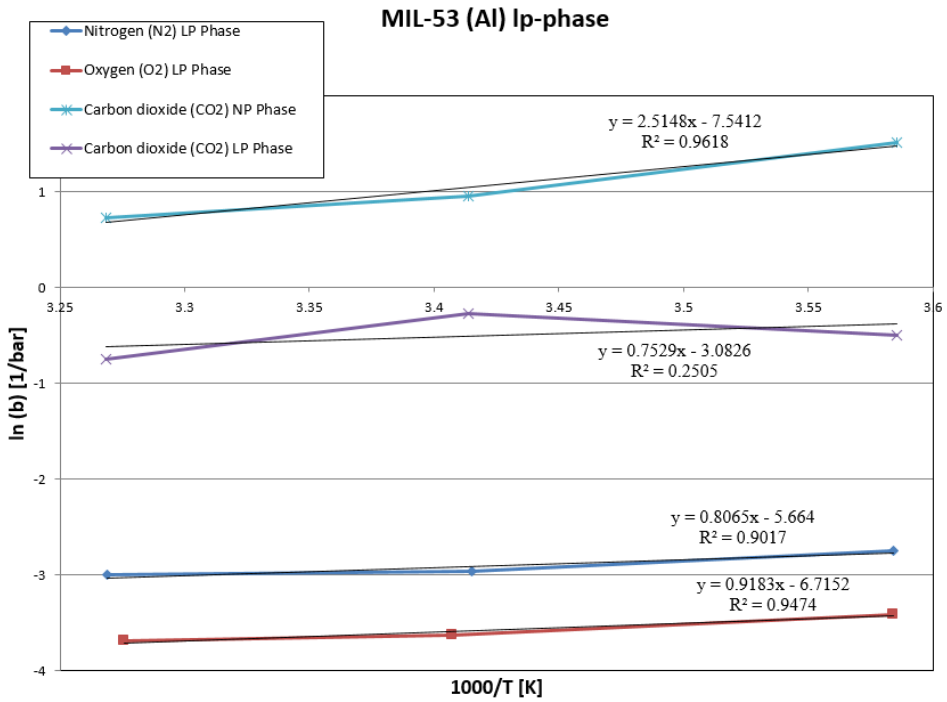

Figure 5.13 vant Hoff plot showing temperature dependency of experimental Henry's constant for all gases.

Figure 5.14 exhibits temperature dependency of N_{max}. In theory, Langmuir model equation is derived for a constant saturation capacity (N_{max}). However as seen in the figure, it is usually found to decrease with temperature when the experimental adsorption data is fitted with model equation. As a result N_{max} is inconsistent with the finite value of dN_{max}/dT[33]. Thermodynamically, the monolayer saturation capacity cannot be a function of temperature in Langmuir model. If the model fits experimental data for two or more adsorption isotherms, then the saturation capacity (N_{max}) at a different temperature can be predicted from those isotherms.

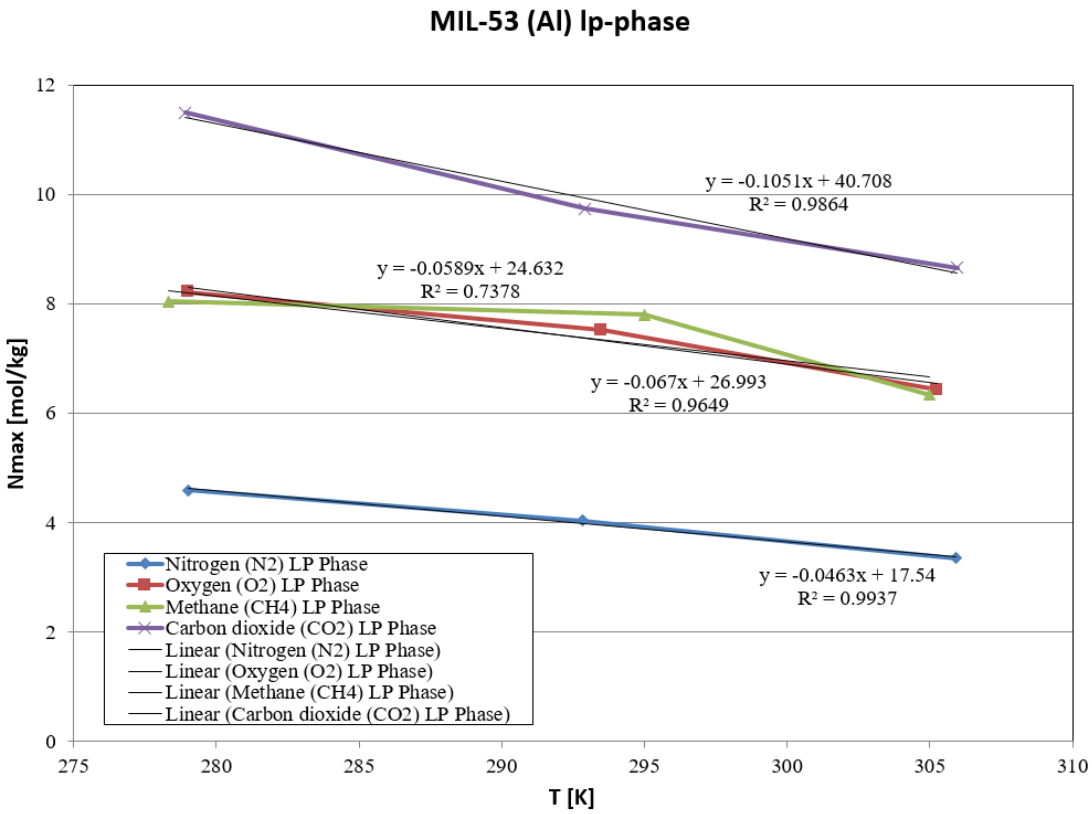

Figure 5.14 Temperature dependency of N_{max} for all experimental gases.

5.5 Temperature Dependency of Crystal Transformation

A logarithmic form of the Arrhenius equation is used to demonstrate the temperature dependence of solid phase transition between np and lp phases (see Figure 5.15). A $\ln(\delta)_{Pc}$ versus T^{-1} [where $(\delta)_{Pc}$ represents a difference in the spreading pressure/grand potential between two phases at critical pressure (Pc)] is plotted for the experimental gases at all three temperatures. The slope obtained represents a ratio of change in internal energy (ΔE) and the gas constant (R) i.e. $[-\Delta E/R]$. It is exactly equivalent to the difference in the Helmholtz free energy (ΔF) between lp and np phases of the solid. In the figure below, we see that slopes in case of nitrogen and oxygen are almost identical (2.0069 and 1.9542 respectively) which implies that ΔE of the solid is identical for the two components. This shows that the amount of work done during transition from np to lp phase is almost the same. For methane, we were unable to

compute the critical pressure (Pc) as a result of the unusual behavior exhibited by the experimental data at 279K and 293K. Hence ΔF and ΔE could not be computed accurately. In case of carbon dioxide, ΔE calculated is different compared to nitrogen and oxygen since the sample behaves in a different manner as explained in earlier sections.

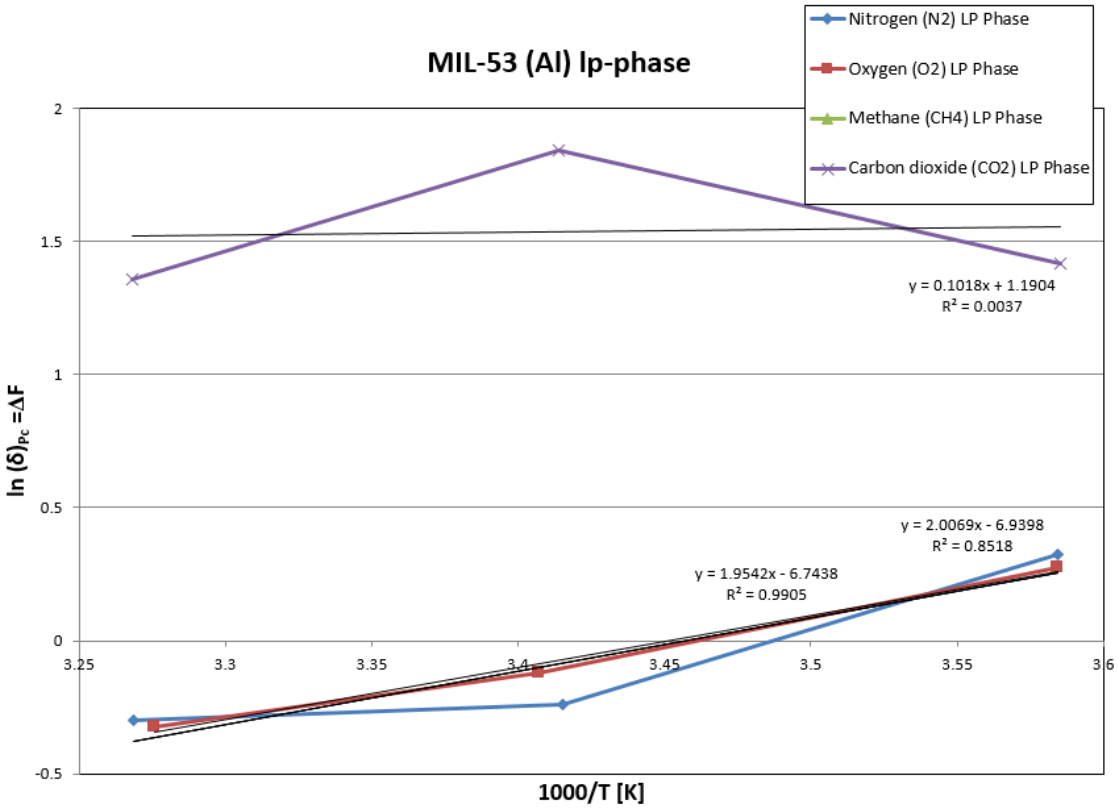

Figure 5.15 Temperature dependency of the transition process.

CHAPTER VI

CONCLUSION AND RECOMMENDATONS

6.1 Conclusions

The goal of this study was to investigate the adsorption induced phase transitions inMIL-53(Al) metal organic framework. The material is a flexible MOF which undergoes structural transformation by changing the temperature, pressure or by introducing guest molecules. The differences in the adsorption characteristics were analyzed by measuring isotherms for nitrogen, oxygen, methane and carbon dioxide at three experimental temperatures of 278K, 293K and 306K between the pressure range of 0-30 bar. The data is compared to literature where available and confirms well given they are different samples.

As evident by the results and discussion chapter, there are some key takeaways. First, the narrow pore (np) form was shown to have a very low affinity for nitrogen, oxygen and methane in the low pressure region resulting in very low to negligible adsorption. In the high pressure region, the amount of gas adsorbed for individual component at a particular temperature was identical irrespective of the phase history (i.e. either starting with np or lp phase) of the solid as evident from the isotherms.

Second, the so called “breathing” phenomena or double transition in case of CO_2 was found to be a consequence of very high affinity for the gas in the low pressure

region. This resulted in a significant amount being adsorbed before undergoing a transition as evident in the isotherm plots.

Third, Internal energy of transition determined from temperature dependency of Helmholtz energy using Arrhenius plot is similar for oxygen and nitrogen. For methane it could not be determined while carbon dioxide stands out because of double transition.

6.2 Recommendations

In order to have a more detailed insight about the adsorptive behavior of MIL-53(Al), additional isotherm measurements should be performed at higher temperatures and pressure ranges for the gases studied in this work in addition to other gases.

Furthermore, synthesis techniques to control the crystal size distribution should be investigated. A sample with uniform crystal size should then be tested to examine its effect on transition process.

REFERENCES

1. Yang, R. *Gas Separation by Adsorption Processes*. *Gas Separation & Purification* **2**, (1987).
2. Rouquerol, F., Roquerol, J., Sing, K. Adsorption by powders and porous solids : principles, methodology and applications. in 647 (1999).
3. D.M.Ruthven. Principles of adsorption and adsorption processes : By D. M. Ruthven; published by John Wiley and Sons Ltd., Chichester, 1984; 433 pp. *Chem. Eng. Process. Process Intensif.* (1985). doi:10.1016/j.nimb.2016.03.044
4. Gumma, S. Automation of volumetric multi-component adsorption equilibrium measurements. (1999).
5. Neimark, A. V., Coudert, F. X., Boutin, A. & Fuchs, A. H. Stress-based model for the breathing of metal-organic frameworks. *J. Phys. Chem. Lett.* **1**, 445–449 (2010).
6. Yaghi, O. M., Li, H., Davis, C., Richardson, D. & Groy, T. L. *Synthetic Strategies, Structure Patterns, and Emerging Properties in the Chemistry of Modular Porous Solids †*. (1998).
7. Mellot-Draznieks, C., Serre, C., Surblé, S., Audebrand, N. & Rard Fé Rey, G. Very Large Swelling in Hybrid Frameworks: A Combined Computational and Powder Diffraction Study. (2005). doi:10.1021/ja054900x
8. Ramsahye, N. A. *et al.* On the breathing effect of a metal-organic framework upon CO 2 adsorption: Monte Carlo compared to microcalorimetry experiments{ COMMUNICATION www.rsc.org/chemcomm | ChemComm. (2007). doi:10.1039/b702986a
9. Finsy, V. *et al.* Framework breathing in the vapour-phase adsorption and separation of xylene isomers with the metal-organic framework MIL-53. *Chem.*

- *A Eur. J.* **15**, 7724–7731 (2009).

10. Loiseau, T. *et al.* A Rationale for the Large Breathing of the Porous Aluminum Terephthalate (MIL-53) Upon Hydration. *Chem. - A Eur. J.* **10**, 1373–1382 (2004).
11. Serre, C. *et al.* Very Large Breathing Effect in the First Nanoporous Chromium(III)-Based Solids: MIL-53 or Cr III (OH),{O 2 C-C 6 H 4-CO 2 },{HO 2 C-C 6 H 4-CO 2 H} x ,H 2 O. (2002). doi:10.1021/ja0276974
12. Mishra, P., Uppara, H. P., Mandal, B. & Gumma, S. Adsorption and Separation of Carbon Dioxide Using MIL-53(Al) Metal-Organic Framework. (2014). doi:10.1021/ie5006146
13. Boutin, A. *et al.* The Behavior of Flexible MIL-53(Al) upon CH_4 and CO_2 Adsorption. *J. Phys. Chem. C* **114**, 22237–22244 (2010).
14. Mishra, P., Edubilli, S., Uppara, H. P., Mandal, B. & Gumma, S. Effect of adsorbent history on adsorption characteristics of mil-53(al) metal organic framework. *Langmuir* **29**, 12162–12167 (2013).
15. Thomas, W. J. & Crittenden, B. *Adsorption Technology and Design*. *Butterworth Heinemann: Oxford, U.K.* (1998). doi:10.1016/B978-075061959-2/50002-1
16. Moran, A. A. A PSA Process for an Oxygen Concentrator. (2014).
17. Donohue, M. D. & Aranovich, G. L. Classification of Gibbs adsorption isotherms. *Adv. Colloid Interface Sci.* (1998). doi:10.1016/S0001-8686(98)00044-X
18. Gumma, S. & Talu, O. Net Adsorption: A Thermodynamic Framework for Supercritical Gas Adsorption and Storage in Porous Solids. *Langmuir* **26**, 17013–17023 (2010).
19. Myers, A. L. Thermodynamics of adsorption in porous materials. *AIChE J.* **48**,

145–160 (2002).

20. Myers, A. L. (2004). *Chemical Thermodynamics for Industry - Google Books*.

21. Laidler, K. J. *The Development of the Arrhenius Equation Journal of Chemical Education, 61(6), 494*. **14**, (UTC, 1984).

22. Bourrelly, S. *et al.* Different adsorption behaviors of methane and carbon dioxide in the isotypic nanoporous metal terephthalates MIL-53 and MIL-47. *J. Am. Chem. Soc.* **127**, 13519–13521 (2005).

23. Rallapalli, P. *et al.* Sorption studies of CO 2 , CH 4 , N 2 , CO, O 2 and Ar on nanoporous aluminum terephthalate [MIL-53(Al)]. doi:10.1007/s10934-010-9371-7

24. Himeno, S., Tomita, T., Suzuki, K. & Yoshida, S. Characterization and selectivity for methane and carbon dioxide adsorption on the all-silica DD3R zeolite. (2006). doi:10.1016/j.micromeso.2006.05.018

25. Peter, S. A., Sebastian, J. & Jasra, R. V. Adsorption of Nitrogen, Oxygen, and Argon in Mono-, Di-, and Trivalent Cation-Exchanged Zeolite Mordenite. (2005). doi:10.1021/ie050128v

26. Coudert, F. X., Jeffroy, M., Fuchs, A. H., Boutin, A. & Mellot-Draznieks, C. Thermodynamics of guest-induced structural transitions in hybrid organic-inorganic frameworks. *J. Am. Chem. Soc.* **130**, 14294–14302 (2008).

27. EFFECT OF HISTORY ON THE BINARY ADSORPTION EQUILIBRIA OF ALUMINIUM TEREPHTHALATE (MIL-53 (Al)) UFUOMA I . KARA Bachelor of Engineering in Chemical Engineering University of Benin April 2014 submitted in partial fulfillment of the requirements for the d. **53**, (2018).

28. Weireld, G. De, Frère, M. & Jadot, R. Automated determination of gas adsorption isotherms using a magnetic suspension balance. *Meas. Sci. Technol.*

10, 117–126 (1999).

29. *Rubotherm-your specialist for gravimetric analysis*.

30. Harale, A. Automation of Magnetic Suspension Balance for High Pressure Adsorption Measurements. (2004).

31. Kentish, S., Scholes, C. & Stevens, G. Carbon Dioxide Separation through Polymeric Membrane Systems for Flue Gas Applications. *Recent Patents Chem. Eng.* **1**, 52–66 (2012).

32. Rallapalli, P. *et al.* Sorption studies of CO2, CH4, N2, CO, O2and Ar on nanoporous aluminum terephthalate [MIL-53(Al)]. *J. Porous Mater.* **18**, 205–210 (2011).

33. 88 AIChE_TALU, MYERS_Rigorous thermodynamic treatment of gas adsorption.pdf.

APPENDIX A: EXPERIMENTAL DATA

Large Pore = 1, Narrow Pore = 2

Isotherm #	Gas	T (K)	P (bar)	N net (mmol/gm)	N excess (mmol/gm)	LP/NP
1	N_2	279	0.00	0.00	0.00	1
1	N_2	279	0.41	0.11	0.12	1
1	N_2	279	1.92	0.48	0.53	1
1	N_2	279	2.91	0.70	0.78	1
1	N_2	279	3.94	0.90	1.00	1
1	N_2	279	4.96	1.09	1.22	1
1	N_2	279	5.99	1.25	1.41	1
1	N_2	279	8.15	1.56	1.77	1
1	N_2	279	10.19	1.80	2.07	1
1	N_2	279	13.56	2.13	2.49	1
1	N_2	279	16.93	2.38	2.83	1
1	N_2	279	19.65	2.54	3.06	1
2	N_2	279	0.00	0.00	0.00	2
2	N_2	279	0.97	0.00	0.03	2
2	N_2	279	1.91	0.02	0.07	2
2	N_2	279	2.94	0.09	0.16	2
2	N_2	279	3.95	0.23	0.33	2
2	N_2	279	4.96	0.45	0.58	2
2	N_2	279	5.99	0.71	0.87	2

2	N_2	279	8.12	1.32	1.53	2
2	N_2	279	10.21	1.78	2.05	1
2	N_2	279	13.59	2.13	2.48	1
2	N_2	279	16.96	2.38	2.83	1
2	N_2	279	19.48	2.52	3.03	1
3	N_2	293	0.00	0.00	0.00	1
3	N_2	292	0.31	0.06	0.07	1
3	N_2	292	3.09	0.56	0.64	1
3	N_2	292	6.23	1.01	1.16	1
3	N_2	293	10.23	1.43	1.68	1
3	N_2	292	13.62	1.71	2.05	1
3	N_2	293	17.00	1.93	2.36	1
3	N_2	294	20.38	2.10	2.61	1
3	N_2	294	23.76	2.25	2.84	1
3	N_2	294	27.13	2.36	3.04	1
3	N_2	292	29.39	2.36	3.10	1
4	N_2	293	0.00	0.00	0.00	2
4	N_2	292	0.74	0.01	0.03	2
4	N_2	292	1.99	0.07	0.12	2
4	N_2	292	2.98	0.18	0.25	2
4	N_2	292	3.98	0.34	0.44	2
4	N_2	292	5.00	0.54	0.66	2

4	N_2	292	6.03	0.75	0.90	2
4	N_2	292	8.20	1.16	1.36	1
4	N_2	292	10.25	1.43	1.68	1
4	N_2	292	13.62	1.72	2.06	1
4	N_2	292	15.78	1.82	2.22	1
5	N_2	306	0.00	0.00	0.00	1
5	N_2	306	0.43	0.07	0.08	1
5	N_2	306	1.89	0.29	0.33	1
5	N_2	306	2.91	0.43	0.50	1
5	N_2	305	3.93	0.56	0.65	1
5	N_2	306	4.95	0.67	0.80	1
5	N_2	306	5.98	0.79	0.94	1
5	N_2	306	8.13	1.00	1.20	1
5	N_2	306	10.20	1.17	1.43	1
5	N_2	306	13.50	1.41	1.75	1
5	N_2	306	17.00	1.61	2.03	1
5	N_2	306	19.50	1.73	2.22	1
6	N_2	305	0.00	0.00	0.00	2
6	N_2	306	0.93	0.02	0.04	2
6	N_2	306	1.87	0.05	0.10	2
6	N_2	306	2.90	0.11	0.19	2
6	N_2	306	3.92	0.21	0.30	2

6	N_2	306	4.93	0.32	0.45	2
6	N_2	306	5.97	0.46	0.61	2
6	N_2	306	8.13	0.78	0.99	2
6	N_2	306	10.20	1.07	1.33	2
6	N_2	306	13.60	1.41	1.76	1
6	N_2	306	16.90	1.62	2.05	1
6	N_2	306	19.70	1.76	2.25	1
7	O_2	279	0.00	0.00	0.00	1
7	O_2	279	0.40	0.11	0.12	1
7	O_2	279	1.94	0.49	0.54	1
7	O_2	279	2.92	0.72	0.80	1
7	O_2	279	3.95	0.95	1.06	1
7	O_2	279	4.98	1.17	1.30	1
7	O_2	279	6.01	1.37	1.53	1
7	O_2	279	8.15	1.75	1.96	1
7	O_2	279	10.20	2.08	2.35	1
7	O_2	279	13.60	2.55	2.91	1
7	O_2	279	17.00	2.94	3.39	1
7	O_2	279	19.60	3.19	3.71	1
8	O_2	279	0.00	0.00	0.00	2
8	O_2	279	0.86	0.01	0.03	2
8	O_2	279	1.97	0.04	0.09	2

8	O_2	279	2.94	0.11	0.19	2
8	O_2	279	3.97	0.28	0.38	2
8	O_2	279	4.98	0.54	0.67	2
8	O_2	279	6.00	0.87	1.03	2
8	O_2	279	8.14	1.57	1.79	2
8	O_2	279	10.20	2.05	2.32	1
8	O_2	279	13.60	2.54	2.90	1
8	O_2	279	17.00	2.93	3.39	1
8	O_2	279	19.70	3.20	3.72	1
9	O_2	293	0.00	0.00	0.00	1
9	O_2	293	0.42	0.08	0.09	1
9	O_2	293	1.94	0.37	0.42	1
9	O_2	293	2.96	0.55	0.62	1
9	O_2	294	3.98	0.72	0.82	1
9	O_2	293	4.99	0.89	1.01	1
9	O_2	294	6.02	1.04	1.20	1
9	O_2	294	8.17	1.35	1.55	1
9	O_2	294	10.20	1.61	1.87	1
9	O_2	294	13.60	2.00	2.34	1
9	O_2	294	17.00	2.33	2.76	1
9	O_2	293	19.30	2.52	3.01	1
10	O_2	293	0.00	0.00	0.00	2

10	O_2	293	0.98	0.01	0.04	2
10	O_2	293	1.96	0.05	0.10	2
10	O_2	293	2.96	0.14	0.21	2
10	O_2	293	3.98	0.29	0.39	2
10	O_2	293	4.99	0.50	0.62	2
10	O_2	293	6.00	0.73	0.88	2
10	O_2	293	8.15	1.23	1.43	2
10	O_2	293	10.20	1.59	1.85	1
10	O_2	293	13.60	2.00	2.34	1
10	O_2	294	17.00	2.32	2.75	1
10	O_2	293	18.80	2.47	2.94	1
11	O_2	305	0.00	0.00	0.00	1
11	O_2	304	0.43	0.07	0.08	1
11	O_2	305	1.94	0.30	0.34	1
11	O_2	305	2.98	0.45	0.52	1
11	O_2	305	3.97	0.59	0.68	1
11	O_2	305	4.99	0.72	0.84	1
11	O_2	305	6.01	0.85	0.99	1
11	O_2	306	8.19	1.10	1.29	1
11	O_2	306	10.20	1.31	1.56	1
11	O_2	306	13.60	1.64	1.96	1
11	O_2	306	17.00	1.92	2.33	1
11	O_2	305	19.00	2.06	2.52	1

12	O_2	306	0.00	0.00	0.00	2
12	O_2	306	0.44	0.00	0.01	2
12	O_2	306	1.93	0.05	0.10	2
12	O_2	306	2.94	0.13	0.20	2
12	O_2	306	3.97	0.24	0.34	2
12	O_2	306	4.99	0.39	0.51	2
12	O_2	306	6.02	0.57	0.71	2
12	O_2	306	8.15	0.95	1.15	2
12	O_2	306	10.20	1.28	1.52	1
12	O_2	306	13.60	1.64	1.97	1
12	O_2	306	17.00	1.92	2.33	1
12	O_2	306	19.60	2.11	2.59	1
13	CH_4	279	0.00	0.00	0.11	1
13	CH_4	279	1.01	0.03	1.05	1
13	CH_4	279	2.05	0.77	1.82	1
13	CH_4	279	3.07	1.35	2.43	1
13	CH_4	278	4.12	1.83	2.93	1
13	CH_4	278	5.15	2.21	3.35	1
13	CH_4	278	5.91	2.47	3.62	1
13	CH_4	278	7.00	2.79	3.97	1
13	CH_4	278	8.02	3.04	4.25	1
13	CH_4	278	10.00	3.45	4.71	1

13	CH_4	278	13.50	3.97	5.34	1
13	CH_4	278	16.80	4.33	5.78	1
14	CH_4	279	0.00	0.00	0.14	2
14	CH_4	278	1.02	0.13	0.30	2
14	CH_4	278	2.00	1.64	1.83	1
14	CH_4	278	3.08	2.24	2.47	1
14	CH_4	278	4.11	2.71	2.96	1
14	CH_4	278	5.13	3.09	3.36	1
14	CH_4	279	6.12	3.40	3.71	1
14	CH_4	278	7.13	3.69	4.03	1
14	CH_4	279	7.63	3.82	4.17	1
14	CH_4	278	10.00	4.32	4.73	1
14	CH_4	278	13.50	4.84	5.35	1
14	CH_4	278	16.80	5.20	5.80	1
15	CH_4	295	0.00	0.00	0.01	1
15	CH_4	295	1.03	0.03	0.71	1
15	CH_4	295	2.07	0.60	1.32	1
15	CH_4	295	3.09	1.07	1.81	1
15	CH_4	295	4.12	1.46	2.23	1
15	CH_4	295	5.14	1.79	2.59	1
15	CH_4	295	5.79	1.99	2.79	1
15	CH_4	295	7.17	2.34	3.18	1

15	CH_4	295	8.17	2.55	3.42	1
15	CH_4	295	10.20	2.92	3.84	1
15	CH_4	295	13.60	3.40	4.41	1
15	CH_4	295	16.90	3.74	4.84	1
16	CH_4	295	0.01	0.00	0.04	2
16	CH_4	295	1.04	0.03	0.26	2
16	CH_4	295	2.07	1.19	1.28	1
16	CH_4	295	3.10	1.73	1.84	1
16	CH_4	295	4.14	2.13	2.27	1
16	CH_4	295	5.14	2.45	2.62	1
16	CH_4	295	6.17	2.74	2.93	1
16	CH_4	295	7.15	2.99	3.21	1
16	CH_4	295	8.15	3.20	3.45	1
16	CH_4	295	10.20	3.57	3.86	1
16	CH_4	295	11.80	3.84	4.18	1
16	CH_4	295	16.90	4.40	4.88	1
17	CH_4	305	0.00	0.00	0.05	1
17	CH_4	305	1.11	0.03	0.67	1
17	CH_4	305	2.08	1.03	1.13	1
17	CH_4	305	3.09	1.43	1.55	1
17	CH_4	305	4.12	1.78	1.92	1

17	CH_4	305	4.90	2.00	2.17	1
17	CH_4	305	6.17	2.33	2.53	1
17	CH_4	305	7.11	2.55	2.77	1
17	CH_4	305	8.14	2.75	3.00	1
17	CH_4	305	10.10	3.09	3.39	1
17	CH_4	305	13.00	3.48	3.85	1
17	CH_4	305	15.20	3.72	4.14	1
18	CH_4	306	0.00	0.00	0.08	2
18	CH_4	306	1.03	0.03	0.21	2
18	CH_4	306	2.04	0.41	0.62	2
18	CH_4	306	3.06	1.34	1.58	1
18	CH_4	306	4.14	1.70	1.97	1
18	CH_4	305	5.15	1.99	2.28	1
18	CH_4	306	6.17	2.27	2.58	1
18	CH_4	306	7.10	2.47	2.80	1
18	CH_4	306	8.07	2.66	3.02	1
18	CH_4	305	9.17	2.87	3.26	1
18	CH_4	306	13.40	3.45	3.95	1
18	CH_4	305	16.70	3.78	4.36	1
19	CO_2	279	0.00	0.00	0.00	2
19	CO_2	279	0.01	0.07	0.07	2
19	CO_2	279	0.04	0.27	0.27	2

19	CO_2	279	0.06	1.40	1.40	2
19	CO_2	279	0.26	2.24	2.24	2
19	CO_2	279	0.51	2.51	2.52	2
19	CO_2	279	0.72	2.66	2.68	2
19	CO_2	279	0.92	2.78	2.80	2
19	CO_2	279	1.16	2.89	2.92	2
19	CO_2	279	1.36	2.98	3.02	2
19	CO_2	279	1.64	3.07	3.12	2
19	CO_2	279	1.92	3.16	3.21	2
19	CO_2	279	2.27	3.25	3.31	2
19	CO_2	277	2.61	3.32	3.39	2
19	CO_2	279	2.96	3.38	3.46	2
19	CO_2	279	3.30	3.45	3.54	2
19	CO_2	279	3.89	4.22	4.33	1
19	CO_2	279	4.43	6.23	6.35	1
19	CO_2	279	5.15	8.10	8.24	1
19	CO_2	279	5.93	8.91	9.07	1
19	CO_2	279	6.03	9.11	9.27	1
19	CO_2	279	7.46	9.42	9.63	1
19	CO_2	279	8.15	9.57	9.80	1
19	CO_2	279	8.82	9.69	9.93	1
19	CO_2	279	9.51	9.78	10.10	1
20	CO_2	293	0.00	0.00	0.00	2

20	CO_2	293	0.03	0.10	0.10	2
20	CO_2	292	0.06	0.18	0.18	2
20	CO_2	293	0.09	0.27	0.27	2
20	CO_2	293	0.12	0.49	0.49	2
20	CO_2	292	0.16	0.98	0.98	2
20	CO_2	292	0.25	1.72	1.73	2
20	CO_2	292	0.47	2.20	2.21	2
20	CO_2	294	0.78	2.44	2.46	2
20	CO_2	294	1.01	2.56	2.58	2
20	CO_2	294	1.23	2.65	2.69	2
20	CO_2	294	1.53	2.76	2.80	2
20	CO_2	294	1.89	2.87	2.92	2
20	CO_2	292	2.24	2.96	3.01	2
20	CO_2	292	2.59	3.04	3.10	2
20	CO_2	292	2.94	3.10	3.17	2
20	CO_2	292	3.29	3.16	3.24	2
20	CO_2	292	3.97	3.26	3.36	2
20	CO_2	293	4.64	3.39	3.51	1
20	CO_2	293	5.21	4.53	4.66	1
20	CO_2	293	5.81	6.43	6.58	1
20	CO_2	293	6.48	7.46	7.63	1
20	CO_2	293	7.40	8.10	8.30	1
20	CO_2	294	8.11	8.34	8.55	1
20	CO_2	294	8.81	8.51	8.74	1

20	CO_2	293	9.43	8.63	8.88	1
21	CO_2	306	0.00	0.00	0.00	2
21	CO_2	306	0.02	0.04	0.04	2
21	CO_2	306	0.05	0.11	0.11	2
21	CO_2	306	0.16	0.61	0.61	2
21	CO_2	306	0.28	1.08	1.08	2
21	CO_2	306	0.46	1.92	1.93	2
21	CO_2	306	0.71	2.15	2.17	2
21	CO_2	306	0.91	2.26	2.28	2
21	CO_2	306	1.13	2.36	2.39	2
21	CO_2	305	1.34	2.46	2.49	2
21	CO_2	306	1.55	2.51	2.55	2
21	CO_2	306	1.90	2.60	2.65	2
21	CO_2	306	2.25	2.69	2.74	2
21	CO_2	306	2.60	2.76	2.82	2
21	CO_2	306	2.94	2.81	2.89	2
21	CO_2	306	3.28	2.87	2.95	2
21	CO_2	306	3.97	2.96	3.05	2
21	CO_2	306	4.65	3.03	3.14	2
21	CO_2	306	5.32	3.09	3.22	2
21	CO_2	306	5.99	3.18	3.32	2
21	CO_2	306	5.99	3.32	3.46	2
21	CO_2	306	7.39	4.27	4.45	1

21	CO_2	306	8.02	5.31	5.51	1
21	CO_2	306	8.71	6.32	6.54	1
21	CO_2	306	9.44	7.03	7.27	1

APPENDIX B: LANGMUIR PLOTS

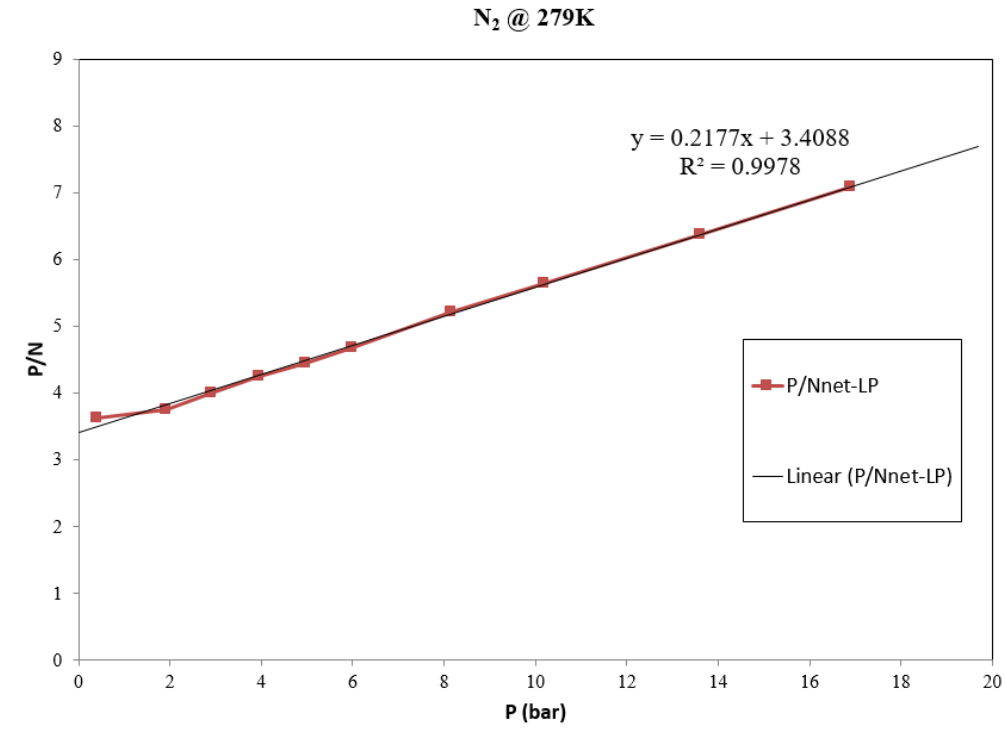

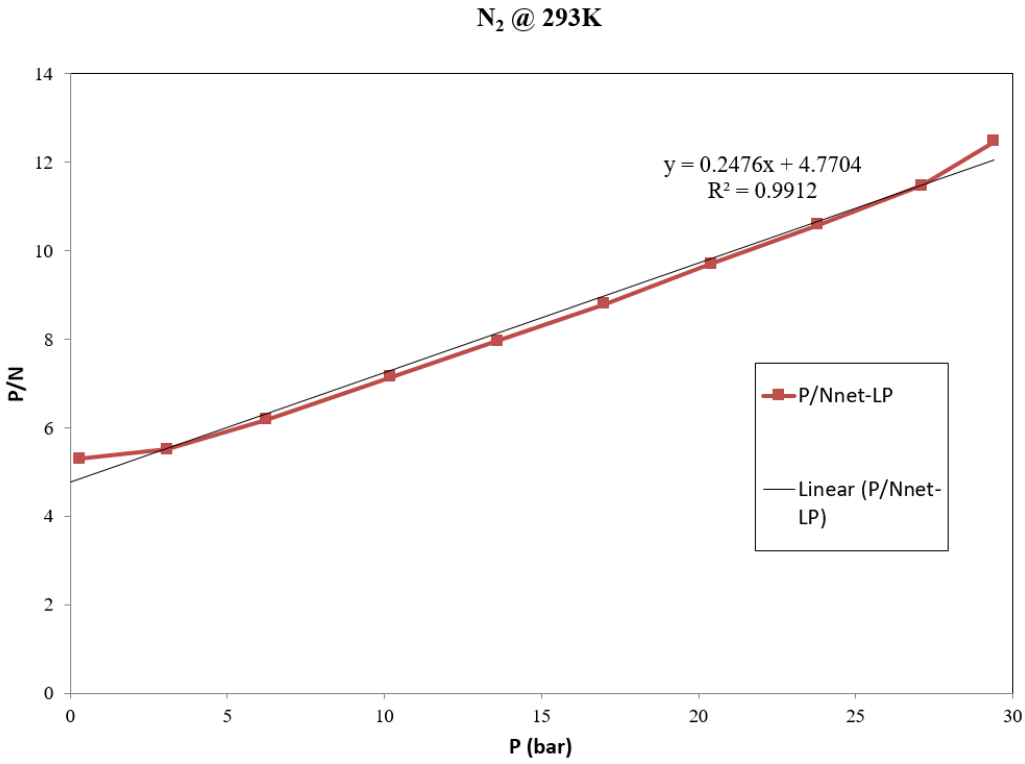

N_2 @ 306K

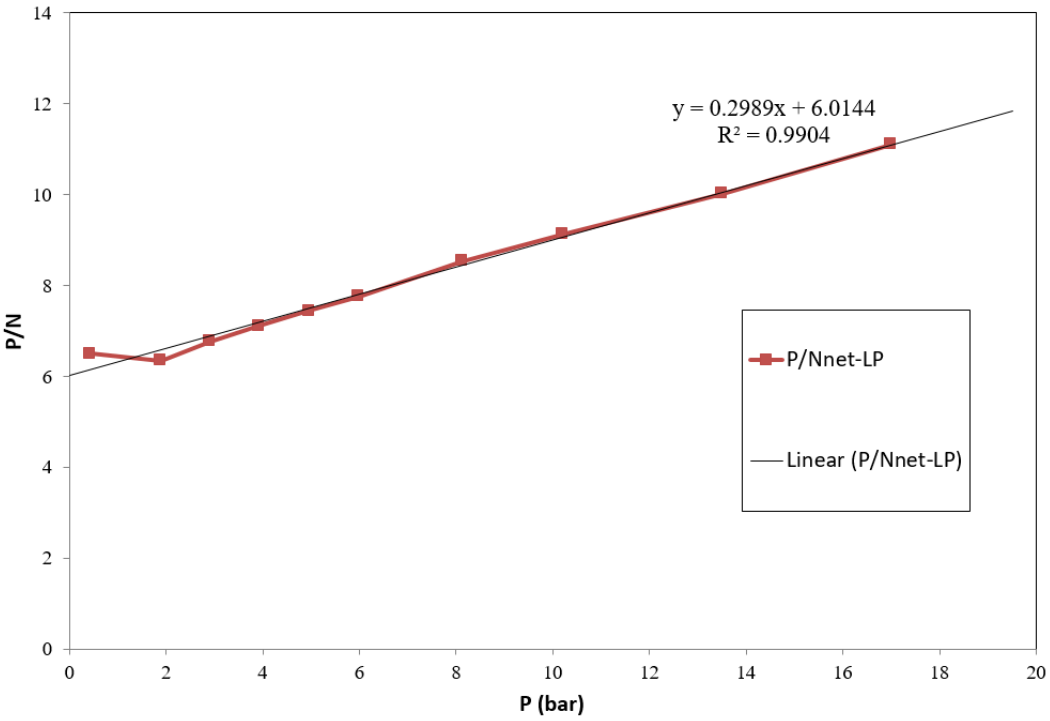

O_2 @ 279K

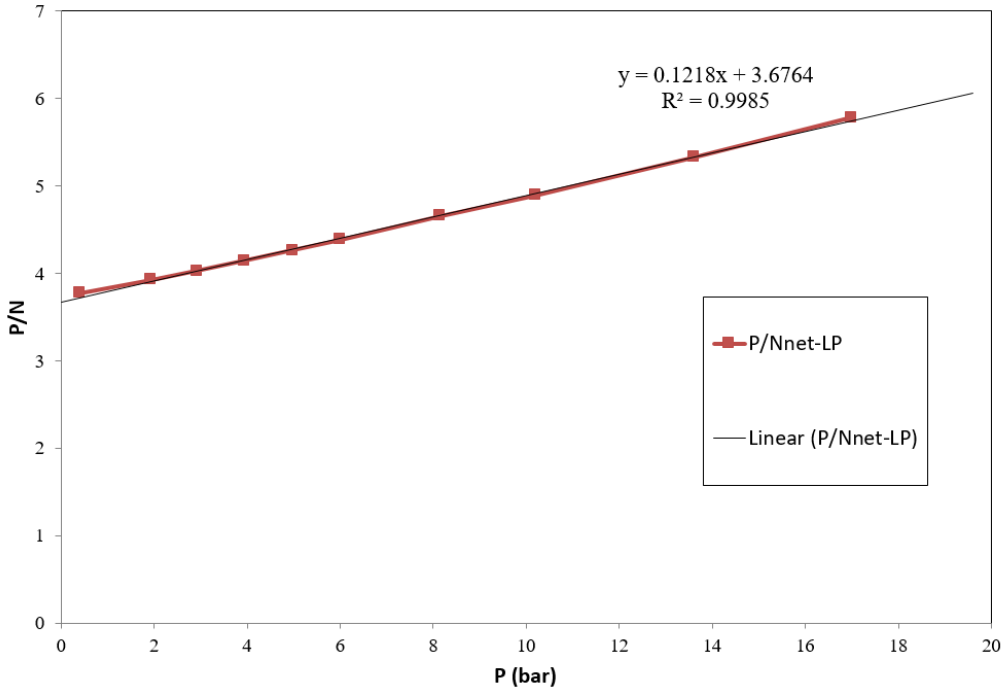

O_2 @ 293K

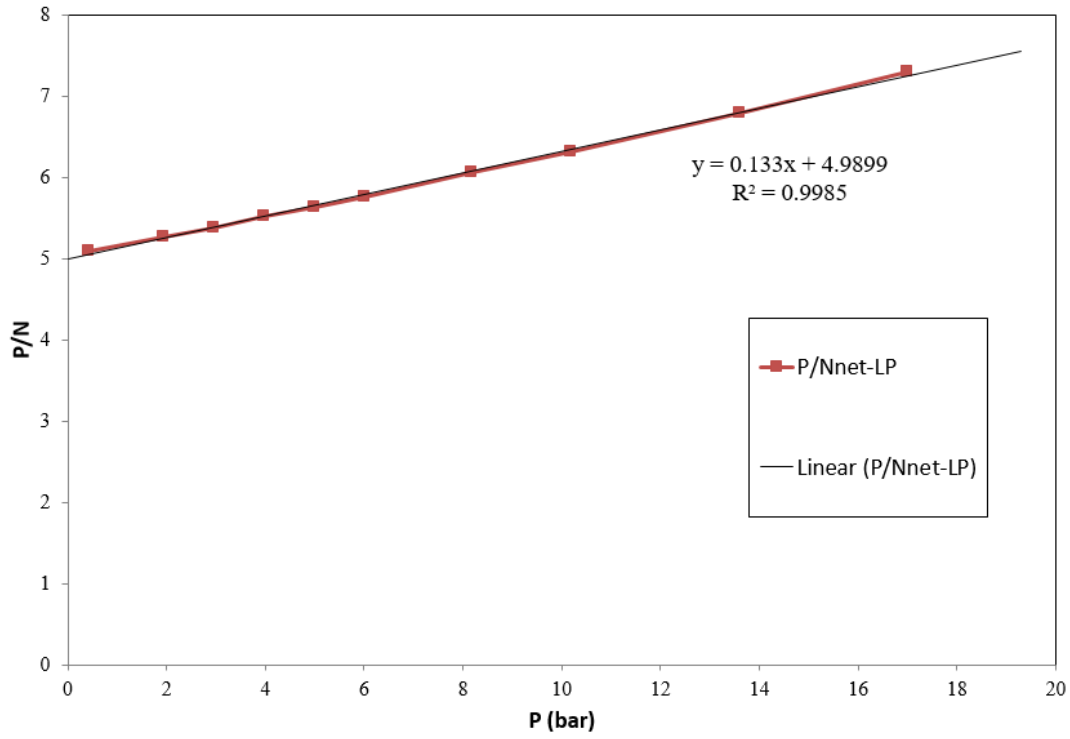

O_2 @ 306K

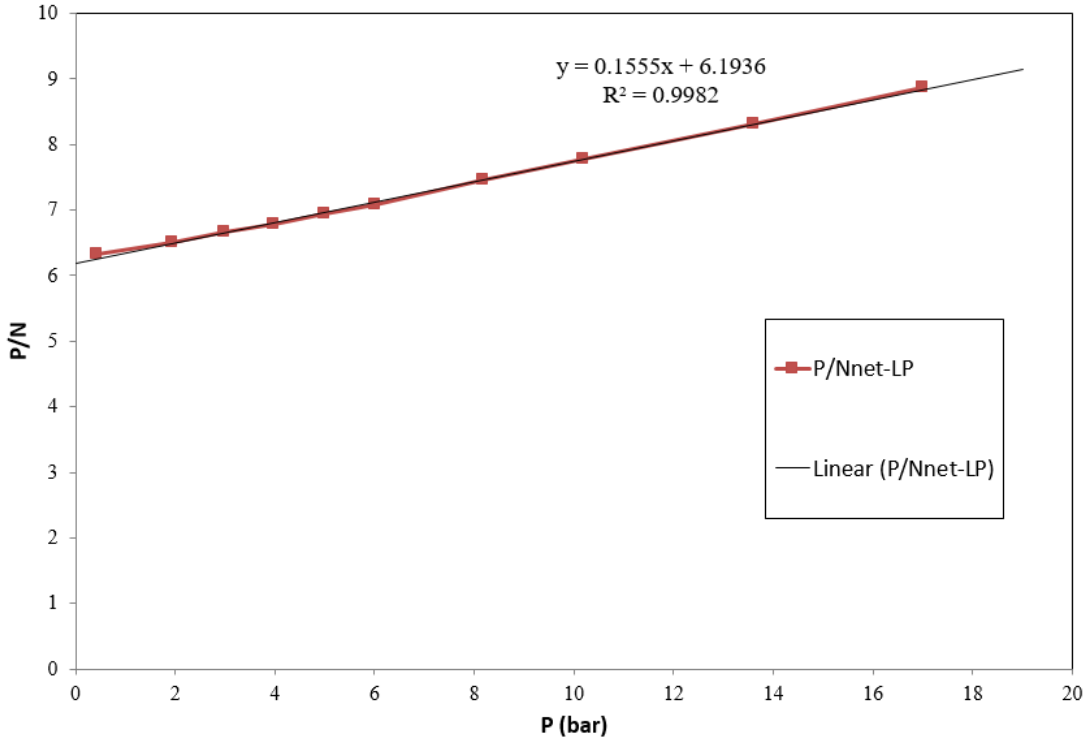

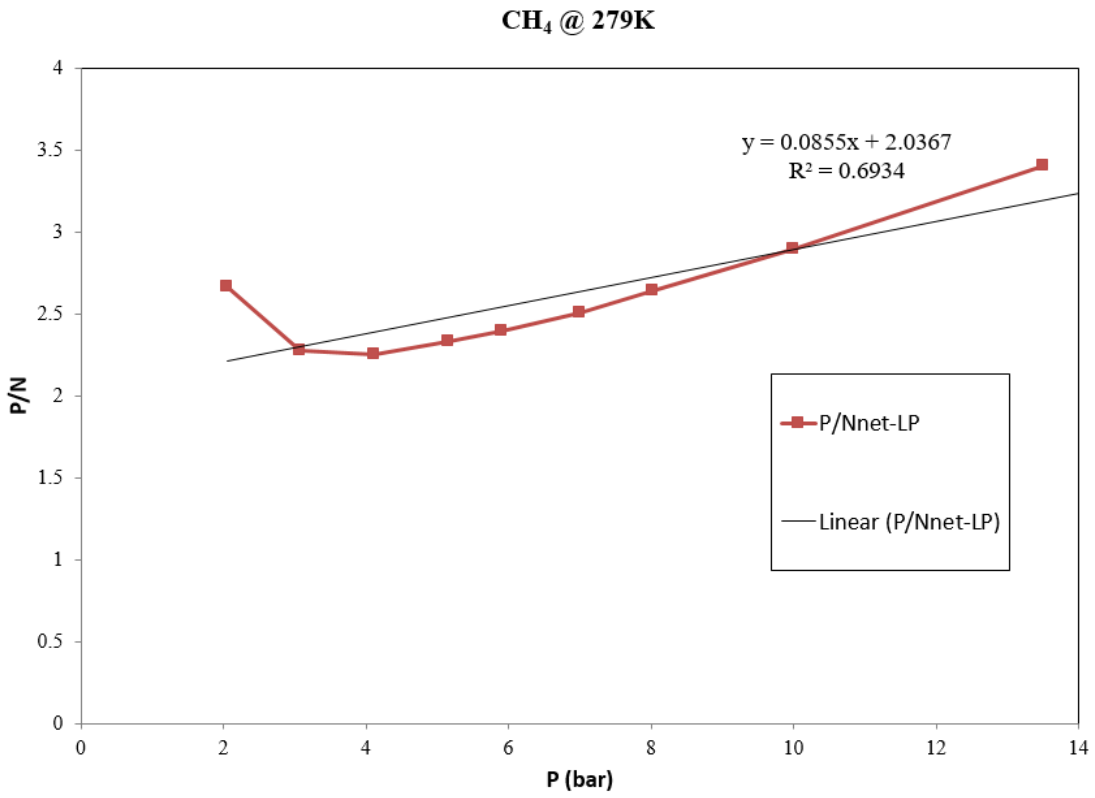
CH4 @ 279K
y = 0.0855x + 2.0367
R² = 0.6934
P/Nnet-LP
Linear (P/Nnet-LP)
P/N
P (bar)
0
0.5
1
1.5
2
2.5
3
3.5
4
0
2
4
6
8
10
12
14

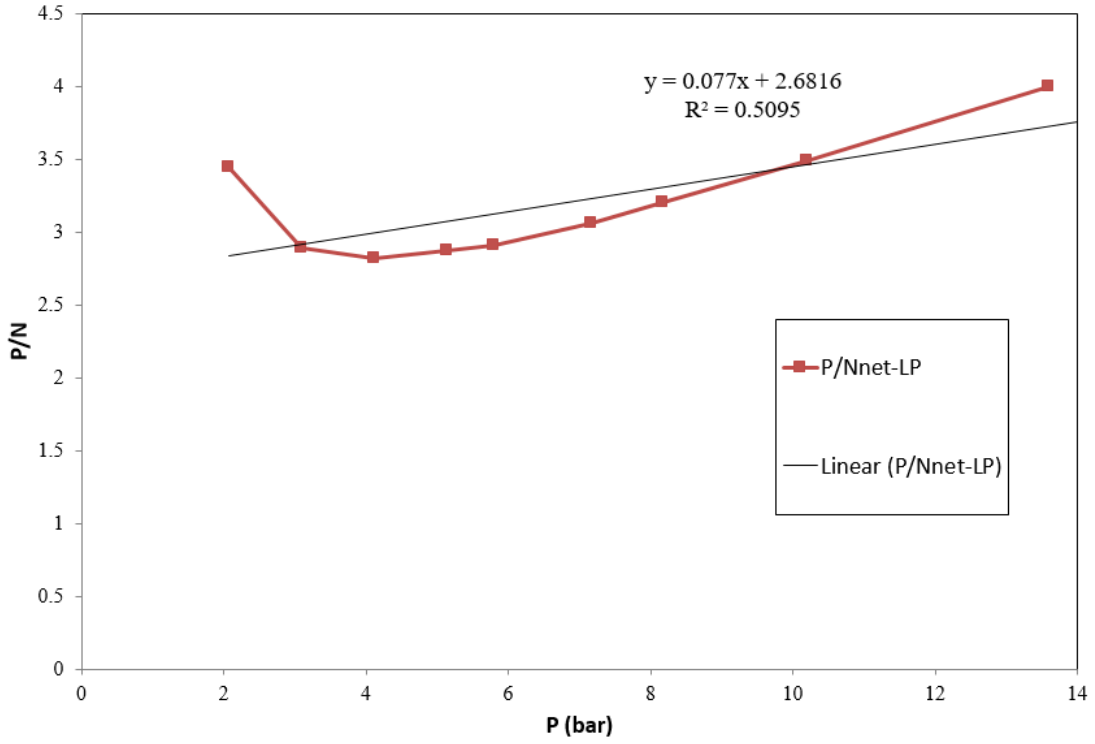
CH4 @ 293K
y = 0.077x + 2.6816
R² = 0.5095
P/Nnet-LP
Linear (P/Nnet-LP)
P/N
P (bar)
0
0.5
1
1.5
2
2.5
3
3.5
4
4.5
0
2
4
6
8
10
12
14

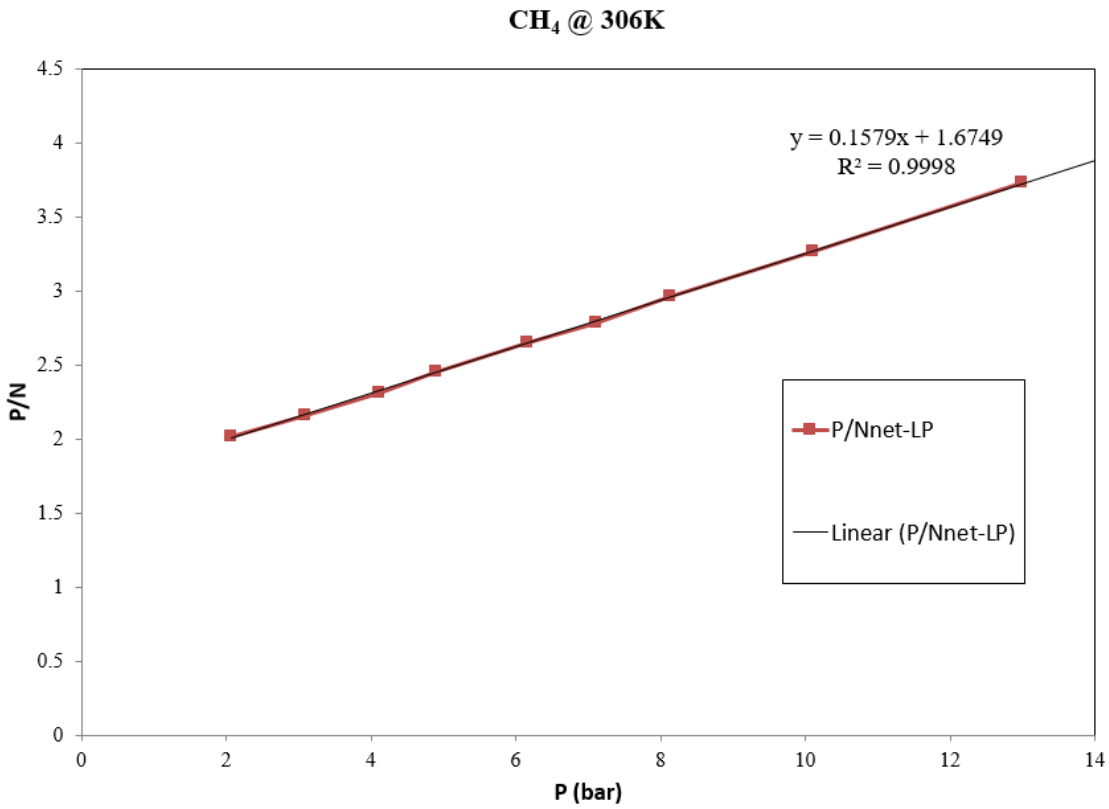
CH4 @ 306K
y = 0.1579x + 1.6749
R² = 0.9998
P/Nnet-LP
Linear (P/Nnet-LP)
P/N
P (bar)
0
0.5
1
1.5
2
2.5
3
3.5
4
4.5
0
2
4
6
8
10
12
14

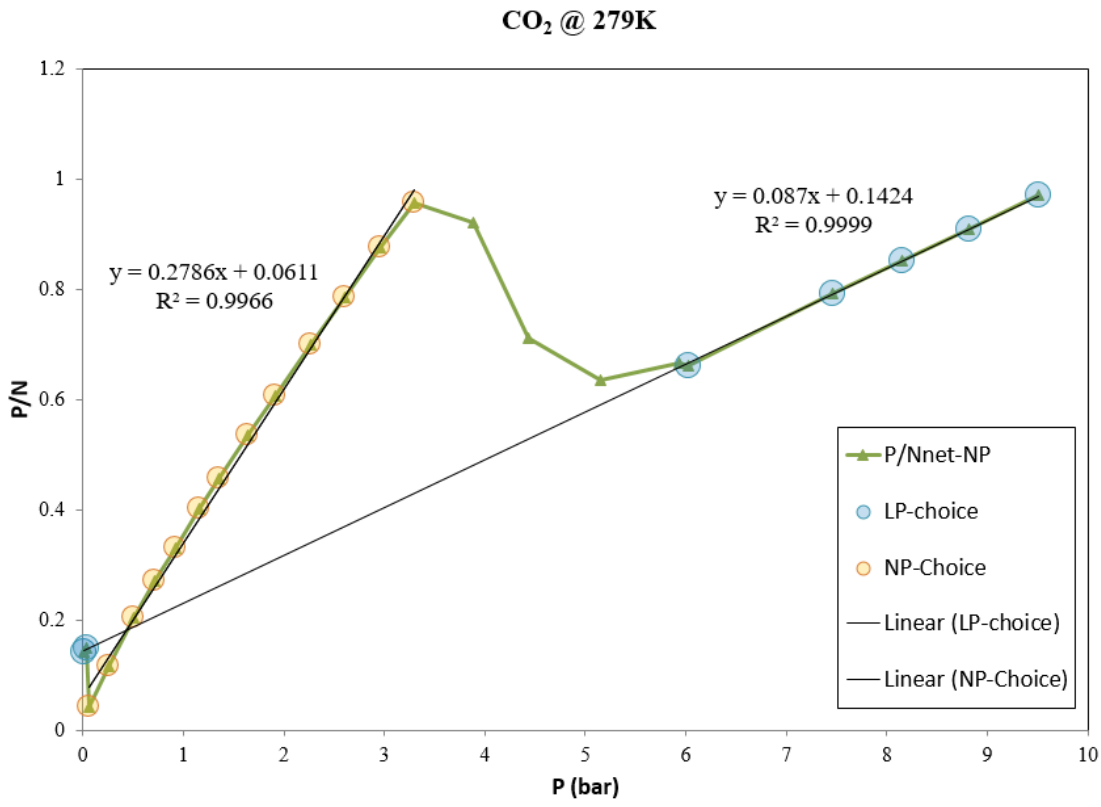
CO2 @ 279K
y = 0.2786x + 0.0611
R² = 0.9966
y = 0.087x + 0.1424
R² = 0.9999
P/Nnet-NP
LP-choice
NP-Choice
Linear (LP-choice)
Linear (NP-Choice)
P/N
P (bar)
0
0.2
0.4
0.6
0.8
1
1.2
0
1
2
3
4
5
6
7
8
9
10

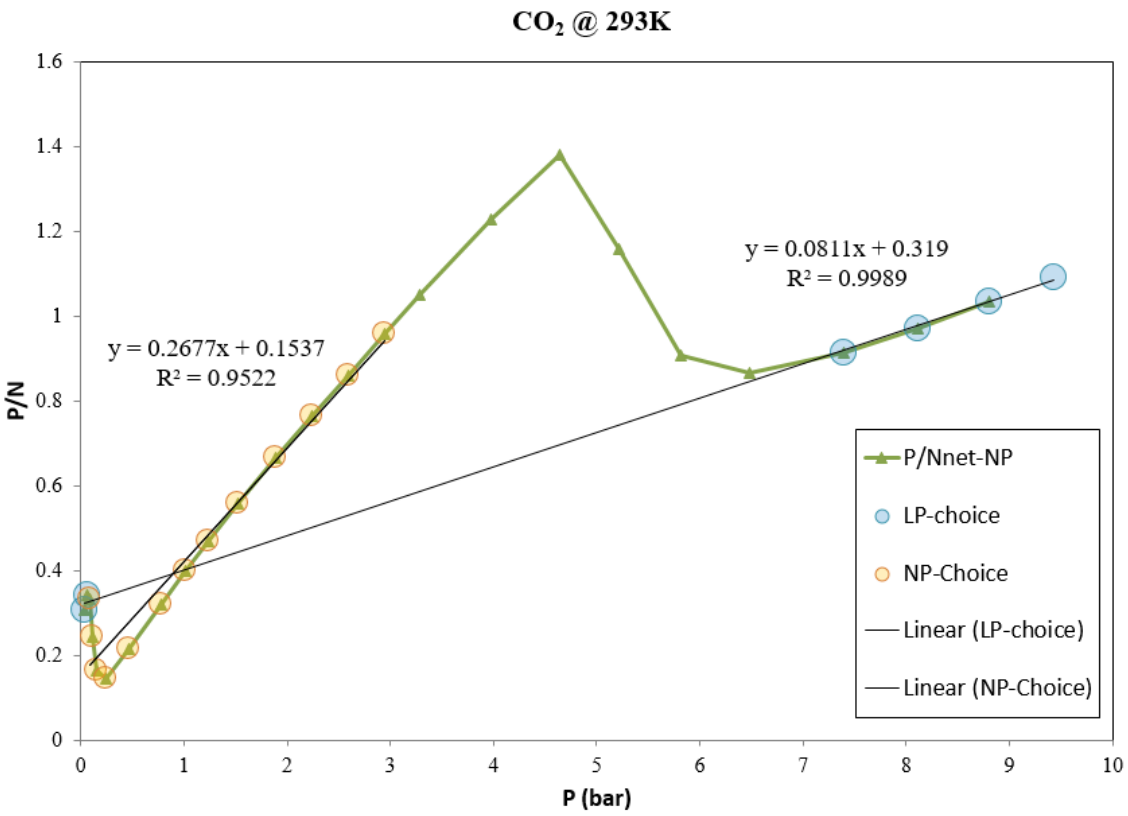
CO2 @ 293K
y = 0.2677x + 0.1537
R² = 0.9522
y = 0.0811x + 0.319
R² = 0.9989
P/N
P (bar)
P/Nnet-NP
LP-choice
NP-Choice
Linear (LP-choice)
Linear (NP-Choice)

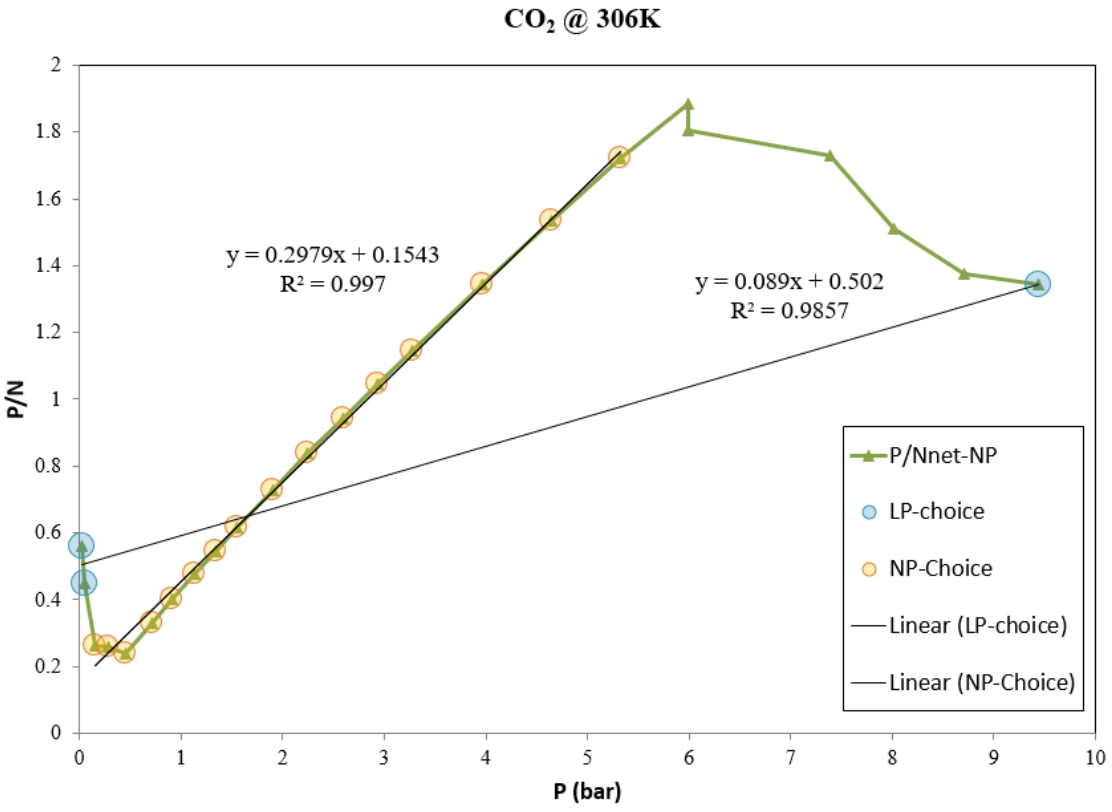
CO2 @ 306K
y = 0.2979x + 0.1543
R² = 0.997
y = 0.089x + 0.502
R² = 0.9857
P/N
P (bar)
P/Nnet-NP
LP-choice
NP-Choice
Linear (LP-choice)
Linear (NP-Choice)

APPENDIX C: CO_2 RIGID HOST ISOTHERMS

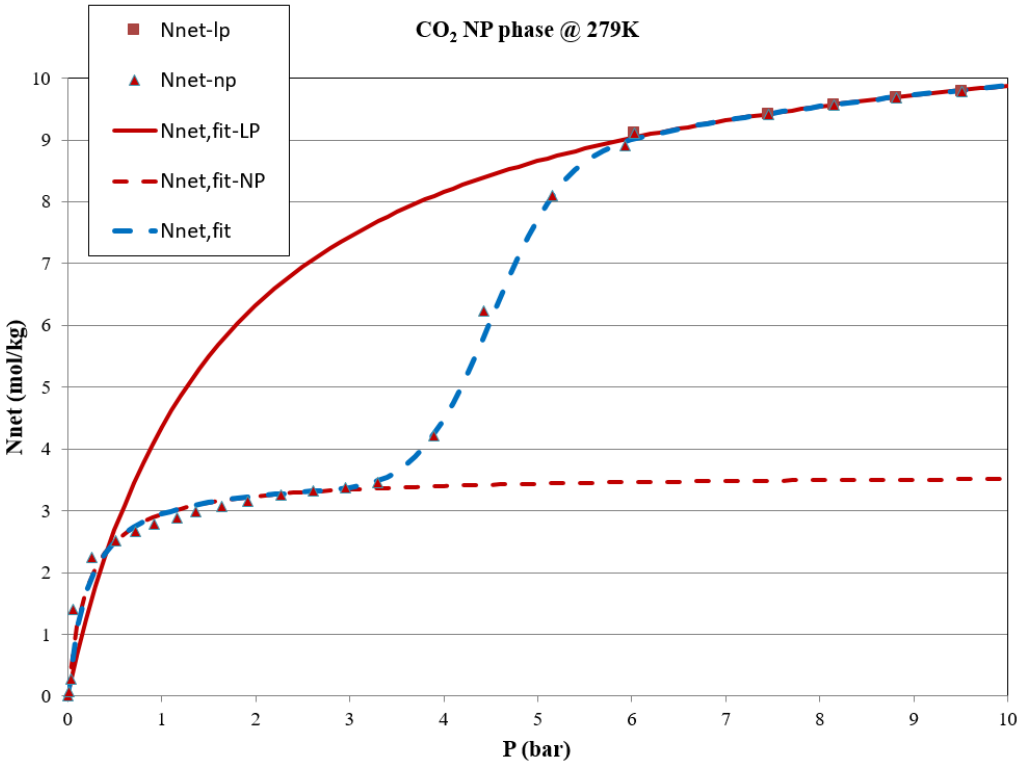

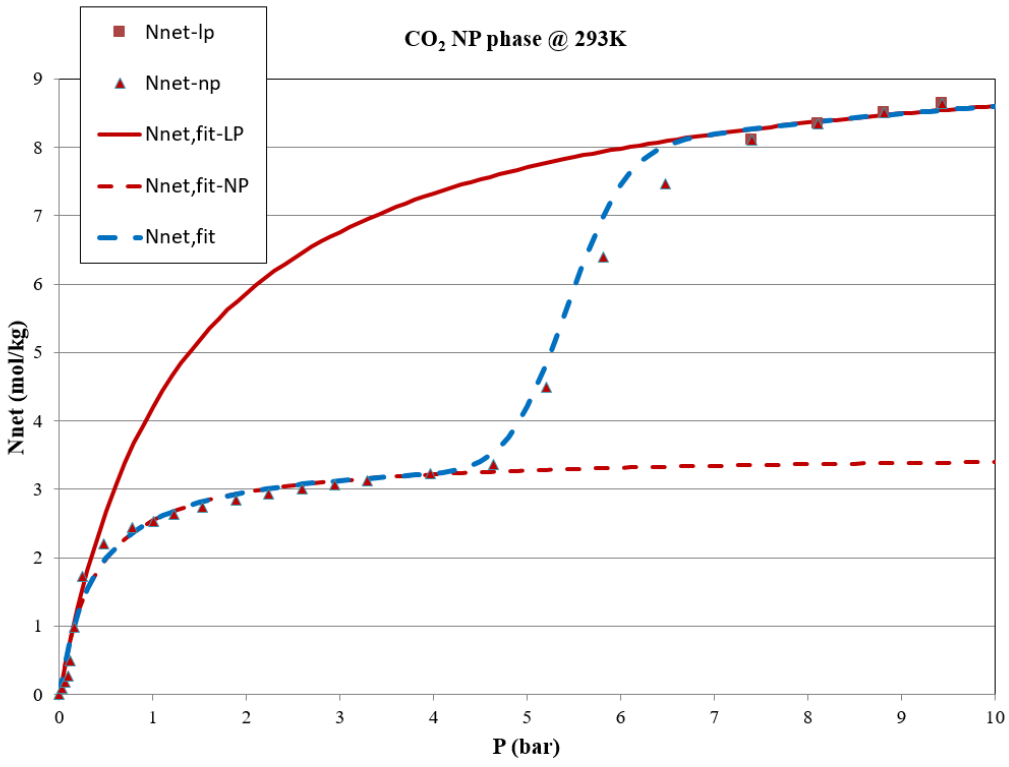

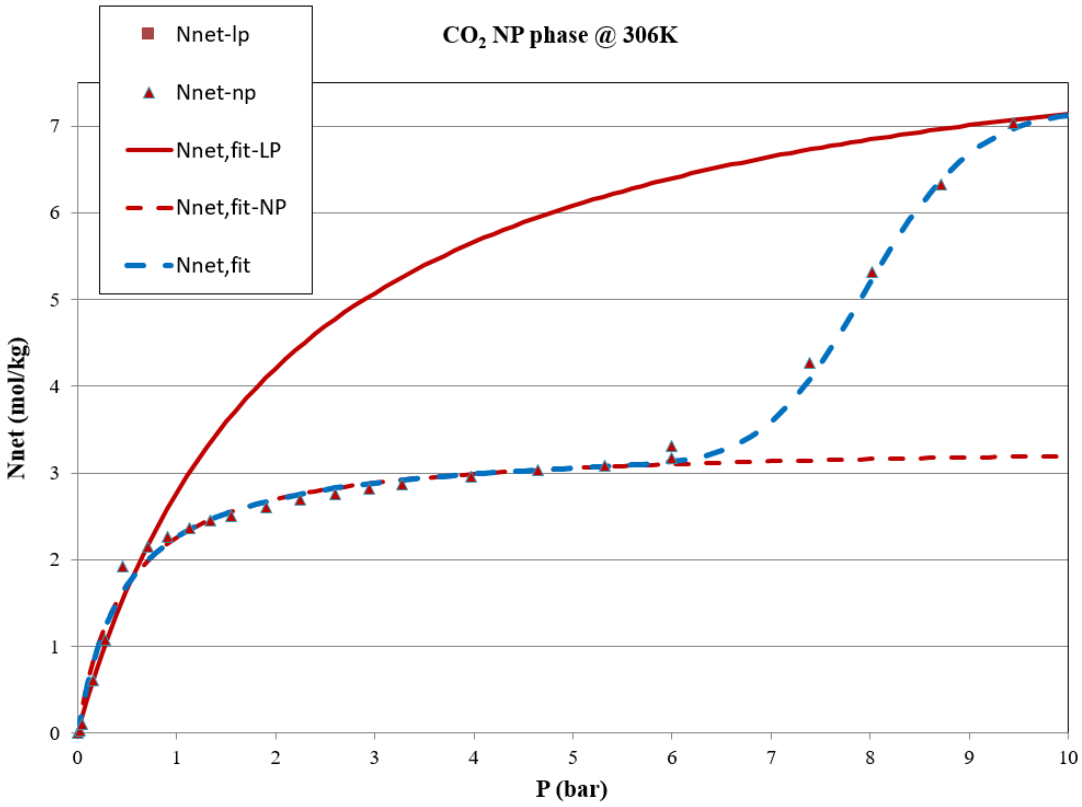
Nnet-lp
Nnet-np
Nnet,fit-LP
Nnet,fit-NP
Nnet,fit
CO2 NP phase @ 306K
Nnet (mol/kg)
P (bar)
0
1
2
3
4
5
6
7
8
9
10

APPENDIX D: SUMMARY TABLE														
Compound	**T (K)**	**N~-LP**	**b-LP**	**N~-NP**	**b-NP**	**Pc**	**Pc-stdev**	**N-LP-Pc**	**N-NP-Pc**	**f-Pc**	**N-com-Pc**	**ψ-LP-Pc**	**ψ-NP-Pc**	**δ_{Pc}**
Nitrogen (N2) LP Phase	279	4.593	0.064	0.00	0.00	5.500	2.45	1.194	0.000	0.500	0.597	1.383	0.00	1.383
Nitrogen (N2) LP Phase	293	4.039	0.052	0.00	0.00	4.150	2.45	0.716	0.000	0.500	0.358	0.788	0.00	0.788
Nitrogen (N2) LP Phase	306	3.346	0.050	0.00	0.00	5.000	3.95	0.666	0.000	0.500	0.333	0.742	0.00	0.742
Oxygen (O2) LP Phase	279	8.210	0.033	0.00	0.00	5.250	2.25	1.216	0.000	0.500	0.608	1.317	0.00	1.317
Oxygen (O2) LP Phase	294	7.519	0.027	0.00	0.00	4.700	2.50	0.837	0.000	0.500	0.419	0.887	0.00	0.887
Oxygen (O2) LP Phase	305	6.431	0.025	0.00	0.00	4.750	3.15	0.685	0.000	0.500	0.343	0.725	0.00	0.725
Methane (CH4) LP Phase	278	8.039	0.074	n/a	n/a	n/a	n/a	n/a	n/a	n/a	n/a	n/a	n/a	n/a
Methane (CH4) LP Phase	295	7.800	0.058	n/a	n/a	n/a	n/a	n/a	n/a	n/a	n/a	n/a	n/a	n/a
Methane (CH4) LP Phase	305	6.333	0.094	n/a	n/a	n/a	n/a	n/a	n/a	n/a	n/a	n/a	n/a	n/a
Carbon dioxide (CO2) LP Phase	279	11.494	0.611	3.589	4.56	4.450	0.60	8.403	3.421	0.500	5.912	15.096	10.977	4.119
Carbon dioxide (CO2) NP Phase	293	9.737	0.760	3.530	2.59	5.400	0.50	7.830	3.294	0.500	5.562	15.874	9.558	6.315

APPENDIX E: EXPERIMENTAL HISTORY LOG											
Data	**Sample ID**	**Treatment**	**Gas**	**Isotherm lable**	**Vac. P (Psi)**	**ZP (gm)**	**MP1 (gm)**	**MP2 (gm)**	**Sample wt (gm)**	**MP1-ZP**	**MP2-MP1**
14-May-18	Dr.Gumma	Isotherm	N2	N2 buoyancy (empty bucket) @ 23C	0.071	5.62088	15.89886	35.48083	N/A	10.27798	19.58197
	Dr.Gumma	Desorption	N2								
1-Jun-18	Dr.Gumma	Isotherm	He	He buoyancy on MIL-53(Al) @ 23C	0.128	5.42415	17.40657	36.98859	1.547522	11.98242	19.58202
	Dr.Gumma	Desorption	He								
	Dr.Gumma	Temp changed to 20C									
1-Jun-18	Dr.Gumma	Isotherm	N2	Isotherm on lp phase @ 20C	0.106	5.42483	17.40727	36.98931	1.547542	11.98244	19.58204
2-Jun-18	Dr.Gumma	Desorption									
4-Jun-18	Dr.Gumma	Isotherm	CO2	Isotherm @ 20C	-3.806	5.42892	17.41168	36.99378	1.547862	11.98276	19.5821
	Dr.Gumma	Desorption	CO2								

7-Jun-18	Dr.Gumma	Isotherm	N2	np phase @ 20C	-3.771	5.42827	17.41134	36.99338	1.548172	11.98307	19.58204
8-Jun-18	Dr.Gumma	Desorption									
8-Jun-18	Dr.Gumma	Phase change	CO2	at 20C							
8-Jun-18	Dr.Gumma	Desorption									
9-Jun-18		Isotherm	N2	np phase @ 20C	-3.751	5.42761	17.41082	36.99287	1.548311 5	11.98321	19.58205
	Dr.Gumma	Desorption									
	Dr.Gumma	Phase change	CO2	at 20C							
13-Jun-18	Dr.Gumma	Isotherm	O2	np phase @ 20C	0.1	5.42765	17.41122	36.99332	1.548671 5	11.98357	19.5821
	Dr.Gumma	Desorption	O2								
14-Jun-18	Dr.Gumma	Isotherm	O2	lp phase @ 20C	0.086	5.42767	17.41138	36.99347	1.548811 5	11.98371	19.58209
	Dr.Gumma	Desorption	O2								
	Dr.Gumma	temp changed to 32C									
15-Jun-18	Dr.Gumma	Isotherm	O2	lp phase @ 32C	0.092	5.42714	17.41084	36.99287	1.548801 5	11.9837	19.58203

	Dr.Gumma	Phase change	CO2	at 32C							
29-Jun-18	Dr.Gumma	Isotherm	O2	np phase @ 32C	0.146	5.48328	17.46489	37.04683	1.5467115	11.98161	19.58194
	Dr.Gumma	Desorption	O2								
	Dr.Gumma	temp changed to 5C									
1-Jul-18	Dr.Gumma	Isotherm	O2	lp phase @ 5C	0.157	5.48501	17.46687	37.04881	1.5469615	11.98186	19.58194
	Dr.Gumma	Desorption	O2								
	Dr.Gumma	Phase change	CO2	at 5C							
3-Jul-18	Dr.Gumma	Isotherm	O2	np phase @ 5C	0.169	5.48699	17.46769	37.04962	1.5458015	11.9807	19.58193
	Dr.Gumma	Desorption	O2								
5-Jul-18	Dr.Gumma	Isotherm	CO2	isotherm @ 5C	0.187	5.49014	17.47094	37.0529	1.5459015	11.9808	19.58196
	Dr.Gumma	Desorption	CO2								
9-Jul-18	Dr.Gumma	Isotherm	N2	np phase @ 5C	0.13	5.49928	17.47963	37.06172	1.5454515	11.98035	19.58209
	Dr.Gumma	Desorption	N2								

10-Jul-18	Dr.Gumma	Isotherm	N2	lp phase @ 5C	0.145	5.49786	17.47806	37.06009	1.5453015	11.9802	19.58203
	Dr.Gumma	temp changed to 32C									
13-Jul-18	Dr.Gumma	Isotherm	CO2	at 32C	0.133	5.50426	17.48322	37.06526	1.5440615	11.97896	19.58204
	Dr.Gumma	Desorption	CO2								
17-Jul-18	Dr.Gumma	Isotherm	N2	np phase @ 32C	0.155	5.50454	17.4077	36.98967	1.4682615	11.90316	19.58197
	Dr.Gumma	Desorption	N2								
19-Jul-18	Dr.Gumma	Isotherm	N2	lp phase @ 32C	0.133	5.50962	17.41289	36.99493	1.4683715	11.90327	19.58204
	Dr.Gumma	Desorption	N2								
25-Jul-18	Dr.Gumma	Isotherm	CH4	lp phase @ 32C	0.129	5.51216	17.41535	36.99746	1.4682915	11.90319	19.58211
8-Nov-18	Dr.Talu	Sample Changed				5.41959	12.84876	32.42587	1.34000	7.42917	19.57711
18-Dec-18	Dr.Talu	Sample Activation				5.45689	12.76365	32.34496		7.30676	19.58131
21-Dec-18	Dr.Talu	Isotherm	He	buoyancy on MIL-53(Al) @ 20C	0	5.45734	12.76442	32.34640	1.313980	7.30708	19.58198
	Dr.Talu	Desorption	He								

28-Dec-18	Dr.Talu	Isotherm	CH4	lp phase @ 20C	0.05	5.45916	12.76642	32.34839	1.314160	7.30726	19.58197
	Dr.Talu	Desorption	CH4								
	Dr.Talu	Phase change	CO2	at 20C							
4-Jan-19	Dr.Talu	Isotherm	CH4	np phase @ 20C	0	5.45985	12.76778	32.34971	1.314830	7.30793	19.58193
	Dr.Talu	Desorption	CH4								
	Dr.Talu	Temp changed to 32C									
7-Jan-19	Dr.Talu	Isotherm	CH4	lp phase @ 32C	0	5.4588	12.76696	32.34884	1.315060	7.30816	19.58188
	Dr.Talu	Desorption	CH4								
9-Jan-19	Dr.Talu	Phase change	CO2	at 32C							
8-Feb-19	Dr.Talu	Isotherm	CH4	np phase at 32C	0	5.43349	12.74239	32.32412	1.31570	7.3089	19.58173
	Dr.Talu	Desorption	CH4								
	Dr.Talu	temp changed to 5C									
19-Feb-19	Dr.Talu	Isotherm	CH4	lp phase @ 5C	0	5.43573	12.74508	32.3267	1.31625	7.30935	19.58162
	Dr.Talu	Desorption	CH4								
	Dr.Talu	Phase change	CO2	at 5C		5.43602	12.74611	32.32777		7.31009	19.58166
21-Feb-19	Dr.Talu	Isotherm	CH4	np phase @ 5C	-0.2	5.43602	12.74608	32.32778	1.31696	7.31006	19.5817